

# **Synthesis, Characterization, and Applications of Organic-Inorganic Hybrid Mesoporous Silica Materials**

Von der Fakultät Chemie der Universität Stuttgart  
zur Erlangung der Würde eines  
Doktors der Naturwissenschaften (Dr. rer. nat.)  
genehmigte Abhandlung

Vorgelegt von

**Tahira Yasmin**

aus Pakistan

Hauptberichter:	Prof. Dr. K. Müller
Mitberichter:	Prof. Dr. E. Roduner
Mitprüfer und Prüfungsvorsitzender:	Prof. Dr. Th. Schleid
Tag der mündlichen Prüfung:	02 November 2010

**Institut für Physikalische Chemie  
der Universität Stuttgart**

**2010**



**Dedicated to my beloved parents and my husband**



# Acknowledgments

All praises are due to almighty God, the Creator and Sustainer of the Universe. First of all, I want to express my thanks to my supervisor and first referee on this thesis, Prof. Dr. Klaus Müller. He initiated and supported this work with his great experiences and gave me the opportunity to work on this challenging domain. His guidance helped me in all the time of research and writing of this thesis. I could not have imagined having a better advisor and mentor for my Ph.D. study. I warmly thank Prof. Dr. Emil Roduner for his interest in my work and his willingness to act as the second referee on this thesis. I also thank Prof. Dr. Thomas Schleid, co-examiner for my doctoral thesis.

I would like to thank the Higher Education Commission of Pakistan (**HEC**) and Deutscher Akademischer Austausch Dienst (**DAAD**) for their financial support for this research.

I would like to acknowledge Prof. Dr. Emil Roduner (Institute of Physical Chemistry, University of Stuttgart) for allowing me to use the nitrogen sorption instrument and Dr. Alexander Fels (Institute of Electron microscopy microanalyses, University of Stuttgart) for performing the SEM measurements. I also thank Prof. Dr. Frank Gießelmann and Ms. Nadia Kapernaum (Institute of Physical Chemistry, University of Stuttgart) for their help in XRD measurements and Mr. H. Beuttler (Institute of Technical Biochemistry, University of Stuttgart) and Dr. Klaus Dirnberger (Institute of Polymer Chemistry, University of Stuttgart) for support during the HPLC experiments.

I would like to thank all my group fellows who helped me in brainstorming and providing information for this study. However, there are a few people that I would like to specially acknowledge and extend my heartfelt gratitude who have made the completion of this research possible: Beatrice Omiecienski, Matthias Abele, Kamalakannan Kailasam and Fabrizia Poli.

Finally, I like to express my deepest thanks to my loving parents, my dearest husband and my caring brother and sisters for their all time support and encouragement during the time that I was engaged in this study. Their sacrifices for this research work are highly valuable and influential for my life. Their affection and love motivated me to complete this work.

Stuttgart, November, 2010

Tahira Yasmin



# Contents

<b>1</b>	<b>Introduction</b>	<b>9</b>
1.1	Mesoporous Silica Materials .....	10
1.1.1	MCM-41 Silica Materials .....	11
1.1.2	SBA-15 Silica Materials .....	13
1.2	Organic-Inorganic Hybrid Mesoporous Silica Materials.....	15
1.3	Materials Studied in the Present Work .....	19
<b>2</b>	<b>Characterization Techniques</b>	<b>21</b>
2.1	Nitrogen Sorption Studies .....	22
2.1.1	Classification of Isotherms .....	23
2.1.2	Hysteresis Loops .....	23
2.1.3	BET Surface Area .....	24
2.1.4	Pore Volume .....	25
2.1.5	Pore Size and Pore Size Distribution (PSD) .....	26
2.2	Small Angle X-Ray Diffraction (XRD) .....	27
2.3	Scanning Electron Microscopy (SEM) .....	29
2.4	Solid-State NMR Spectroscopy .....	30
2.4.1	Theory .....	30
2.4.2	Organic-Inorganic Hybrid Silica Materials and Solid-State NMR Spectroscopy.....	40
2.5	Fourier Transform Infrared Spectroscopy (FTIR) .....	42
2.6	High Performance Liquid Chromatography (HPLC) .....	44
2.6.1	Operation.....	45
2.6.2	Organic-Inorganic Hybrid Mesoporus Silica Materials and HPLC .....	49
<b>3</b>	<b>Material Characterization</b>	<b>51</b>
3.1	Elemental Analysis .....	51
3.2	Nitrogen Sorption Studies .....	51
3.3	Scanning Electron Microscopy .....	52
3.4	Small Angle X-Ray Diffraction .....	52
3.5	Solid-State NMR Measurements.....	52
3.6	FTIR Measurements .....	53
3.7	HPLC Experiments .....	53

<b>4</b>	<b>Synthesis and Surface Characterization of Octadecyl Modified MCM-41 Silica Materials and Their Application in HPLC</b>	<b>55</b>
4.1	Introduction .....	55
4.2	Sample Preparation .....	56
4.2.1	Chemicals .....	56
4.2.2	Synthesis of MCM-41 Silica Material .....	56
4.2.3	Reaction of Silylating Agents with MCM-41 Silica Material ...	56
4.3	Results and Discussion .....	57
4.3.1	Synthesis and Surface Modification of MCM-41 Silica Material	57
4.3.2	Nitrogen Sorption Studies.....	59
4.3.3	Scanning Electron Microscopy .....	62
4.3.4	Small Angle X-ray Diffraction .....	63
4.3.5	<sup>29</sup> Si NMR Spectroscopy .....	66
4.3.6	<sup>13</sup> C NMR Spectroscopy .....	68
4.3.7	FTIR Spectroscopy .....	70
4.3.8	HPLC Measurements.....	72
4.4	Concluding Remarks .....	75
<b>5</b>	<b>Synthesis and Surface Modification of MCM-41 Silica Materials with Shorter Alkyl Chains using Surface Polymerization Method</b>	<b>77</b>
5.1	Introduction .....	77
5.2	Sample Preparation .....	78
5.2.1	Chemicals .....	78
5.2.2	Synthesis of MCM-41 Silica Material .....	78
5.2.3	Reaction of Silylating Agents with MCM-41 Silica Material ...	79
5.3	Results and Discussion .....	79
5.3.1	Synthesis and Surface Modification of MCM-41 Silica Material	79
5.3.2	Nitrogen Sorption Studies .....	81
5.3.3	Scanning Electron Microscopy .....	85
5.3.4	Small Angle X-ray Diffraction .....	86
5.3.5	<sup>29</sup> Si NMR Spectroscopy.....	87
5.3.6	<sup>13</sup> C NMR Spectroscopy.....	92
5.3.7	FTIR Measurements .....	94
5.3.8	HPLC Measurements .....	97
5.4	Concluding Remarks ... ..	101
<b>6</b>	<b>Structural Characterization of Alkyl Bonded MCM-41 Silica Materials Prepared by Supercritical Fluid Method</b>	<b>103</b>
6.1	Introduction .....	103
6.2	Sample Preparation .....	104
6.2.1	Chemicals .....	104
6.2.2	Reaction of Silylating Agents with MCM-41 Silica Material ...	104
6.3	Results and Discussion.....	105
6.3.1	Synthesis and Surface Modification of MCM-41 Silica Materials .....	105
6.3.2	Nitrogen Sorption Studies.....	107
6.3.3	Scanning Electron Microscopy .....	110
6.3.4	Small Angle X-ray Diffraction .....	110
6.3.5	<sup>29</sup> Si NMR Spectroscopy.....	110
6.3.6	<sup>13</sup> C NMR spectroscopy .....	113



6.3.7	FTIR Measurements .....	115
6.4	Concluding Remarks .....	118
<b>7</b>	<b>Synthesis and Characterization of Surface Modified SBA-15 Silica Materials and Their Application in Chromatography</b>	<b>119</b>
7.1	Introduction .....	119
7.2	Sample Preparation .....	119
7.2.1	Chemicals .....	119
7.2.2	Synthesis and Surface Modification of SBA-15 Silica material..	119
7.3	Results and Discussion.....	121
7.3.1	Synthesis and Surface Modification of SBA-15 Silica material..	121
7.3.2	Scanning Electron Microscopy .....	123
7.3.3	Nitrogen Sorption Studies.....	123
7.3.4	Small Angle X-ray Diffraction .....	127
7.3.5	<sup>29</sup> Si NMR Spectroscopy .....	128
7.3.6	<sup>13</sup> C NMR Spectroscopy .....	130
7.3.7	FTIR Measurements .....	134
7.3.8	HPLC Measurements .....	138
7.4	Concluding Remarks .....	140
<b>8</b>	<b>Summary</b>	<b>143</b>
<b>9</b>	<b>Zusammenfassung</b>	<b>149</b>
	<b>References</b>	<b>155</b>



# Chapter 1

## Introduction

Liquid chromatography is a separation technique where analytes are separated by virtue of different solubilities between a liquid mobile phase and a liquid or solid stationary phase. Normal phase or adsorption chromatography make use of a polar adsorbent such as silica or alumina, and a nonpolar mobile phase. Reversed-phase liquid chromatography on the contrary uses a nonpolar stationary phase and a polar, largely aqueous mobile phase [1].

Reversed-phase liquid chromatography is the most popular analytical technique for separating complex mixtures. The separation is achieved by the interactions of analytes with the stationary phase. The stationary substrate or adsorbent acts as a support for the silylating agents to be bonded to the surface. The substrate must be rigid and impermeable for the better interaction with the analytes. In reversed-phase liquid chromatography, the analytes are separated using their hydrophobicity. A solute with more hydrophobic character will be retained on the column longer than the one with lesser hydrophobic nature. Also, polar solutes will interact with the silica surface to cause peak tailing. Water is generally one of the mobile phase components of a binary mixture in reversed-phase liquid chromatography and it does not interact with the hydrophobic stationary phase chains. The most popular mobile phase organic solvents used in reversed-phase liquid chromatography are methanol and acetonitrile because these two solvents can mix well with water at any ratio and do not have significant UV absorption within the UV detection range. In general, water/acetonitrile combinations provide greater efficiency, especially for compounds containing an aromatic ring.

The most important criteria for the chromatographic performance of an adsorbent are particle size, particle porosity, and surface area [2]. Particles should be spherical and the particle size should be between 3-10  $\mu\text{m}$  with a very small size distribution. This greatly enhances the packing of a column and hence the column efficiency. The particle porosity is described by the pore size, shape, and pore size distribution of the adsorbent. The pores

of an adsorbent can be modeled with either a cylinder with a small neck that widens, or with parallel slits. The average pore diameters for common adsorbents used in chromatography are between 9-30 nm. Each adsorbent can exhibit different types of pores depending on the manufacturing processes. The surface area is very important for the chromatographic performance and usually ranges between 100 and 500 m<sup>2</sup> g<sup>-1</sup>.

There are numerous types of adsorbents that have been studied over the years. Among them, silica is the most common substrate. Silica gel, SiO<sub>2</sub>, is a partially hydrated and highly porous form of silica, which is made from the most abundant elements in the earth's crust. Since the 1970's, silica gel has been the most widely used support for reversed-phase liquid chromatography. The improvement of starting silica materials with very controllable particle and pore sizes has enhanced chromatography immensely. In the past few decades, the most promising development for reversed-phase liquid chromatography was the introduction of microparticles and chemically bonded stable phases [3]. These particles with various pore sizes permit optimum reverse-phase interaction with solutes of different molecular weight.

## 1.1 Mesoporous Silica Materials

Porous inorganic materials that can be used in applications such as catalysis and separations have been intensely studied over the last 50 years due to their potential stability, ease of recovery and high surface areas. According to IUPAC, these materials are classified according to their types of predominant pore size as: (a) micropores with diameters less than 2.0 nm, (b) mesopores with diameters between 2.0 and 50 nm, and (c) macropores with diameters greater than 50 nm [4]. In Figure 1.1, the pore diameter of three representative classes of silica materials with micro-, meso- and macropores are depicted.

Amorphous oxides, while widely used industrially, are complex due to their inherent disorder. From a fundamental viewpoint inorganic solids which are crystalline, or at least ordered, should be easier to understand. With this in mind, zeolites have received considerable interest in the second half of the last century. Zeolites, an example of microporous materials, are crystalline and have therefore very well defined pore diameters. Silica gel with macropores is purely amorphous and its pores vary considerably in diameter. Mesoporous silicas are in between these two materials. Mesoporous silica materials represent a good compromise between the high structural

uniformity of zeolites and easily modified macroporous surfaces and thus possess the potential for a much larger range of effective chemical functions than micro- or macroporous materials. This is why the development of ordered mesoporous silica materials in the early 1990's was met with excitement and enthusiasm.

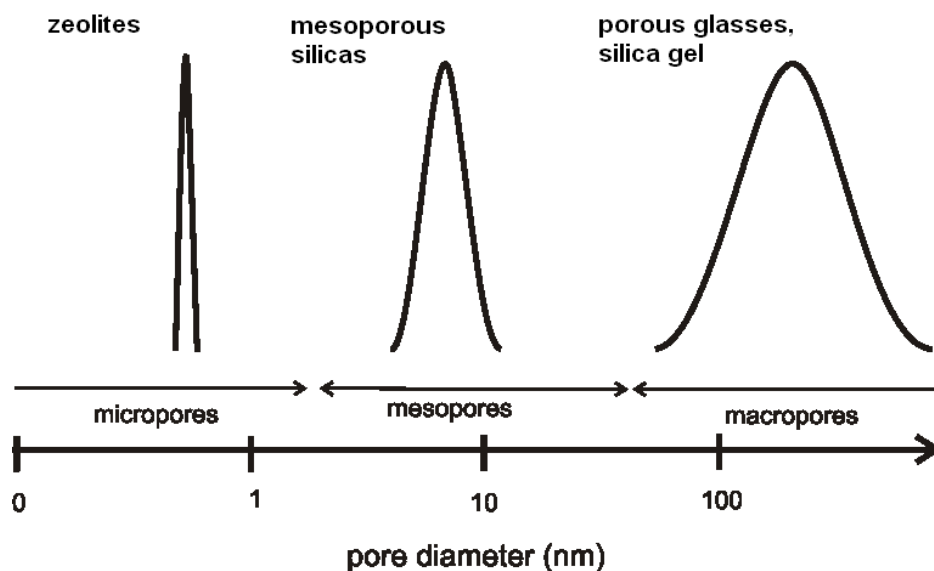


Figure 1.1: Pore diameter ranges according to IUPAC.

In the present dissertation, we are interested in mesoporous silica materials. Many applications of these materials in the field of catalysis, separation, adsorption, and drug delivery have been proposed and developed [5-7]. Among them, the use as stationary phases in chromatography is a promising field for further investigations. The unique properties of these silica materials are their high surface areas, extremely narrow pore size distribution, perfectly adjustable pore size, and the presence of silanol groups, which are promising for chromatographic separations.

### 1.1.1 MCM-41 Silica Materials

Since the first report on the M41S family of silica based mesoporous materials in 1992 by the Mobil Corporation [8-9], numerous studies have been performed dealing with their synthesis and surface modification which aimed to a further improvement of the bulk properties in view of the envisaged applications of these materials [10-18]. The most well-known and widely studied member of this type of materials is MCM-41. The framework of the MCM-41 type materials consists of hexagonally arranged cylindrical mesopores (which can vary from 2.5 to 10 nm in diameter depending on the template

used) with high surface area and narrow pore size distribution. The MCM-41 materials have a P6mm space group and the wall thickness is usually between 0.6 and 1.2 nm [19]. A great deal of research has been undertaken to examine the synthesis, characterization and potential applications of MCM-41 silica materials. They are formed under basic conditions using surfactants as the structure directing agent, which is usually cetyltrimethylammonium bromide (CTAB). Using CTAB, a typical pore size for MCM-41 is 4.0 nm. They are synthesized using self-assembly approaches where surfactant arrays co-assemble with inorganic precursors into nanoscale structures through favourable intermolecular interactions. Removal of the surfactants by calcination gives mesoporous oxide structures.

A liquid-crystal templating (LCT) mechanism was proposed by Beck et al. [9] to explain the formation of MCM-41 (Figure 1.2). The mechanism involves long-chain quaternary ammonium surfactants which minimize their energy in solution by assembling into micelles. Under certain conditions these micelles can adopt a rod-like shape and even organize into long-range hexagonal arrays (with rod diameters in the mesopore range 2.0 to 4.0 nm). In these arrangements the charged head groups point toward the solution and the long hydrocarbon chains (hydrophobic) point toward the centre of the micelles. The formation of the micellar rods and their organization into hexagonal arrays is strongly dependent on the surfactant alkyl chain length, concentration, the nature of the halide counter-ion, and the temperature of the solution [5,20-21]. Upon addition of a silicate precursor, the negatively charged silica species ( $\Gamma$ ) condense and polymerize on the surface of the positively charged micelles ( $S^+$ ), giving rise to the corresponding hexagonal  $S^+\Gamma$  organic-inorganic complex. Calcination of the complex yields the solid framework of this particular mesoporous molecular sieve (denoted as MCM-41).

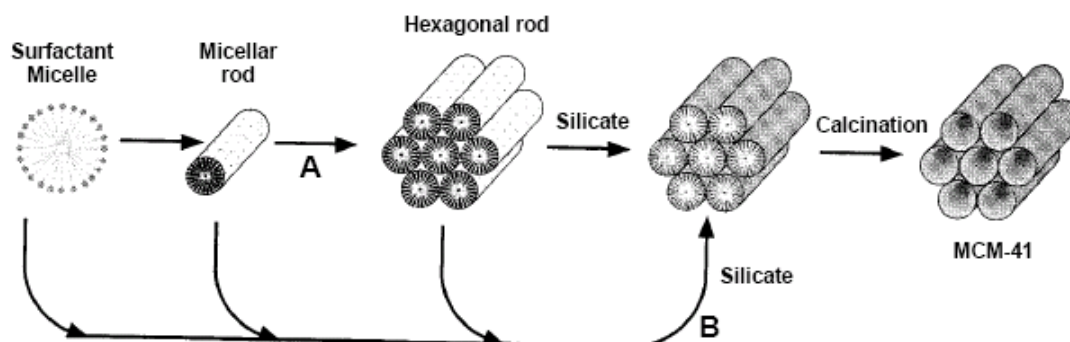


Figure 1.2: Liquid-crystal templating mechanism proposed by Beck et al. [9] showing two pathways for the formation of MCM-41: (A) liquid-crystal-initiated and (B) silicate-initiated.

MCM-41 silicas have been used as stationary phases, catalysis, etc. For instance, in catalysis the control of the particle size represents an important issue for the transfer of catalytic reactions from batch experiments to continuous processes where efficient mass transfer plays a key role [22]. In separation science, the average particle size is found to affect the plate height of the columns and thus their separation efficiency. In this context, the preparation of mesoporous silica spheres of tuneable size is very attractive because they allow a homogeneous filling of the chromatographic columns which in turn should improve the separation performance [23-24]. The first application of mesoporous materials in chromatography dates back by about a decade [6,25-26]. So far, MCM-41 silica materials have been proposed as stationary phases for normal-phase HPLC [27], size-exclusion chromatography [28], capillary gas chromatography [29], chiral HPLC [30] and reversed-phase liquid chromatography (RPLC) [23]. Although there were many attempts to prepare optimized systems that meet the requirements for chromatographic application, quite often only MCM-41 spheres with large particle size-distribution and agglomeration could be obtained [25-26,31-32]. However, there is still a need for further improvement of the basic materials.

Recently, the pseudomorphic synthesis was introduced which represents a new synthetic strategy for MCM-41 preparation with optimized procedures for particle shaping and mesophase self-assembly [22-23,33]. In this method, commercially available preformed silica particles of well-determined shape, size and size-distribution are used as silica source. The term pseudomorphism originates from the field of mineralogy, where a pseudomorph denotes an altered mineral with an outward appearance of another mineral species. In the present context, the pseudomorphic synthesis provides MCM-41 spheres which are pseudomorphs of the parent silica spheres. The key parameter in maintaining the morphology of the silica particles during the transformation process is to find the optimum synthetic conditions for which the rate of templated silica precipitation is equal to the rate for silica dissolution.

### **1.1.2 SBA-15 Silica Materials**

After the first report on surfactant templated synthesis of hexagonally ordered mesoporous MCM-41 silica materials in 1992, a broad spectrum of other mesoporous materials has been discovered. A major breakthrough in this area was the synthesis of large pore ordered mesoporous silica of the SBA-15 type using commercially available

block copolymers. It is one of a series of mesoporous materials developed in the mid-late 1990's in the University of California at Santa Barbara by Stucky et al. [34-35]. They reported that using triblock copolymers as structure directing agents, mesoporous silica can be synthesized in a wide range of sizes. Generally, the preparation includes the synthesis of a silica-surfactant composite, an aging step of the synthesis mixture under hydrothermal conditions, filtration with an optional washing step, followed by the removal of the organic polymer. The synthesis is based on cooperative self-assembly of the silica precursor and micelles of the triblock copolymer as structure directing agents under acidic conditions. A schematic pathway for the formation of SBA-15 silica material is shown in Figure 1.3. SBA-15 materials have a hexagonal pore-network like MCM-41, with uniform pore sizes up to approximately 30 nm [35]. A typical pore size for SBA-15 is 8.0 nm. The specific surface areas and specific pore volumes are somewhat smaller than those of MCM-41 materials, but pore walls are thicker (between 3.1 and 6.4 nm) as compared to MCM-41 materials. Therefore also the thermal and hydrothermal stability of these materials are better [36]. The pore diameters can be varied by the reaction conditions.

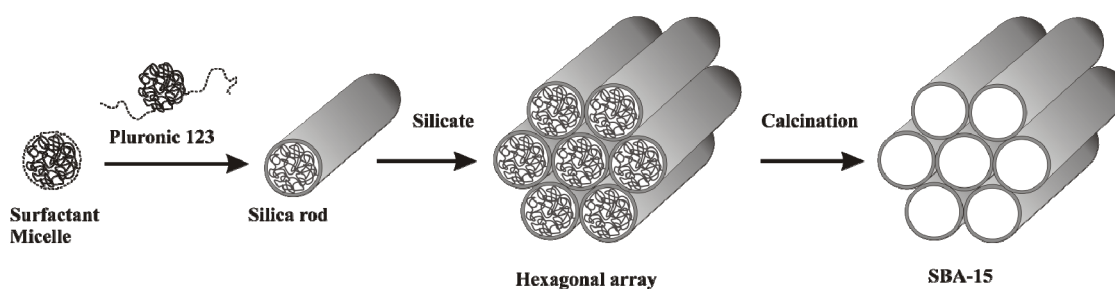


Figure 1.3: A schematic pathway for the formation of SBA-15 silica material.

The morphology of SBA-15 can be well controlled by using block copolymers, co-surfactants or co-solvent [37], which makes such uniform materials useful for catalysis [38] and adsorption/desorption processes [39]. However, the application of large pore SBA-15 as a substrate in high performance liquid chromatography (HPLC) needs monodisperse and micrometer-sized spherical particles. These materials can be used as a good packing in HPLC to separate both small aromatic molecules and large biomolecules such as proteins.

Here, we report on the synthesis of well-ordered hexagonal SBA-15 mesoporous silica spheres with large uniform pore sizes, which are obtained by the use of an



amphiphilic block copolymer, poly(ethylene oxide)-poly(propylene oxide)-poly(ethylene oxide), a high molecular weight non-ionic surfactant, commercially available as Pluronic P123 (EO<sub>20</sub>PO<sub>70</sub>EO<sub>20</sub>), as organic structure directing agent in combination with a cosurfactant (CTAB) and ethanol as a cosolvent in strong acid media. It was observed by Mesa et al. [40] that the adjustment of the size and shape of the particles was not possible without the presence of the cosurfactant CTAB. They observed that in the absence of the cosurfactant, the majority of the particles are very small with non-defined shape which indicates that this cosurfactant is the one that determines mainly the morphology of SBA-15 mesoporous silica. The cosolvent ethanol also plays an important role for the formation of perfect spherical morphology. The addition of ethanol may decrease the polarity of the solvent and thus decreases the rate of nucleation and growth of the mesostructures products because of the slower tetraethyl orthosilicate (TEOS) hydrolysis and mesostructure assembly, which could contribute to the formation of silica spheres with smooth surfaces [41-42].

## 1.2 Organic-Inorganic Hybrid Mesoporous Silica Materials

When an inorganic material, such as the aforementioned mesoporous silicas, are surface modified with an organic material they are referred to as organic-inorganic hybrid materials or, simply, hybrid materials. Such materials are both physically robust and possess the potential to perform complex separations, highly selective catalysis, and sensing. Surface modification of mesoporous silica materials with organic groups permits a tuning of the surface properties like hydrophilicity, hydrophobicity and surface reactivity [43]. Surface modification with organic groups via silylation is the commonly used method for preparation of organic-inorganic hybrid materials [44]. Here, reaction of the solid substrate with the silylating agents leads to a covalent bonding between the organic and inorganic components [45]. The interest in such organic-inorganic hybrid materials arises from the (combined) advantages that the organic and inorganic moieties bring in. Whereas the inorganic components provide sufficient mechanical, thermal and structural stability, by a proper choice of the organic components it is possible to match the special needs required, for instance, in separation science, catalysis or sensor design [46]. In connection with the former area of application, MCM-41 and SBA-15 silica materials have been proposed as stationary phases for HPLC. For this application, the

control of size and morphology, and the amount of surface coverage represent important issues.

In this context, mono-, di-, and trifunctional silanes ( $\text{RSiX}_n$ ;  $n = 0-3$ ; R = alkyl chains of length  $\text{C}_4$ ,  $\text{C}_8$ ,  $\text{C}_{12}$ ,  $\text{C}_{18}$ ,  $\text{C}_{22}$ ,  $\text{C}_{30}$ , etc.; X = chloro or alkoxy groups) have been attached to the surfaces of various oxide materials. The pore dimensions could be progressively decreased depending on the nature of the alkyl chain. In particular, trifunctional silanes have been frequently used as silylating reagents for surface modification of such oxide substrates which provide closely packed and highly ordered monolayers with enhanced stability [47-49]. However, the application of trifunctional silanes may also result in undesired vertical polymerization [50]. In commercial columns modification is therefore done by means of monofunctional silanes which provide reproducible surface coverages while vertical polymerization is avoided. It should be mentioned that the modification of mono-, di-, or trifunctional silanes on the oxide substrates depends on the targeted applications.

Monofunctional silane modified stationary phase materials can be obtained by the attachment of alkyl chains through single bonds. When di- or trifunctional silanes are used, two or more bonds per ligands will be formed with the inorganic support along with cross-linking of the neighboring silanes. The resulting bonding situation for mono- and trifunctional silane attached phases is shown in Figure 1.4.

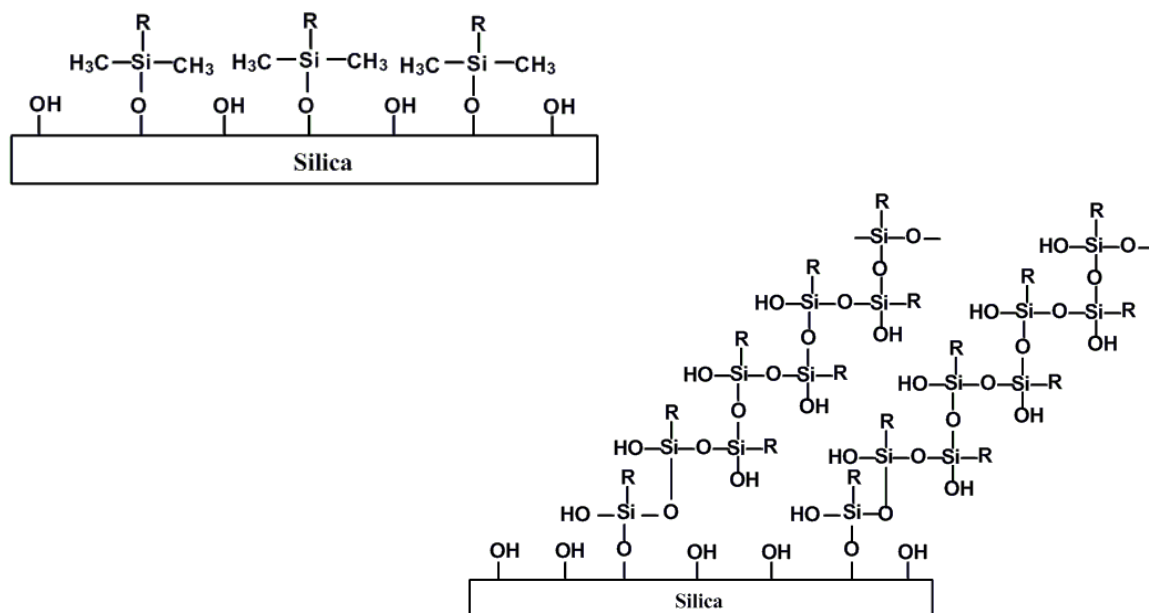


Figure 1.4: Representative structure of the alkyl modified stationary phases. Top – Phases formed from the monofunctional silane, Bottom – Phases formed from the trifunctional silane. R is representing alkyl chain ( $\text{C}_4$ ,  $\text{C}_8$  and  $\text{C}_{18}$ ).

The procedures used for the polymeric phase synthesis have been described as “solution polymerization” and “surface polymerization” to distinguish the introduction of water for initiating the polymerization (see Figure 1.5). For solution polymerization, water is added to slurry of silica containing silane. Polymerization occurs in the solution with subsequent deposition onto the silica [51-52]. Deposition of the silane polymer on the silica results in a surface with some heterogeneity. Most likely, vertical polymerization occurs in this case, and the degree of polymerization is due to the amount of water added to the reaction medium.

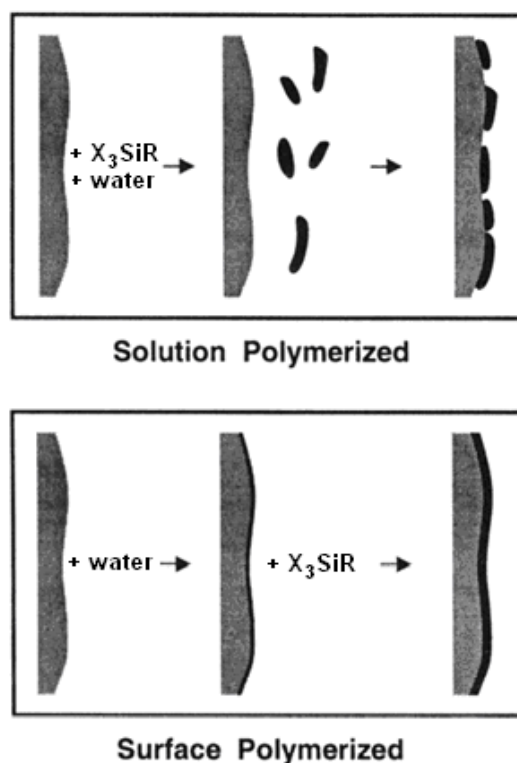


Figure 1.5: Diagram distinguishing two approaches to the synthesis of polymeric stationary phases, where X is representing functional group (e.g., OCH<sub>3</sub>) and R is alkyl chain. Silane polymerization occurs in solution or at the silica surface depending on the order of addition of reagents.

For surface polymerization, water is added to dry silica either through exposure to humid air or by direct addition prior to silanization [52-53]. Here, a monolayer coverage of the water molecules on the silica surface is achieved. Later, wet silica is introduced into a solution containing the silane. The “surface polymerization” procedure is a self-assembled monolayer approach, where higher surface coverage of alkyl chains on the surface and a more regular bonded surface can be reached [54-55]. These phases are mostly horizontally polymerized and have more alkyl moieties which are bonded to the

surface and have the ability to run at the high and low pH extremes [56]. Vertical polymerization also takes place here which actually depends on the amount of water present on the surface and on the type of silylating agent [57-58].

Supercritical carbon dioxide (sc-CO<sub>2</sub>) has been demonstrated as another effective reaction medium for the generation of chromatographic stationary phases as demonstrated by Healy et al. [59]. Supercritical CO<sub>2</sub> has certain properties that make it an attractive solvent as compared with traditional organic solvents. It is nonflammable, more environmentally friendly, and considerably less hazardous than most organic solvents. McCool and Tripp demonstrated that silica silanols which are inaccessible in organic solvents are accessible in (sc-CO<sub>2</sub>) which can be attributed to the unique properties of the supercritical fluid such as its gas-like diffusivities and liquid-like solubilities [60]. The supercritical state can be achieved at comparably low temperatures (31.1 °C) and pressures (73.8 bar) when compared to other substances. The density and solvating power can be “tuned” by varying temperature and pressure. High diffusivity and mass-transfer kinetics in sc-CO<sub>2</sub> should provide improved access to silanol groups in porous silica and faster reactions than in conventional solvents. Organosilanes have been used before to modify materials using supercritical fluids as the reaction solvent [61-62]. In the present work, we report on the sc-CO<sub>2</sub> surface modification of mesoporous MCM-41 silica materials for the preparation of alkyl bonded phases with surface coverages comparable to organic solvent produced bonded phases.

After derivatization with alkyl silanes (usually with C<sub>8</sub> to C<sub>18</sub> systems), residual silanols remain on the surface [63]. In order to eliminate these silanols, low molecular weight (C<sub>1</sub> to C<sub>3</sub>) alkyl silane reagents are used to endcap the surface. These smaller silanes will react with as many silanols as possible. Endcapped alkyl modified phases were shown to provide better chromatographic results [64-65]. The main compound used for endcapping is hexamethyldisilazane (HMDS) [66]. In the present study, endcapping was done with HMDS after the attachment of mono- and trifunctional alkyl silanes to the mesoporous supports. Figure 1.6 provides a schematic drawing of endcapped silica gels after surface modification with mono- and trifunctional alkyl chains.

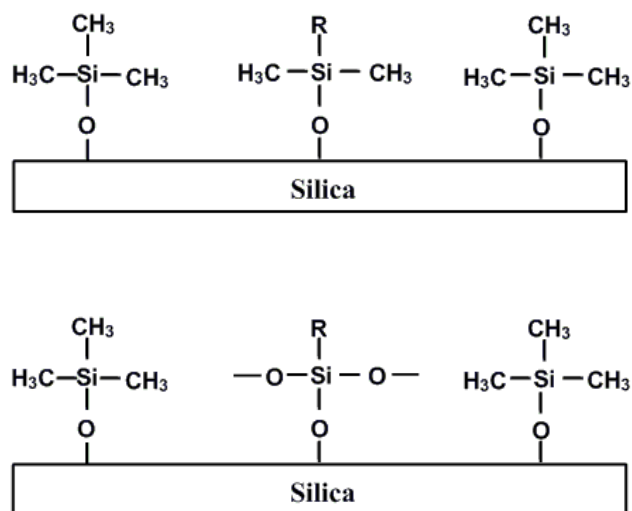


Figure 1.6: Schematic drawing of endcapped silica gels after surface modification with monofunctional (top) and trifunctional (bottom) alkyl chains. R is representing alkyl chain (C<sub>8</sub> and C<sub>18</sub>).

### 1.3 Materials Studied in the Present Work

In this dissertation, mesoporous silica materials were surface modified with different alkyl silylating agents to prepare the stationary phases with different surface coverages. The attachment of these alkyl chains was performed using direct attachment, surface polymerization and supercritical fluid methods. The physical and chemical properties of mesoporous silica materials can be modified by the attachment of organic components either on the outer silica surface or in the interior of the channels. The molecular length of the silylating reagent is very crucial for the surface coverage with organic components. Because of steric hindrance, longer chains primarily bind to the outer surface and only few chains are attached within the mesopores, leaving a large fraction of non-reacted surface silanol groups. These residual silanol groups are weakly acidic, and cause peak tailing for basic solutes which reduces the resolution and column efficiency in chromatographic applications. Endcapping of these silanols, for instance, by hexamethyldisilazane (HMDS) overcomes this problem and provides a better performance during chromatographic separation.

In the present contribution, Prontosil MCM-41 silica spheres with trimodal pore size distribution were prepared by the pseudomorphic route using the spheres of Prontosil silica. Thus the transformation of Prontosil silica spheres results in the presence of primary and secondary mesopores along with the parental silica pores left in these materials as observed from the nitrogen sorption isotherms. *n*-Octadecylsilyl groups (C<sub>18</sub>)

were attached to this calcined MCM-41 silica material with *n*-octadecyltrimethoxysilane using direct grafting and surface polymerization methods. The preparation of MCM-41 silica materials with uniform mesopores was carried out by increasing the reaction time and changing the silica source to Kromasil. Since the alkyl modified MCM-41 silica spheres prepared after the surface polymerization method results in higher surface coverages as compared to the direct grafting method, a series of surface modified MCM-41 silica materials using mono- and trifunctional butyl (C<sub>4</sub>) and octylsilanes (C<sub>8</sub>) using surface polymerization method has been prepared. In the case of C<sub>8</sub> modified materials, the residual silanol groups were further endcapped with HMDS. The various samples, i.e., MCM-41 materials before and after surface modification, were comprehensively characterized by nitrogen sorption experiments, small angle X-ray diffraction (XRD), scanning electron microscopy (SEM), FTIR, solid-state <sup>13</sup>C and <sup>29</sup>Si NMR spectroscopy as well as HPLC. MCM-41 silica materials were also surface modified using supercritical carbon dioxide (sc-CO<sub>2</sub>) as reaction medium and the results are compared with other surface modified samples prepared in the traditional way.

SBA-15 silica materials were surface modified with C<sub>4</sub>, C<sub>8</sub> and C<sub>18</sub> alkyl chains using surface polymerization method using tri- and monofunctional silanes. In case of materials surface modified with C<sub>8</sub> and C<sub>18</sub> alkyl chains, subsequent endcapping of remaining silanols was carried out using HMDS. SBA-15 silica materials before and after surface modification, were also comprehensively characterized by the techniques mentioned above and their chromatographic performance was also tested.

## **Chapter 2**

### **Characterization Techniques**

Inorganic oxides with covalently bound organic groups are used in a variety of technological applications. The determination of the physical and chemical properties of chemically modified surfaces is of considerable importance for an improved understanding of interfacial phenomena in various fields, such as catalysis, electrochemistry, and chromatography, etc. Alkyl bonded substrates prepared by the reaction of silanes with porous silica are widely used in liquid chromatography for the separation of polar and nonpolar analytes. Such bonded phase layers have unique properties that differ from the solid and liquid states of matter. By nature of the covalent bond, the degrees of freedom of the attached chains are reduced, and chain motion is intermediate to that of the corresponding alkane melts liquids and crystalline solids. An understanding of the physical nature of the bonded phase is a requisite for a complete description of the analyte retention mechanisms. Properties such as surface coverage or ligand density of chemically bonded stationary phases are routinely calculated from sorbent bulk properties (e.g., substrate surface area and percentage of carbon), but these measurements do not provide any insight into the phase structure at the molecular level. In the past, a variety of techniques were employed to probe the inorganic oxide substrates and their alkyl bound structures.

#### **2.1 Nitrogen Sorption Studies**

Nitrogen sorption analysis is probably the most important characterization method in this work. This analysis allows the determination of the specific surface area, the pore volume and the pore size distribution. With a careful and appropriate interpretation, nitrogen sorption analysis is one of the most powerful tools for the determination of porosity in solid materials and, therefore, also one of the most common techniques used.

The data evaluation, however, relies on models of the adsorption process in order to estimate material properties [67]. Nevertheless, they have to be handled with care with respect to accuracy, reliability and characterization capability. Here, we will discuss the strength and weaknesses of the most commonly used methods to evaluate porosity.

### 2.1.1 Classification of Isotherms

In gas adsorption techniques, the physisorption of a gas molecule (adsorptive) to a solid material (adsorbent) is evaluated. The amount of gas adsorbed to the material as a function of relative pressure is measured at a constant temperature, and is therefore called isotherm. The shape of the isotherm contains information about interactions between adsorbent and adsorptive.

According to the IUPAC classification system, adsorption isotherms are classified into six groups as shown in Figure 2.1 [4]. Type I is obtained when adsorption is limited to only a few molecular layers. Type II shows the isotherm for nonporous or macroporous materials with unrestricted monolayer-multilayer adsorption. The inflection point B indicates the change of monolayer coverage to multilayer coverage. The convex shape of type III implies a relatively weak interaction between adsorbent and adsorbate (as between some polymers and nitrogen). This type is not very common. Type IV isotherms are typical for mesoporous materials. The hysteresis loop is due to pore condensation. The lower part of this isotherm shows the same behavior as type II. Type V is a combination of type IV and type III, and type VI is a special case that represents step-by-step adsorption of multilayers.



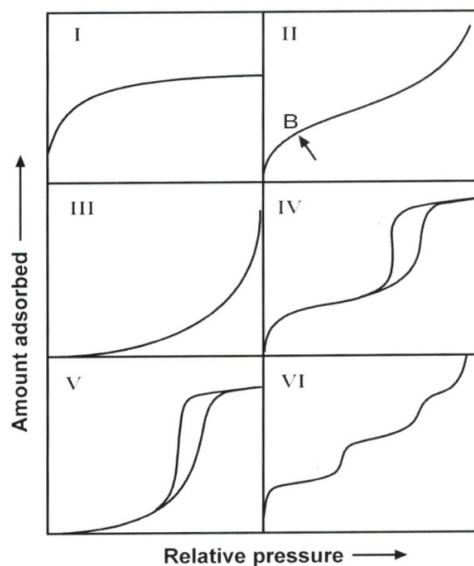


Figure 2.1: IUPAC classification of sorption isotherms [4].

### 2.1.2 Hysteresis Loops

The phenomenon of hysteresis was examined in several studies [68-70]. During the adsorption analysis the pore system of the sample is gradually filled with the analysis gas. For mesoporous materials, at first a monolayer and then multilayers of adsorbed gas molecules are formed. At a critical value of the relative pressure  $p/p_0$  a meniscus forms, resulting in a capillary condensation of the adsorptive. Usually the capillary desorption does not occur at the same relative pressure as the capillary condensation. The hysteresis can be the result of two contributions, thermodynamic and network effects, and is generally observed for mesoporous materials with pore diameters exceeding 5.0 nm [67]. For example, this occurs when larger pores have access to the gas phase only through narrow pores. Then, the larger pores remain filled with the condensed adsorptive until the adsorptive from connecting smaller pores is evaporated.

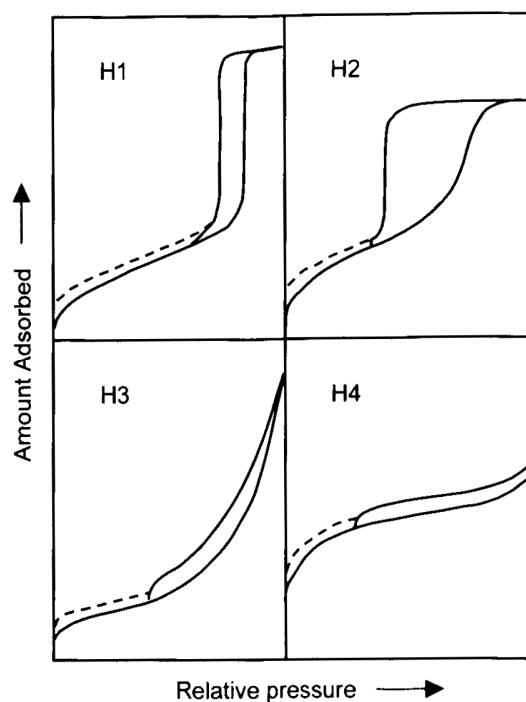


Figure 2.2: IUPAC classification of hysteresis loops in sorption isotherms [4].

The IUPAC also recommended that hysteresis loops should be classified as shown in Figure 2.2 [4]. According to this classification system, type H1 hysteresis is symmetrical with nearly parallel adsorption and desorption branches and often found in cylindrical pore systems in materials like MCM-41, MCM-48 or SBA-15. For many porous inorganic oxides, the adsorption isotherm contains a hysteresis of triangular shape with a steep desorption branch, which is defined as type H2. It is generally believed that the shape of the adsorption branch of the hysteresis loop is related to the absence or presence of pore network connectivity in the mesoporous materials. The type H1 hysteresis loop is usually assigned to a mesoporous materials made up of unconnected pores, whereas the type H2 hysteresis loop is expected for mesoporous materials with a connected pore structure [71]. Isotherms with type H3 loops do not level off close to the saturation pressure, which is often indicative of loose aggregates of plate-like particles. The type H4 hysteresis loops consist of nearly parallel adsorption and desorption branches. They are observed for materials with narrow slit-like pores.

### 2.1.3 BET Surface Area

The BET method is widely used in surface science for the calculation of surface areas of solids by physical adsorption of gas molecules. The BET theory is an extension of the

Langmuir theory for monolayer molecular adsorption, and is applicable to multilayer adsorption with the following assumptions: (a) gas molecules physically adsorb on a solid in layers infinitely; (b) there is no interaction within the adsorption layer and (c) the Langmuir theory can be applied to each layer. The resulting BET equation [72] is expressed by:

$$\frac{p}{V_a(p-p_0)} = \frac{(C-1)}{V_m C} \frac{p}{p_0} + \frac{1}{V_m C} \quad (2.1)$$

where  $p$  and  $p_0$  are the equilibrium and the saturation pressure of adsorbates at the temperature of adsorption,  $V_a$ , the volume of gas adsorbed at pressure  $p$  and  $V_m$  is the volume of gas required to form a monolayer.  $C$ , the BET constant is related to the energy of adsorption of the first layer.

Equation 2.1 is an adsorption isotherm and can be plotted as a straight line with  $p/[V_a(p/p_0)]$  on the y-axis and  $p/p_0$  on the x-axis. This plot is called a BET plot. The linear relationship of this equation is maintained only in the range of  $0.05 < p/p_0 < 0.35$ . The value of the slope  $A$  and the y-intercept  $I$  of the line are used to calculate the monolayer adsorbed gas quantity  $V_m$  and the BET constant  $C$ .

The BET surface area,  $S_{BET}$ , is evaluated by the following equation:

$$S_{BET} = V_m N s \quad (2.2)$$

where  $N$ , Avogadro's number; and  $s$ , the adsorption cross section.

In this study, the surface area measurements are based on the BET method on the basis of adsorption data in the range of relative pressures from  $p/p_0 = 0.05$  to  $0.3$  for the normal silica gels, from  $p/p_0 = 0.05$  to  $0.2$  for MCM-41 silica materials [73], and from  $p/p_0 = 0.05$  to  $0.3$  for SBA-15 silica materials [74]. The BET surface areas were calculated assuming a cross-sectional area for nitrogen  $a(N_2) = 13.5 \text{ \AA}^2$  [75].

#### 2.1.4 Pore Volume

The calculation of the pore volume is in accordance with the Gurvitsch rule [76]. The amount adsorbed at a relative pressure close to 0.99 represents complete filling of all pores with liquid adsorbate, provided that the isotherm shows a course parallel to the relative pressure axis [70]. Then  $V_{tp}$  is calculated as

$$V_{tp} = X_a V \quad (2.3)$$

where  $X_a$  is the amount of adsorbed gas, and  $V$  is the molar volume of adsorbent gas at the adsorption temperature. The rule implies that  $V_{lp}$  is independent of the type of adsorptive, and a close agreement was found in practice in the case of different types of adsorbents [70].

### 2.1.5 Pore Size and Pore Size Distribution (PSD)

Several geometrical and classical methods have been applied for determination of the mesopore diameter ( $D_{\text{pore}}$ ) of MCM-41 and SBA-15 silica materials. For cylindrical mesopores of uniform shape and width, pore condensation can be described on the basis of the Kelvin equation, i.e., the shift of the gas-liquid phase transition of a confined fluid with respect to the bulk material is expressed by macroscopic quantities like the surface tension  $\gamma$  of the bulk fluid, the densities of the coexistent liquid  $\rho^l$  and gas  $\rho^g$  ( $\Delta\rho = \rho^l - \rho^g$ ) and the contact angle  $\theta$  of the liquid meniscus against the pore wall. For cylindrical pores the modified Kelvin equation [70] is given by

$$\ln \frac{p}{p_0} = \frac{-2\gamma}{RT\Delta\rho(r_p - t_c)} \cos \theta \quad (2.4)$$

where  $R$  is the universal gas constant,  $r_p$  is the pore radius and  $t_c$  is the thickness of an adsorbed multilayer film, which is formed prior to pore condensation. The occurrence of pore condensation is expected as long as the contact angle is below  $90^\circ$ . A contact angle of  $0^\circ$  is usually assumed in case of nitrogen adsorption at 77 K.

The Kelvin equation provides a relationship between the pore diameter and the pore condensation pressure, and predicts that pore condensation shifts to a higher relative pressure with increasing pore diameter and temperature. The modified Kelvin equation (Equation 2.4) serves as basis for many techniques applied for mesopore analysis, including the widely used Barrett-Joyner-Halenda method (BJH).

The pore size distribution (PSD) of porous materials is another important characteristic that has received significant attention. Accordingly, several studies have been conducted to determine the PSD of MCM-41 and SBA-15 silica materials using the adsorption of nitrogen. The BJH method for calculating PSD is based on a model of the adsorbent as a collection of cylindrical pores [77]. The theory accounts for capillary condensation in the pores using the classical Kelvin equation, which in turn assumes a hemispherical liquid-vapor meniscus and a well-defined surface tension. The BJH theory also incorporates thinning of the adsorbed layer through the use of a reference isotherm;

the Kelvin equation is only applied to the “core” fluid. PSD were calculated from adsorption/desorption branches of the nitrogen isotherms with the corrected form of the Kelvin equation for capillary condensation in cylindrical pores [78]:

$$r(p/p_0) = 0.416 [\log(p_0/p)]^{-1} + t(p/p_0) + 0.3 \quad (2.5)$$

where  $r$ , the pore radius and  $t(p/p_0)$ , the statistical film thickness curve (t-curve) as a function of the relative pressure.

It is found that the classical method of BJH cannot describe the sorption and phase behaviour of fluids in narrow mesopores (for widths  $< 100 \text{ \AA}$ ) correctly, leading to an underestimation of the pore diameters [79]. Rather, a density functional theory (DFT) [69] based analysis appears as the most accurate method for pore size and pore size distribution determination. This approach takes into account the details of the fluid-fluid interactions and the adsorption potential, which depends on the strength of fluid wall interactions and the pore geometry. The DFT approach is based on a combination of statistical mechanical calculations and experimental observations for macroporous silicas, zeolites, and MCM-41 as well as SBA-15 silica materials. The pore-filling pressures were determined as a function of the pore size from sorption isotherms on MCM-41 and SBA-15 silica materials. The variation of the pore fluid density with pressure and pore size has been accounted for by DFT calculations.

## 2.2 Small Angle X-Ray Diffraction (XRD)

Periodic mesoporous silica materials exhibit a periodic arrangement of mesopores while the silica matrix is amorphous at the atomic scale. The periodic arrangement of the mesopores produces characteristic Bragg reflexes in the small-angle diffraction, as shown in the XRD pattern in Figure 2.3 (left). The reason for the appearance of Bragg-reflexes is that the mesopores in the materials are well ordered. The peaks are attributed to the two dimensional hexagonal unit cell with the lattice constant  $a_0$ . For this reason a crystallographic formulation can be used for the small angle X-ray scattering of these materials. Specifically, MCM-41 and SBA-15 materials comprise a two dimensional hexagonal pore lattice (space group P6mm) as indicated in Figure 2.3 (right).

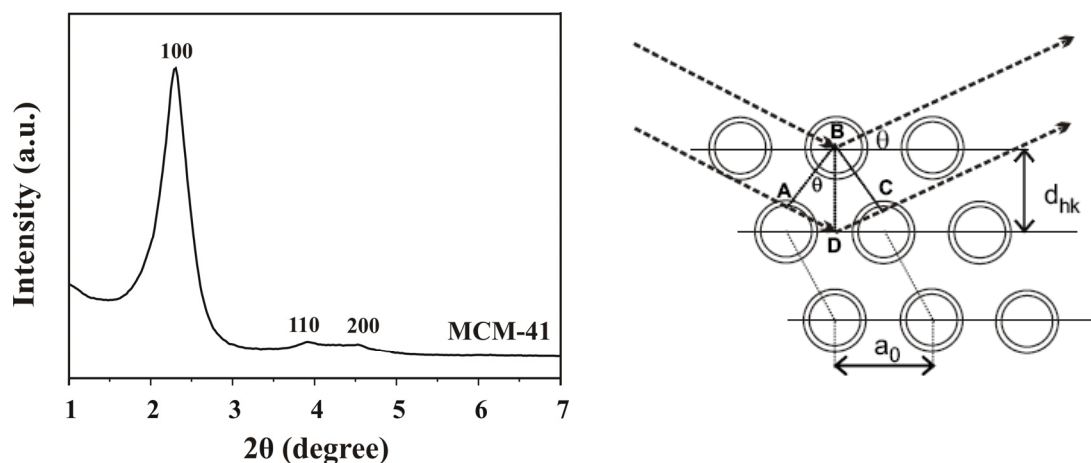


Figure 2.3: XRD pattern of MCM-41 (left) and derivation of Bragg's law for X-ray diffraction in hexagonal ordered materials (right).

Figure 2.3 (right) illustrates the principle of diffraction of monochromatic X-rays of wavelength  $\lambda$  by the lattice planes of a 2D hexagonal crystal lattice. If the lattice planes are considered as semipermeable mirrors, a portion of incident X-rays is reflected and the rest is transmitted. A Bragg-reflex originates if X-rays reflected at numerous parallel lattice planes interfere constructively. This happens when the path lengths of the X-rays reflected at two neighboring lattice planes differ by an integer multiple of  $\lambda$ , i.e.,  $ADC = n \cdot \lambda$ . This is described by the Bragg equation. For our 2D ordered pore system where the lattice planes can be labeled with Miller indices  $hk$  one has

$$n \cdot \lambda = 2 \cdot d_{hk} \cdot \sin(\theta_{hk}). \quad (2.6)$$

The Bragg equation is the basic equation of diffractometry. It ties together the wavelength  $\lambda$ , the lattice plane spacing  $d_{hk}$  and the glancing angle  $\theta_{hk}$  between the incident wave and the lattice plane  $d_{hk}$ ;  $n$  is an integer and its physical interpretation is the interference order. Thus, at a given wavelength first-order reflection of X-rays by lattice planes occurs only at a certain angle  $\theta_{hk}$ . If the wavelength is known, the interplanar spacing  $d_{hk}$  can be calculated by measuring the glancing angle  $\theta_{hk}$ . For its determination in this work diffraction in the small angle region is applied. In small angle scattering the scattering angle  $2\theta$  lies in range of  $0.05^\circ < 2\theta < 5^\circ$ .

In MCM-41 and SBA-15 materials, the individual crystal domains contain approximately 100 and 1000 pores, respectively. The Bragg-reflexes are determined by the type of crystalline system and the *lattice parameter*  $a_0$  of the unit cell. For a 2D

hexagonal lattice, the lattice parameter is obtained by the following equation from the interplanar spacing

$$a_0 = \frac{2}{\sqrt{3}} \cdot d_{hk} \cdot \sqrt{h^2 + hk + k^2} \quad (2.7)$$

Information about the pore diameter  $D$  and the nature of the pore walls can be determined by XRD structure modeling. This can be achieved by applying the so called-continuous density function (CDF) technique [80] in combination with the derivative difference minimization (DDM) method [81]. Alternatively, the intensities of the Bragg-reflections may be fitted by modeling the form factor of the cylindrical pores in an appropriate way [82-83]. Both of these techniques yield quantitative information about the pore diameter  $D$  and the wall thickness  $w$  along the pore center-to-center line, which are related to the lattice parameter  $a_0$  by  $a_0 = D + w$ .

### 2.3 Scanning Electron Microscopy (SEM)

SEM measurements provide the particle morphology of the material under investigation, their diameter and also the particle size distribution. A scanning electron microscope is a high magnification microscope, which uses a focused scanned electron beam to produce high-resolution images of a specimen. The X-rays emitted are characteristic for the elements in the top few  $\mu\text{m}$  of the sample. After the primary electron beam interacts with the sample, ionized atoms can relax by electron shell-to-shell transitions, which leads to either X-ray emission or Auger electron ejection. Images obtained by SEM provide information on the physical properties of mesoporous silica materials including particle size, shape, surface morphology, and adherence to surfaces.

The types of signals made by an SEM can include secondary electrons, back scattered electrons, characteristic X-rays and light (cathodoluminescence). These signals come from the beam of electrons striking the surface of the specimen and interacting with the sample at or near its surface. In its primary detection mode, secondary electron imaging, the SEM can produce very high-resolution images of a sample surface, revealing details about 1 to 5 nm in size. Due to the way these images are created, SEM micrographs have a very large depth of focus yielding a characteristic three-dimensional appearance useful for understanding the surface structure of a sample. Characteristic X-rays are the second most common imaging mode for an SEM. X-rays are emitted when the electron beam removes an inner shell electron from the sample, causing a higher

energy electron to fill the shell and give off energy. These characteristic X-rays are used to identify the elemental composition of the sample. Back-scattered electrons (BSE) that come from the sample may also be used to form an image. BSE images are often used in analytical SEM along with the spectra made from the characteristic X-rays as clues to the elemental composition of the sample.

For conventional imaging, SEM requires that specimens be conductive for the electron beam to scan the surface and that the electrons have a path to ground. All samples are generally mounted on some sort of holder. Nonconductive solid specimens are coated with a layer of conductive material. An ultrathin coating of electrically-conducting material such as, gold, gold/palladium alloy, platinum, tungsten or graphite is deposited on the sample either by low vacuum sputter coating or by high vacuum evaporation. This is done to prevent the accumulation of static electric charge on the specimen during electron irradiation. Another reason for coating, even when there is more than enough conductivity, is to improve contrast and resolution, a situation most common when using samples with low atomic number.

## 2.4 Solid-State NMR Spectroscopy

### 2.4.1 Theory

NMR spectroscopy is a widely employed physical method, since it provides a powerful tool to investigate the structure and the dynamics of chemical systems. While molecular substances in solution give spectra characterized by sharp peaks, the spectra in the solid state, by contrast, are broad and featureless owing to various internal and external interactions which are described below in detail.

The nuclei with a spin possess a magnetic moment  $\vec{\mu}$ , which interacts with its surroundings. Generally, these interactions can be divided into two classes that are described by an external and an internal Hamiltonian, [84-85] i.e.,

$$\hat{H} = \hat{H}_{ext} + \hat{H}_{int} \quad (2.8)$$

The first term on the right hand side includes the interactions of a spin system with the external static magnetic field  $\vec{B}_0$  (Zeeman interaction,  $\hat{H}_z$ ) and the pulsed radio-frequency (r.f.) fields ( $\hat{H}_{rf}$ ). The second term includes the interactions of a spin system with internal local fields originating from the chemical shift interaction ( $\hat{H}_{CS}$ ), direct



dipole-dipole or simply dipolar interaction (homo-nuclear,  $\hat{H}_{IS}$  and hetero-nuclear,  $\hat{H}_{II}$ ), quadrupole interaction ( $\hat{H}_Q$ ), and indirect J-coupling ( $\hat{H}_J$ ). Thus, Equation 2.8 can also be expressed as [84,86],

$$\hat{H} = \hat{H}_Z + \hat{H}_{rf} + \hat{H}_{CS} + \hat{H}_{II} + \hat{H}_{IS} + \hat{H}_Q + \hat{H}_J \quad (2.9)$$

The external interactions have an identical influence on the whole spin system and contain no structural and dynamic information about the nucleus of interest which are conversely included in the internal interactions. All internal Hamiltonian contributions reflect tensoral interactions, which depend on the orientation of the interaction tensor with respect to the external magnetic field direction. In comparison with the external static field, the internal or local interactions are normally small. Therefore they typically act only as a first-order perturbation in the high field (secular) limit and produce small shifts and splittings of the Zeeman energy levels which depend on the nature and extent of the couplings and on the number of interacting spins.

### The Zeeman Interaction

The interaction of the magnetic moment,  $\vec{\mu}$ , of a nucleus with the static external magnetic field,  $\vec{B}_0$  is called Zeeman interaction and is written as

$$\hat{H}_Z = -\gamma\hbar B_0 \hat{I}_z \quad (2.10)$$

where  $\gamma$  is the gyromagnetic ratio of the nuclear spin  $\hat{I}$ ,  $\hbar$  is the Planck's constant  $h$  divided by  $2\pi$  and  $\vec{B}_0$ , the external magnetic field along the z-direction of the laboratory frame.

Assuming that the Zeeman interaction is the only contribution in the spin Hamiltonian, the magnetic moment of the nucleus experiences a precession around the direction of the magnetic field with the well-known Larmor frequency  $\omega_0$ , which is given by

$$\omega_0 = -\gamma B_0 \quad (2.11)$$

For an allowed transition between two states, characterized by the magnetic spin quantum number  $m$  and  $m'$  ( $m' = m \pm 1$ ), the energy difference is given by

$$\Delta E = \pm\gamma\hbar B_0 \quad (2.12)$$

Equation 2.12 shows that the energy difference  $\Delta E$  is directly proportional to the magnitude of the magnetic field. The energy difference between the two states alters along with the variation of the external magnetic field strength. Once the energy of the photon generated by the radio-frequency irradiation matches the energy difference between the two spin states, absorption of energy by the sample occurs.

When a group of spins is exposed to a magnetic field, the number of spins in the lower energy level,  $N^+$  and the number in the upper energy level,  $N^-$ , follow the Boltzmann statistics, as given by

$$\frac{N^-}{N^+} = e^{-\Delta E/kT} \quad (2.13)$$

where  $k$  is the Boltzmann's constant,  $1.3805 \times 10^{-23}$  J/Kelvin, and  $T$  is the temperature in Kelvin. At room temperature ( $N^-/N^+ = 0.99998$ ), the population difference between the two states is very small. Moreover, the ratio  $N^-/N^+$  decreases with decreasing temperature.

The signal in NMR spectroscopy results from the difference between the energy absorbed by the spins which make a transition from the lower to the higher energy state, and the energy emitted by the spins which simultaneously make a transition from the higher to the lower energy state. The signal is thus proportional to the population difference between the states, as described by Equation 2.13.

### Interaction with Radio-Frequency Fields

In NMR experiments, an radio-frequency (r.f.) field is created by the probe coil passing an alternating current at the Larmor frequency, and employed to manipulate the effective Hamiltonian of the spin system. The amplitude of the oscillating r.f. field is substantially smaller than that of the static magnetic field, so  $\hat{H}_{rf}$  acts as a perturbation on the spin system, which does not change the energy levels but only induces transitions between them. If an oscillating r.f. magnetic field,  $\vec{B}_1 = (B_1, 0, 0)$ , is applied along the x-axis perpendicular to the static magnetic field in the laboratory frame, the interaction of a nuclear spin with this field can be expressed by the Hamiltonian:

$$\hat{H}_{rf} = -2\gamma\hbar\vec{B}_1 \cos(\omega t + \varphi)\hat{I} = -2\gamma\hbar B_1 \cos(\omega t + \varphi)\hat{I}_x \quad (2.14)$$

where  $\omega$  is the carrier frequency and  $\varphi$  is the phase. When the r.f. field oscillates close to the resonance frequency  $\omega_0$ , which corresponds to the Zeeman energy splitting, a transition between the spin states will occur.

The introduction of the r.f. pulse complicates the motion of the spin in the magnetic field. On one hand, the spin precesses around the  $B_0$  field with the Larmor frequency, while on the other hand, it nutates due to the action of the r.f. field. In order to facilitate the interpretations, it is useful to introduce the “rotating frame”, which rotates around the z-axis of the applied static magnetic field with frequency  $\omega$ . The effective Hamiltonian in the rotating frame becomes

$$\hat{H}_{\text{eff}} = -\gamma\hbar(\vec{B}_0 - \vec{B}_1)\hat{I}_z + \gamma\hbar\vec{B}_1\hat{I}_x = (\omega_0 - \omega)\hbar\hat{I}_z - \omega_1\hbar\hat{I}_x \quad (2.15)$$

where  $(\omega_0 - \omega)$  is the so-called resonance offset. When  $\omega_0 = \omega$ , the irradiation is said to be on-resonance.

### Chemical Shift Interaction

The chemical shift, or shielding, interaction originates from the effect of  $B_0$  on the electrons around a nucleus. In a magnetic field, the electrons circulate about the direction of the external magnetic field  $B_0$ . This circulation induces additional small magnetic fields, which may be added to or subtracted from the external magnetic field felt by the nucleus. Therefore, the effective magnetic field experienced by the nucleus is altered, as well as its resonance frequency. The chemical shift interaction is an anisotropic interaction, due to the fact that the electronic distribution in the molecules can be thought of as an ellipsoid. The degree to which the electron density affects the resonance frequency of a nucleus depends on the orientation of the electron cloud (and hence the orientation of the molecule) with respect to  $B_0$ . The chemical shift Hamiltonian is expressed by [87]

$$\hat{H}_{CS} = [\sigma_{\text{iso}} + \frac{1}{2}\delta_{CS}\{3\cos^2\theta - 1 + \eta_{CS}\sin^2\theta\cos(2\phi)\}]h\gamma B_0\hat{I}_z \quad (2.16)$$

Here the angles  $\theta$  and  $\phi$  describe the orientation of the chemical shift tensor with respect to  $B_0$ , while  $\sigma_{\text{iso}}$  is the isotropic chemical shift, typically on the order of  $10^{-6}$  in ppm.

In a solid sample, molecular motion may narrow the chemical shift tensor by partial averaging, and the resulting powder pattern contains motional and orientation information

of the molecules. In solution, the rapid, isotropic motion of the molecule averages the shielding tensor to its isotropic value  $\sigma_{\text{iso}}$ .

Since the chemical shift is a direct consequence of the electronic structure, the chemical shift tensor can provide information about the structure of the molecules and can be used to verify calculations of the electronic structure of molecules. The anisotropic chemical shift interaction contributes significantly to the line broadening of a solid state NMR spectrum, which often obscures the structural information available from the isotropic chemical shifts. This line broadening of the resonances in solid state can be eliminated by spinning the sample at high speed and at a certain angle, the so-called magic angle spinning (see below).

### Dipolar Interactions

Dipolar interactions result from the interaction of the nuclear spin under study with the dipole moments of neighboring nuclear spins. This is a direct through space interaction, which depends on the magnetogyric ratio  $\gamma$  of each nucleus as well as the distance  $r_{ij}$  between two nuclei. The homonuclear dipolar interaction is the interaction between the magnetic dipole moments of like nuclei, while the heteronuclear interaction is the interaction between the magnetic dipole moments of unlike nuclei. The Hamiltonian of the homonuclear interaction describes the dipolar coupling between the nuclei  $i$  and  $j$  having the same nuclear spins  $I$  [88].

$$\hat{H}_{II} = \frac{1}{2} \gamma_I^2 \hbar^2 r_{ij}^{-3} (\hat{I}_i \hat{I}_j - 3 \hat{I}_{iz} \hat{I}_{jz}) (3 \cos^2 \theta_{ij} - 1) \quad (2.17)$$

where  $\gamma_I$  is nuclear magnetogyric ratios of the interacting nuclei  $i$  and  $j$ . Here,  $r_{ij}$  is the internuclear distance, and  $\theta_{ij}$  is the angle between the vectors of  $r_{ij}$  and the external magnetic field  $B_0$ .

In the case of the heteronuclear dipolar interaction between the nuclei of spins  $I$  and  $S$ , the Hamiltonian is given by [88]:

$$\hat{H}_{IS} = \frac{1}{2} \gamma_I \gamma_S \hbar^2 r_{is}^{-3} \hat{I}_z \hat{I}_{Sz} (1 - 3 \cos^2 \theta_{IS}) \quad (2.18)$$

where  $\gamma_I$ ,  $\gamma_S$  are the magnetogyric ratios of nuclei with spins  $I$  and  $S$ ,  $r_{is}$  is the internuclear distance, and  $\theta_{IS}$  is the angle between the vectors of  $r_{ij}$  and the external magnetic field  $B_0$ . The effects of dipolar interactions can be eliminated by spin decoupling (see below).

## Quadrupolar Interactions

In addition to the above-mentioned interactions, the quadrupolar interaction further causes a line-broadening of the NMR signals of nuclei having spins  $I > 1/2$  (e.g.  $^2\text{H}$ ,  $^{11}\text{B}$ , and  $^{27}\text{Al}$  nuclei). It is defined as the interaction of the electric quadrupole moment  $eQ$  of the nucleus with the electric field gradient (EFG) at the site of the nucleus. The EFG is a traceless tensor and it can be expressed by [88]:

$$V_{ij} = \partial^2 V / \partial x_i \partial x_j \quad (2.19)$$

where  $V$  is the electric potential and  $x_i, x_j$  are Cartesian coordinates. In the principle axis system of  $V_{ij}$ , the Hamiltonian of the quadrupolar interaction of nuclei with spin  $I > 1/2$  is

$$\hat{H}_Q = \{e^2 q Q / 4I(2I-1)\} [3I_z^2 - I^2 + \eta(I_x^2 - I_y^2)] \quad (2.20)$$

with  $V_{zz} \geq V_{yy} \geq V_{xx}$  and the z-component  $V_{zz} = eq$  of the EFG. The characteristic parameters of quadrupole nuclei, such as the asymmetry parameter,  $\eta$ , and quadrupole coupling constant,  $C_{\text{QCC}}$ , are defined by [88-89]:

$$\eta = (V_{xx} - V_{yy}) / V_{zz} \quad (2.21)$$

and

$$C_{\text{QCC}} = e^2 q Q / h \quad (2.22)$$

Generally, the quadrupolar interaction is weaker than the Zeeman interaction ( $\hat{H}_Q \ll \hat{H}_Z$ ) and can be considered as a perturbation. In this case, the frequency function of the  $m-1 \rightarrow m$  transition is described by a first- and second-order frequency function [149]:

$$\nu_m = \nu_0 + \nu_m^{(1)} + \nu_m^{(2)} \quad (2.23)$$

In the case of central transition ( $m = -1/2$  to  $+1/2$ ), the second-order frequency function is given by [149]:

$$\nu_{1/2} = -(\nu_Q^2 / 16\nu_L) \{I(I+1) - 3/4\} (1 - \cos^2 \theta) (9 \cos^2 \theta - 1) \quad (2.24)$$

where  $\theta$  is the angle between z-axis in the principle system and the external magnetic field  $B_0$ . The quadrupole frequency is given by [88]:

$$\nu_Q = 3e^2 q Q / 2hI(2I-1) \quad (2.25)$$

## Magic Angle Spinning (MAS)

Magic angle spinning (MAS) is a high-resolution solid-state NMR technique, which involves the rotation of solid samples at spinning rates of several kHz around a fixed axis at an angle of  $54.74^\circ$  with respect to the direction of the external magnetic field. Figure 2.4 indicates the schematic representation of MAS. The angle  $\theta_m = 54.74^\circ$  is obtained from the geometric term  $(3\cos^2\theta_m - 1)$ , which becomes zero leading to a cancellation of the orientation dependent spin interactions. By applying this technique, most of the interactions (i.e., chemical shift, dipolar and first-order quadrupolar interactions) in solid samples can be removed or at least partially averaged, and the MAS NMR signal consists of a narrow central line at the isotropic chemical shift  $\nu_{\text{iso}}$ , and spinning sidebands at [90-91]:

$$\nu_k = \nu_{\text{iso}} + k\nu_{\text{rot}} \quad (2.26)$$

where  $k = \pm 1, \pm 2, \dots$  denotes the order of spinning sidebands, and  $\nu_{\text{rot}}$  is the sample spinning rate. In the case of MAS at low spinning rates, the NMR spectrum consists of many spinning sidebands. The number of spinning sidebands can be reduced by using high spinning rates.

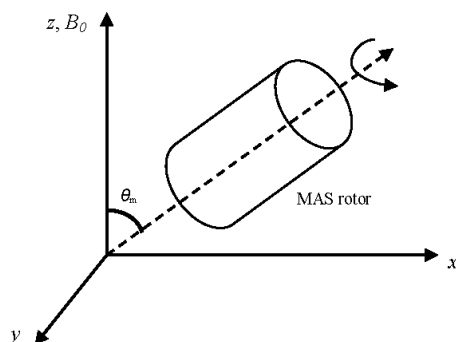


Figure 2.4: Schematic representation of MAS.

MAS can either be used on its own, or be combined with other line-narrowing techniques. For instance, it can be used in conjunction with multiple pulse sequences to obtain high resolution NMR spectra, especially for hydrogen and fluorine nuclei in solids, or with cross-polarization and high power heteronuclear decoupling methods to get high resolution spectra for  $^{13}\text{C}$ ,  $^{29}\text{Si}$  and other low abundant nuclei. In case of spin-1/2 nuclei,

the line broadening mainly arises from chemical shift interaction and dipolar interaction. The effect of MAS on each of them is discussed in the following sections.

### Chemical Shift and Magic Angle Spinning

Under fast spinning conditions, the molecules rapidly experience all possible orientations, and hence, even a strongly asymmetric electron distribution will appear spherical when viewed on the NMR timescale. The chemical shift Hamiltonian can be divided into an isotropic term and an anisotropic term. For the axially symmetric ellipsoid case, in which  $\sigma_{xx} = \sigma_{yy}$ , the chemical shift Hamiltonian can be written as

$$\hat{H}_{CS} = \hbar\omega_0\hat{I}_z\sigma_{iso} + \frac{1}{2}(\sigma_z - \sigma_{iso})(3\cos^2\theta - 1)\hbar\omega_0\hat{I}_z \quad (2.27)$$

When a solid sample is rotated with angular velocity  $\omega_r$  about an axis inclined at angle  $\theta_m$  respect to  $B_0$  and at angle  $\beta$  to the principal axes of the  $\tilde{\sigma}$  tensor, the chemical shift Hamiltonian becomes time dependent and is expressed as

$$\hat{H}_{CS} = \hbar\omega_0\hat{I}_z\sigma_{iso} + \frac{1}{2}(\sigma_z - \sigma_{iso})\left[(3\cos^2\theta_m - 1)(3\cos^2\beta - 1) + \xi(t)\right]\hbar\omega_0\hat{I}_z \quad (2.28)$$

Where  $\xi(t)$  contains the functions of the Euler angles involved in the coordinate transformation.

The first term (isotropic part) in the right hand side of Equation (2.28), is invariant under motion; the first term between the square bracket accounts for the averaged anisotropy of the chemical shift tensor which depends on the angle between the spinner axis and the external magnetic field  $B_0$ . When the angle  $\theta_m$  is  $54.74^\circ$ , the value of the  $(3\cos^2\theta_m - 1)$  term in the chemical shift Hamiltonian is zero, the shift anisotropy is removed from the NMR spectrum. If the angle  $\theta_m$  deviates from the magic angle, a scaled anisotropy is observed. The second term in the square bracket gives rise to sidebands. When the spinning rate is not fast enough to exceed the width of the static line shape, the powder pattern breaks up into relatively narrow lines at the isotropic chemical shift (center band) and sidebands at multiples of  $\omega_r$  from the center band.

### High-Power Spin Decoupling

High-power decoupling is a simple technique which removes the effects of heteronuclear coupling. Consider the case of dipolar-coupled  $^1\text{H}$  and  $^{13}\text{C}$  spins, where the  $^{13}\text{C}$  spins are to be observed. The method (Figure. 2.5) consists of applying a continuous irradiation of

very high power (100–1000 watts) at the frequency of the proton resonance. The required pulse sequence for the  $^{13}\text{C}$  nuclei is then applied, and the  $^{13}\text{C}$  FID measured while continuing the  $^1\text{H}$  irradiation.

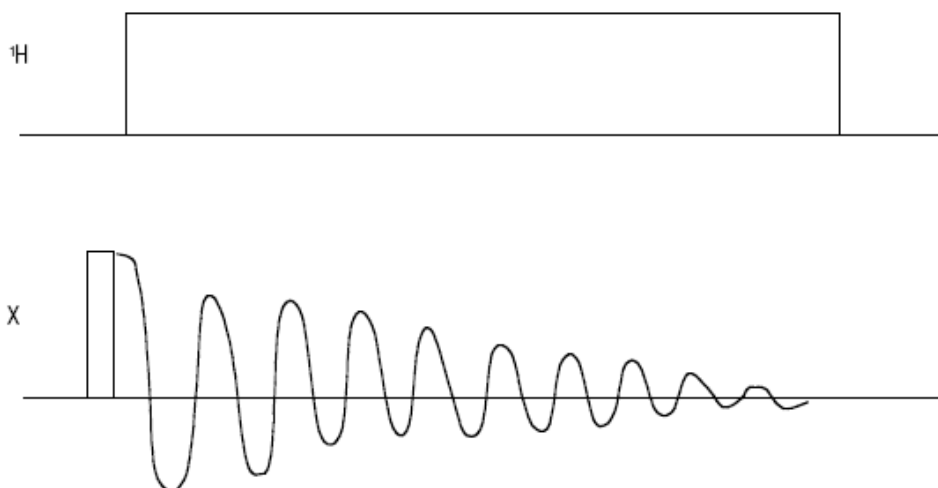


Figure 2.5: High-power decoupling. This removes the effects of  $^1\text{H}$  dipolar coupling from the NMR spectrum of X in this case; it can of course be applied to any abundant spin in place of  $^1\text{H}$  in the same manner. High-power irradiation is simply applied to the  $^1\text{H}$  spins during the acquisition of the X spin spectrum. Here a single pulse is used to generate the X transverse magnetization.

The effect of the close-to-resonance rf irradiation is to cause the  $^1\text{H}$  spins to undergo repeated transitions ( $\alpha \leftrightarrow \beta$ ) at a rate determined by the amplitude of the rf irradiation,  $\omega_1$ . The  $^{13}\text{C}$  spectrum will be affected by the time-averaged dipolar coupling only, providing the rate of transition  $\alpha \leftrightarrow \beta$  on the  $^1\text{H}$  spin is fast relative to the strength of the  $^1\text{H} - ^{13}\text{C}$  dipolar coupling. In turn, the time-averaged dipolar coupling is clearly zero.

### Single Pulse and Cross-polarization NMR Spectroscopy

Normally NMR spectra are obtained by single pulse (SP) experiments and the pulse sequence used for single pulse (SP) NMR experiments is shown in Figure 2.6 (left). However, the nuclei with small magnetogyric ratios and low natural abundance, such as  $^{13}\text{C}$  and  $^{29}\text{Si}$ , are often affected by low signal to noise (S/N) ratios. It is, therefore, necessary to apply double resonance techniques, such as cross polarization (CP) [84,92], as shown in Figure 2.6 (right). In this way, the signal to noise ratio (S/N) can be improved significantly. The CP technique involves the transfer of polarization from abundant nuclei (usually  $^1\text{H}$  nuclei) to a low abundant one such as  $^{13}\text{C}$ . The process of CP occurs through the transfer tendency of the magnetization from highly polarized nuclei to nuclei with



lower polarization when they are brought into contact. This is similar to heat flow from a hot object to a cold object when the two objects are in thermal contact. For homonuclear spins, the magnetization can be exchanged through mutual energy-conserving spin flips. For heteronuclear pairs, such as  $^{13}\text{C}$  and  $^1\text{H}$ , these spin flips are not energy-conserving at high fields. Therefore, the exchange of magnetization must be driven externally by the application of r.f. fields.

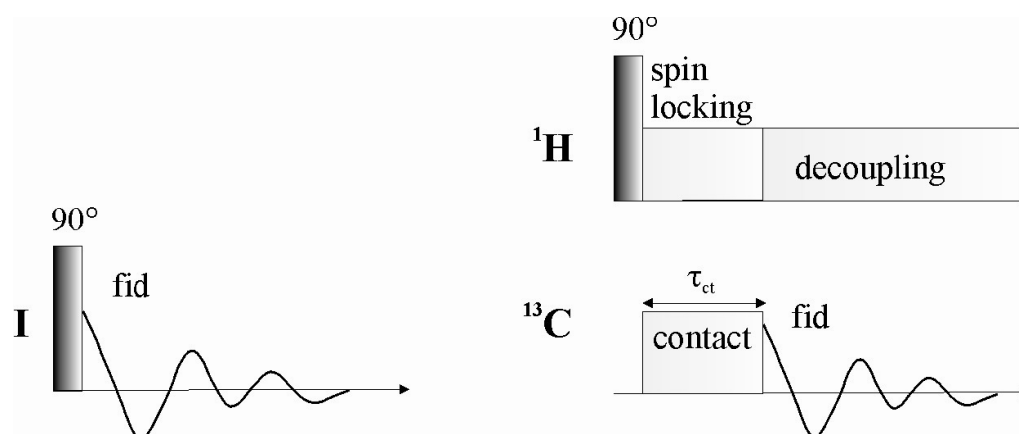


Figure 2.6: Pulse sequences for single pulse (left) and cross-polarization (right) NMR experiments.

Among the techniques for building a dipolar contact between two different spin systems  $I$  and  $S$ , the Hartmann-Hahn approach is particularly effective. This approach requires the simultaneous application of two continuous r.f. fields, one at the resonance frequency of the spin  $I$  and the other at the resonance frequency of the  $S$  spin. The effect of any r.f. field is to rotate the magnetization about the axis of the applied field. The rotation rate depends on the frequency and amplitude of the r.f. field. An r.f. field that oscillates at the spin  $I$  frequency, for instance 300 MHz, would not have any effect on  $S$  spins with a frequency of 75 MHz and vice versa. By applying two r.f. fields, one tuned to the spin  $I$  and the other to spin  $S$ , both  $I$  and  $S$  spins can be rotated independently around a particular axis at rates determined by the amplitudes of two applied fields. When the nutation frequencies of the  $I$  and  $S$  spins are equal, i.e., the Hartman-Hahn condition (i.e., Equation 2.29), given by [93] is satisfied, an energy-conserving dipolar contact between the two spin systems is created.

$$\gamma_I B_{1(I)} = \gamma_S B_{1(S)} \quad (2.29)$$

The maximum enhancement for a CP contact period is  $\gamma_I/\gamma_S$ . It is through this dipolar contact that the polarization is transferred between  $I$  and  $S$  spins.

Thus by employing the CP pulse sequence, the intensity of the signals of the less abundant nuclei can be enhanced and a better signal/noise ratio is obtained. The use of CP also shortens the acquisition time. In this way, excellent spectra of a variety of nuclei in the solid state have been obtained. A careful analysis of these spectra and of the chemical shifts allows distinguishing the different coordinations of an atom. This technique has been extensively employed to study alkyl modified MCM-41 and SBA-15 silica materials presented in this dissertation.

### 2.4.2 Organic-Inorganic Hybrid Silica Materials and Solid-State NMR Spectroscopy

Solid-state NMR spectroscopy has significantly advanced the understanding of stationary phase materials by providing complementary information on chemically modified surfaces. With a combination of MAS, CP, and high-power spin decoupling, solid state NMR has rapidly emerged as one of the most important tools in material science. Solid state NMR measurements of chromatographic materials are used to make structural studies of surface modified stationary phases, in particular for studying the alkyl chain mobility and conformational order of stationary phases.

In the early 1980s, Maciel and Sindorf pioneered the application of solid state NMR techniques in chromatographic stationary phase materials by examining silica surfaces with  $^{29}\text{Si}$  CP/MAS NMR spectroscopy [94]. Later, they explored the structure and mobility of attached monofunctional  $\text{C}_8$  and  $\text{C}_{18}$  ligands with  $^{13}\text{C}$  CP/MAS NMR spectroscopy. However, it has to be kept in mind that NMR spectra measured by CP/MAS are not quantitative since the efficiency of polarization transfer by CP is highly variable. The signal intensity of different nuclei can only be compared if the contact time is maximum and thus  $T_{\text{SiH}}$  (cross-relaxation constant) and  $T_{1\rho\text{H}}$  (proton spin-lattice realaxation time in the rotating frame) values are in the same order. However,  $^{29}\text{Si}$  and  $^{13}\text{C}$  NMR techniques provide detailed information about the different groups present in the substrate and chemically modified surfaces.

## $^{29}\text{Si}$ MAS NMR Spectroscopy

$^{29}\text{Si}$  NMR spectroscopy was employed for the determination of the surface species, the amount of alkyl chain attachment and the degree of cross linking of the attached alkylsilanes. Because of the chemical shift dispersion of about 130 ppm for silane and silica gel signals, structural elements can be assigned quite easily by recording  $^{29}\text{Si}$  NMR spectra. The different structural elements are illustrated in Figure 2.7.

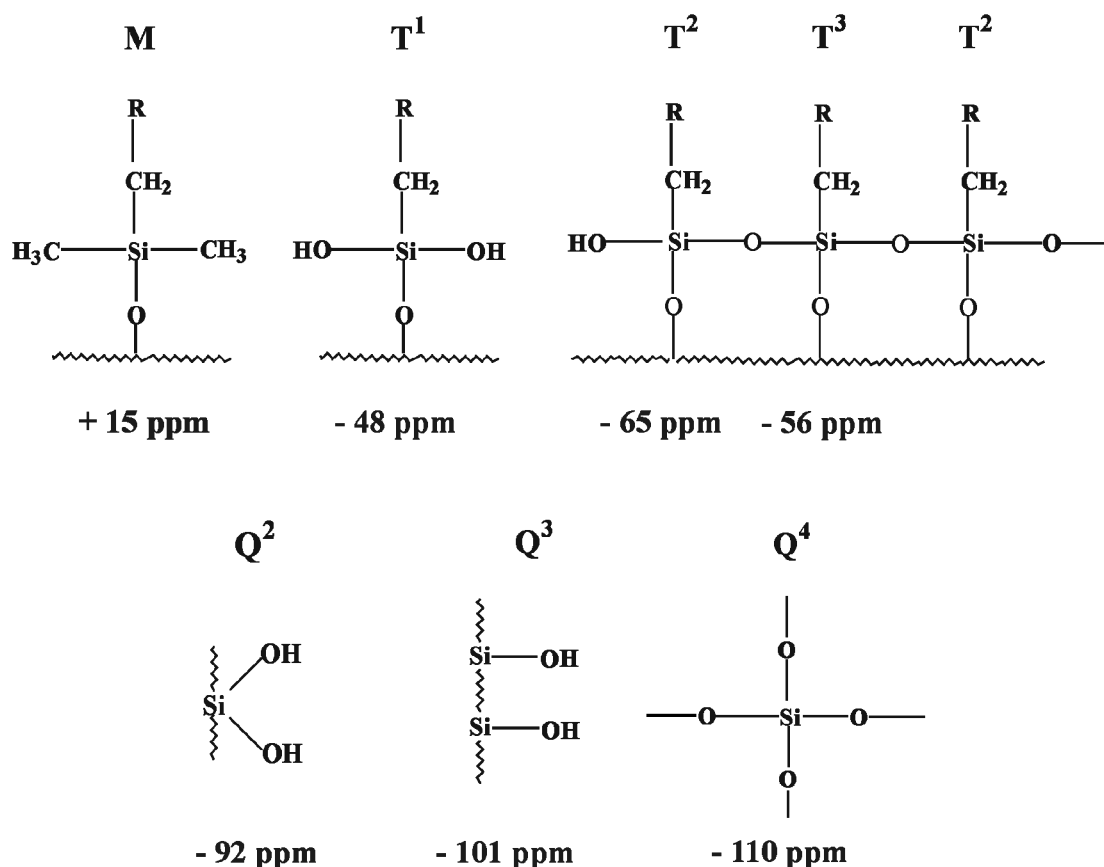


Figure 2.7: Different structural elements of the silicon species present in the alkyl modified silica systems.

The signals from the native silica are  $\text{Q}^2$ ,  $\text{Q}^3$ ,  $\text{Q}^4$  ( $\text{Q}^n$  units =  $\text{Si}(\text{OSi})_n(\text{OH})_{4-n}$ , with  $n = 1$  to 4), and are located in the range from -91 to -110 ppm, in which superscripts indicate the number of Si-O-Si bonds [95-97]. In contrast to FTIR spectroscopy, where isolated and geminal silanols absorb at nearly the same wavenumber,  $\text{Q}^3$  units (silanol groups) and  $\text{Q}^2$  (geminal silanols groups) can be distinguished by their corresponding chemical shifts at -91 and -100 ppm, respectively. The  $^{29}\text{Si}$  NMR signals of the trifunctional silanes ( $\text{T}^n = \text{RSi}(\text{OSi})_n(\text{OH})_{3-n}$ , with  $n = 1, 2, 3$ ) are located in the range from -45 to -70 ppm which refer to trifunctional groups without cross-linking ( $\text{T}^1$ ) at

about -48 ppm, with partial ( $T^2$ ) at about -55 ppm, and with complete cross-linking ( $T^3$ ) at around -66 ppm [54,96]. In the case of monofunctional silane ( $M = R_3Si(OSi)$ ) and the endcapping group ( $Si(CH_3)_3$ ), the peak is found at about +14 ppm [54]. The general trend observed from the  $^{29}Si$  NMR signal is the following: the high-field shift of an NMR signal increases as more oxygen neighbors are located around the observed silicon nuclei ( $Q > T > M$ ).

$^{29}Si$  NMR spectra discussed in the present dissertation are mostly recorded under  $^{29}Si\{^1H\}$  cross polarization conditions to increase the signal-to-noise ratio. Cross-polarization experiments, however, do not give the correct signal intensities, and provide enhanced intensities for the resonances of those  $^{29}Si$  nuclei with adjacent protons. In order to determine the relative amount of silanols on the silica surface and to compare the amounts before and after surface modification, single pulse  $^{29}Si$  NMR spectra can be recorded. The relative intensities are obtained by spectral deconvolution.

### **$^{13}C$ MAS NMR Spectroscopy**

$^{13}C$  CP/MAS NMR spectroscopy was used to study the attached species and to distinguish between regions containing all-trans chains and conformationally disordered chains with gauche bonds. Carbon nuclei offer a wider chemical shift range (220 ppm) than protons (12 ppm) and therefore provide a sensitive indicator of structural changes and the conformational order of immobilized ligands.

For alkylsilanes with longer alkyl chains (i.e., with 10 or more methylene segments), the  $^{13}C$  resonances of the inner methylene groups can be used to get qualitative information about the chain conformational order. But in case of shorter chains, the chain lengths were too small and did not allow a similar discussion of the conformational order. In this context, FTIR spectroscopy appears to be more suitable, as will be outlined in the next subsection.

## **2.5 Fourier Transform Infrared Spectroscopy (FTIR)**

In Fourier Transform Infrared (FTIR) spectroscopy, radiation is passed through the sample in which radiation is partially absorbed by the sample. The resulting spectrum represents the molecular absorption, creating a molecular fingerprint of the sample which corresponds to the frequencies of vibrations of molecular bonds and chemical environments in which these bonds are present. In this technique, molecules only absorb

infrared light at those frequencies where the infrared light affects the dipole moment of the molecule.

Almost all molecules absorb infrared light except monatomic (He, Ne, Ar, etc) and homopolar diatomic (H<sub>2</sub>, N<sub>2</sub>, O<sub>2</sub>, etc) molecules, and each type of molecule only absorbs infrared light at certain frequencies. This property provides a unique characteristic for each molecule. It provides a way to identify the molecule type (qualitative analysis) and the amount of this molecule in the sample (quantitative analysis). Importantly, IR spectroscopy is used for the identification of the functional groups present in the molecules. The major advantage of FTIR spectroscopy is its high sensitivity and relatively easy access to the desired information about the infrared absorption spectrum from the infrared spectral libraries.

FTIR absorption frequencies, band intensities and band shapes have shown to reflect the molecular conformation, configuration and chain packing in polyethylene chains [98]. The spectral features of the polyethylene infrared spectra have been used as a base for studying *n*-alkanes and subsequently those of tethered *n*-alkyl chains due to their structural similarities. FTIR spectroscopy probes on a time scale of less than 10<sup>-10</sup> s and is a versatile tool for examining the chain conformational order in various materials. For instance, it has been proved to be an efficient technique to characterize the conformational features of the chromatographic column materials, i.e., of the tethered long alkyl chains [99-106].

The degree of alkyl chain conformational order of surface modified systems varies substantially from highly ordered (crystalline) to disordered (liquid-like) and is substrate, preparation route and temperature dependent. Alkane chain structure and interfacial properties dictate the function and utility of these materials. In alkane-modified silicas used as stationary phase materials for chromatography, the conformational order of the alkane moieties governs the efficiency and selectivity of the separations [52,55,107]. The understanding at a molecular level of the alkyl chain conformational order behavior is thus crucial for such materials function in their respective applications.

In a pioneering work, Snyder calculated and tabulated the IR frequencies for an extensive number of vibrations in alkanes, including some that are specific to localized bent structures containing gauche bonds [108]. Normal mode calculations detail the assignment of various C-H stretching, scissoring, rocking and wagging modes. The observed wavenumbers, intensities and positions of these bands provide quantitative information about various defect structures responsible for disorder in the system. These

conformational defects have also been observed in other more complex hydrocarbon assemblies, such as model membranes and biomembranes [96] as well as micellar systems [109].

In the present dissertation, two vibrational modes have been used to investigate the conformational order of alkyl modified stationary phase materials. Table 2.1 contains the information related to each investigated vibrational mode.

Table 2.1. Conformation-sensitive IR modes used for *n*-alkyl chain conformational analysis.

Vibrational Mode	Wavenumber (cm <sup>-1</sup> )	Comments
CH <sub>2</sub> stretching		
Symmetric	2853 – 2846	Shift to higher frequency indicates more conformational disorder (qualitative)
Antisymmetric	2926 – 2915	

### Methylene Stretching Bands

The conformational properties of attached alkyl chains can be studied by several conformation-sensitive vibrational bands [110-111]. Among these, the symmetric and antisymmetric CH<sub>2</sub> stretching bands (2800-3000 cm<sup>-1</sup>) are the most intense signals, and in the majority of cases are easily accessible. Their positions as a function of external parameters, like temperature, pressure or sample constitution, can be used for a qualitative discussion of the conformational order in the aliphatic chains. Hence, changes in the positions of these bands are directly related to the alteration of the *trans/gauche* ratios. A band shift towards lower wavenumbers reflects an increase in conformational order (i.e., higher amount of *trans* conformers and reduced mobility), while a shift towards higher wavenumbers points to an increasing conformational disorder with a higher amount of *gauche* conformers and thus enhanced chain flexibility. Similar information can in principle be derived from the bandwidths, although the respective alterations are typically less pronounced [105].

## 2.6 High Performance Liquid Chromatography (HPLC)

High performance liquid chromatography (HPLC) is a form of liquid chromatography to separate compounds that are dissolved in solution. HPLC instruments consist of a reservoir of mobile phase, a pump, an injector, a separation column, and a detector.

HPLC is used to separate components of a mixture by using a variety of chemical interactions between the substance being analyzed (analyte) and the chromatography column.

### 2.6.1 Operation

The basic operating principle of HPLC is to force the analyte through a column of the stationary phase (usually a tube packed with small spherical particles with a certain surface chemistry) by pumping a liquid (mobile phase) at high pressure through the column. The sample to be analyzed is introduced in small volume to the stream of a mobile phase and is retarded by specific chemical or physical interactions with the stationary phase as it traverses the length of the column. The amount of retardation depends on the nature of the analyte, stationary phase and mobile phase composition. The time at which a specific analyte elutes (comes out of the end of the column) is called the retention time and is considered a reasonably unique identifying characteristic of a given analyte. The use of pressure increases the linear velocity (speed) giving the components less time to diffuse within the column, leading to improved resolution in the resulting chromatogram. Common solvents used include any miscible combinations of water and various organic liquids (the most common are methanol and acetonitrile). A further refinement of HPLC is the variation of the mobile phase composition during the analysis; this is known as *gradient elution*. A normal gradient for reversed phase chromatography might start at 5 % methanol or acetonitrile and progress linearly to 50 % over 25 minutes, depending on how hydrophobic the analyte is. The gradient separates the analyte mixtures as a function of the affinity of the analyte for the current mobile phase composition relative to the stationary phase. The choice of solvents, additives and gradient depend on the nature of the stationary phase and the analyte. Often a series of tests are performed on the analyte and a number of generic runs may be processed in order to find the optimum HPLC method for the analyte - the method which gives the best separation of peaks.

### Types of HPLC

There are many ways to classify liquid column chromatography. If this classification is based on the nature of the stationary phase and the separation process, three modes can be specified.

- **Adsorption chromatography:** the stationary phase is an adsorbent (like silica gel or any other silica based packing) and the separation is based on repeated adsorption-desorption steps.
- **Ion-exchange chromatography:** the stationary bed has an ionically charged surface of opposite charge to the sample ions. This technique is used almost exclusively with ionic or ionizable samples. The stronger the charge on the sample, the stronger it will be attracted to the ionic surface and thus, the longer it will take to elute. The mobile phase is an aqueous buffer, where both pH and ionic strength are used to control elution time.
- **Size exclusion chromatography:** the column is filled with material having precisely controlled pore sizes, and the sample is simply screened or filtered according to its solvated molecular size. Larger molecules are rapidly washed through the column; smaller molecules penetrate inside the pores of the packing particles and elute later. This technique is also called gel filtration or gel permeation chromatography.

Concerning the first type, two modes are defined depending on the relative polarity of the two phases: normal and reversed-phase chromatography. In normal phase chromatography, the stationary bed is strongly polar in nature (e.g., silica gel), and the mobile phase is nonpolar (such as n-hexane). Polar samples are thus retained on the polar surface of the column packing for longer than less polar materials.

Reversed-phase chromatography is the inverse of this. The stationary bed is (nonpolar) in nature, while the mobile phase is a polar liquid, such as mixtures of water and methanol or acetonitrile. Here the more nonpolar the material is, the longer it will be retained.

Reverse phase chromatography is used for almost 90% of all chromatographic applications. Eluent polarity plays the major role in all types of HPLC. There are two elution types: isocratic and gradient. In the first type, a constant eluent composition is pumped through the column during the whole analysis. In the second type, eluent composition (and strength) is steadily changed during the run.

HPLC as compared with the classical LC technique is characterised by:

- high resolution
- small diameter (2–5 mm), reusable stainless steel columns
- column packing with very small (3, 5 and 10  $\mu\text{m}$ ) particles



- relatively high inlet pressures and controlled flow of the mobile phase
- continuous flow detectors capable of handling small flow rates and detecting very small amounts
- rapid analysis

Initially, pressure was selected as the principal criterion of modern liquid chromatography and thus the name was “high pressure liquid chromatography” or HPLC. This was, however, an unfortunate term because it seems to indicate that the improved performance is primarily due to the high pressure. This is, however, not true. In fact, high performance is the result of many factors: very small particles of narrow distribution range and uniform pore size and distribution, high pressure column slurry packing techniques, accurate low volume sample injectors, sensitive low volume detectors and, of course, good pumping systems. Naturally, pressure is needed to permit a given flow rate of the mobile phase.

### **Retention Mechanism**

In general, HPLC is a dynamic adsorption process. Analyte molecules, while moving through the porous packing bead, tend to interact with the surface adsorption sites. Depending on the HPLC mode, the different types of the adsorption forces may be included in the retention process:

- Hydrophobic (non-specific) interactions are the main ones in reversed-phase separations.
- Dipole-dipole (polar) interactions are dominated in normal phase modes.
- Ionic interactions are responsible for the retention in ion-exchange chromatography.

All these interactions are competitive. Analyte molecules are competing with the eluent molecules for the adsorption sites. So, the stronger analyte molecules interact with the surface and the weaker the eluent interaction, the longer analyte will be retained on the surface.

SEC (size-exclusion chromatography) is a special case. It is the separation of the mixture by the molecular size of its components. In this mode any positive surface interactions should be avoided (eluent molecules should have much stronger interaction with the surface than analyte molecules).

The basic principle of SEC separation is that bigger molecules have less possibility to penetrate into the adsorbent pore space. Hence, the bigger the molecule the less it will be retained.

### Stationary Phases (Adsorbents)

HPLC separations are based on surface interactions, and depend on the types of the adsorption sites (surface chemistry). Modern HPLC adsorbents are small rigid porous particles with high surface area. Main adsorbent parameters are:

- Particle size: 3 to 10  $\mu\text{m}$
- Pore size: 9 to 30 nm
- Surface area: 100 to 500  $\text{m}^2 \text{g}^{-1}$
- Bonding phase density (number of adsorption sites per surface unit): 1 to 5 per  $\text{nm}^2$

Depending on the type of the ligand attached to the surface, the adsorbent could be normal phase (-OH, -NH<sub>2</sub>), or reversed-phase (C<sub>4</sub>, C<sub>8</sub>, C<sub>18</sub>, Phenyl), and even anion (NH<sub>4</sub><sup>+</sup>), or cation (-COO<sup>-</sup>) exchangers.

Mostly HPLC is performed with the stationary phase attached to the outside of small spherical silica particles. These particles come in a variety of sizes with 5  $\mu\text{m}$  beads being the most common ones. Smaller particles generally provide more surface area and better separations, but the pressure required for optimum linear velocity increases with the inverse of the particle diameter squared [112-113].

### Mobile phases

In HPLC, the type and composition of the eluent is one of the variables influencing the separation. Despite the large variety of solvents used in HPLC, there are several common properties, e.g., purity, detector compatibility, solubility of sample, low viscosity and chemical inertness.

For normal phase mode, solvents are mainly nonpolar; for reversed-phase, eluents are usually a mixture of water with some polar organic solvent such as acetonitrile or methanol. Size-exclusion chromatography (SEC) has special requirements. SEC eluents have to dissolve polymers, but more important is that SEC eluents have to suppress possible interactions of the sample molecule with the surface of the packing material.

### 2.6.2 Organic-Inorganic Hybrid Mesoporous Silica Materials and HPLC

Alkyl modified stationary phases can be characterized by different techniques to determine the attachment, conformational behavior and mobility of the surface-attached alkyl chains. They include systematic analysis of the retention behavior for a certain group of solutes [52,114-116], various spectroscopic measurements of the stationary phase materials [51,54,97,99,117-124], and theoretical calculations [125-128] of the bonded phase structures. The chain conformation of the stationary phases were primarily studied with the help of chromatographic experiments, which provided essential information about the bonded phase as a function of mobile phase, temperature, solute hydrophobicity and polarity [114,129]. These studies have demonstrated that the selectivity differences among the columns are not only due to differences in the starting silica material, but also due to differences in the chain density of the alkyl bonded phases. It turned out that the alkyl chain structure and interfacial properties urge the function and utility of these stationary phase materials. It was also demonstrated that the conformational order of the alkyl chain moieties plays an important role in determining the efficiency and selectivity of separations. Such studies, however, provide only indirect evidence about the bonded phase morphology. On the other hand, experimental techniques—such as NMR [54,100,121-122,130-131] and FTIR [100-102,104-106,132] reveal direct information about the alkyl chain structure, conformation, and dynamics of the stationary phase materials.



## Chapter 3

### Material Characterization

The various MCM-41 and SBA-15 materials before and after surface modification were comprehensively characterized by elemental analysis, nitrogen sorption experiments, small angle X-ray diffraction (XRD), scanning electron microscopy (SEM), Fourier transform infrared spectroscopy (FTIR), solid-state  $^{13}\text{C}$  and  $^{29}\text{Si}$  NMR spectroscopy as well as high performance liquid chromatography (HPLC).

#### 3.1 Elemental Analysis

Carbon and hydrogen contents of the surface modified MCM-41 and SBA-15 silica were determined by a Carlo Erba Strumentazione elemental analyzer 1106 (Milan, Italy). The percentage of carbon was utilized for calculating the surface coverage,  $\alpha_{RP}$  (in  $\mu\text{mol m}^{-2}$ ) with the following equation [97]:

$$\alpha_{RP} = \frac{10^6 P_C}{1200n_C - P_C(M - n_x)} \cdot \frac{1}{S_{BET}}, \quad (3.1)$$

where  $P_C$  is the percentage of carbon determined via elemental analysis,  $n_C$  the number of carbon atoms per silane moiety,  $M$  the molar mass of the silane,  $n_x$  the number of reactive groups in the silane ( $n_x=3$  for  $n$ -alkyltrimethoxysilane), and  $S_{BET}$  the BET surface area of the unmodified support.

#### 3.2 Nitrogen Sorption Studies

Nitrogen sorption (adsorption-desorption) measurements were performed at 77 K on a Micromeritics ASAP 2010 volumetric adsorption analyzer (Neuss, Germany). Here, 150 mg of the unmodified or surface modified MCM-41 and SBA-15 materials were degassed at 393 K for 4 h in the degassing port of the adsorption apparatus. The surface

area measurements were based on the BET method within a pressure range from  $p/p_0 = 0.05$  to  $0.3$  and  $p/p_0 = 0.05$  to  $0.2$  for normal silica (Kromasil) and MCM-41 silica spheres, respectively. For SBA-15 materials, a pressure range from  $p/p_0 = 0.05$  to  $0.3$  was used. BET surface areas were calculated from the adsorption isotherms using the BET equation [72] and a cross section for nitrogen  $a(\text{N}_2) = 13.5 \text{ \AA}^2$  [75].

The pore volume was calculated from the amount of  $\text{N}_2$  adsorbed at a relative pressure of  $0.99$ . For determination of pore diameter and pore size distribution, the majority of studies employs the BJH method [77] which, however, is known to underestimate the pore size for pores smaller than  $100 \text{ \AA}$  [19]. A more reliable method is based on the density functional approach (DFT) [19,69,133]. Therefore, results from both methods are presented to demonstrate this effect. The analyses were made using the DataMaster programme and the DFTplus module from Micromeritics.

### 3.3 Scanning Electron Microscopy

SEM measurements were performed on a CamScan CS44 scanning electron microscope (Waterbeach, UK). The samples were prepared by placing MCM-41 and SBA-15 silica spheres on double-sided carbon adhesive tape mounted on the sample holder. The samples were then gold coated (thickness about  $20 \text{ nm}$ ) by cathodic sputtering.

### 3.4 Small Angle X-ray Diffraction

X-ray diffraction experiments were performed with a Bruker AXS NanoSTAR system ( $\text{CuK}_\alpha$  radiation aligned by Goebel mirrors) equipped with a two-dimensional electronic detector and a temperature controller (MRI Physikalische Geräte GmbH, Karlsruhe, Germany).

### 3.5 Solid-State NMR Measurements

Solid-state NMR measurements were done on a Varian InfinityPlus 400 NMR spectrometer (Varian, Palo Alto/CA, USA), operating at  $9.4 \text{ T}$  and at resonance frequencies of  $100.52 \text{ MHz}$  and  $79.41 \text{ MHz}$  for  $^{13}\text{C}$  and  $^{29}\text{Si}$ , respectively. Magic angle spinning (MAS) experiments were performed with a  $4 \text{ mm}$  MAS probe at a sample rotation frequency of  $5 \text{ kHz}$ . During the  $^{13}\text{C}$  NMR experiments, cross-polarization (CP) excitation, a  $\pi/2$  pulse width of  $3.5 \text{ }\mu\text{s}$ , a contact time of  $5 \text{ ms}$  and recycle delays of  $5 \text{ s}$

were used. The typical number of scans was 4000.  $^{13}\text{C}$  chemical shifts were determined relative to the external standard adamantane.  $^{29}\text{Si}$  CP/MAS NMR spectra were recorded using a  $\pi/2$  pulse length of 3.5  $\mu\text{s}$ , a contact time of 5 ms, and a recycle delay of 5 s. The spinning speed was 5 kHz, and the typical number of scans was 5000. Single pulse  $^{29}\text{Si}$  NMR spectra were recorded using a  $\pi/2$  pulse length of 3.5  $\mu\text{s}$ , a recycle delay of 45 s, and with a typical number of scans of 1300.  $^{29}\text{Si}$  chemical shifts were determined relative to the external standard  $\text{Q}_8\text{M}_8$ , the trimethylsilylester of octameric silicate. Deconvolution of the  $^{29}\text{Si}$  NMR spectra was done by using the Spinsight software package (Varian).

### 3.6 FTIR Measurements

Pellets of surface modified MCM-41 and SBA-15 silica materials and KBr (1/10–1/15 w/w) of 1 mm thickness were prepared under vacuum using a hydraulic press and placed in a brass cell equipped with an external thermocouple in close vicinity to the sample. The same thermocouple was used for monitoring the actual sample temperature. The brass cell was thermostated in a variable temperature transmission cell (L.O.T. – Oriol, Langenberg, Germany) equipped with NaCl windows. FTIR spectra were recorded with a Nicolet Nexus 470 FTIR spectrometer (Nicolet, Madison/WI, USA) equipped with a DTGS detector, and by purging with  $\text{N}_2$  gas. Typically, 256 interferograms covering a spectral range of 4000–400  $\text{cm}^{-1}$  at a resolution of 2  $\text{cm}^{-1}$  were collected within a temperature range from 193 K to 353 K. The recorded interferograms were apodized with a triangular function and Fourier transformed with two levels of zero filling. The background spectrum was recorded with an empty cell using twice the number of scans as for the measurements with the sample, and was automatically subtracted from the experimental spectra of the surface modified MCM-41 and SBA-15 samples. Data from all the samples were acquired at all temperatures. The processing and analysis of the spectra, covering the  $\text{CH}_3$  and  $\text{CH}_2$  stretching band region, were performed with the OMNIC E.S.P.5.1 software (Nicolet). The wavenumbers of the  $\text{CH}_3$  and  $\text{CH}_2$  stretching vibrations were calculated from the interpolated zero crossing in the first derivative spectra.

### 3.7 HPLC Experiments

The chromatographic columns (125 mm x 4.6 mm) were prepared with  $\text{C}_{18}$  alkyl modified MCM-41 materials by the slurry method with isopropanol as solvent. The columns were

packed using a Knauer pneumatic HPLC pump (Berlin, Germany) under 400 bar pressure. Chromatographic tests were performed at 25 °C using a Hewlett Packard HPLC instrument (Series 1100) from Agilent (Waldbronn, Germany) that possesses a UV-Visible diode array detector. Reversed-phase liquid chromatographic performances of these columns were tested with a mixture of alkyl benzenes (C1-C6) with the detection at 210 nm. Chromatographic measurements were made at 293 K using a mobile phase composition of water/methanol of 80/20 v/v at an elution velocity of 1.0 ml min<sup>-1</sup>. HPLC grade methanol and water were obtained from Merck (Darmstadt, Germany).

While the chromatographic columns (125 mm x 4.6 mm) with C<sub>4</sub> and C<sub>8</sub> alkyl modified MCM-41, and C<sub>4</sub>, C<sub>8</sub> and C<sub>18</sub> alkyl modified SBA-15 materials were prepared by the slurry method with acetone as solvent. The chromatographic performance of these columns was tested with the reference mixture SRM 870 received from NIST, which contains five organic components: uracil, toluene, ethylbenzene, quinizarin, and amitriptyline. They were separated on the columns using an acetonitrile/water mixture (50/50, v/v) as mobile phase at an elution velocity of 1.0 ml min<sup>-1</sup> and with a detector operating at 254 nm. HPLC grade acetonitrile and water were obtained from Merck (Darmstadt, Germany).



## Chapter 4

# Synthesis and Surface Characterization of Octadecyl Modified MCM-41 Silica Materials and their Application in HPLC

### 4.1 Introduction

MCM-41 silica spheres are prepared via the pseudomorphic route, using commercial Prontosil silica spheres. The obtained MCM-41 silica spheres are surface modified with octadecyl (C<sub>18</sub>) alkyl chains using trifunctional (*n*-octadecyltrimethoxysilane) silylating agent, by using direct grafting and surface polymerization methods in order to vary the degree of surface hydrophobicity.

The MCM-41 silica materials before and after surface modification are characterized by nitrogen sorption analysis, small angle X-ray diffraction (XRD) and scanning electron microscopy (SEM) measurements. XRD and nitrogen sorption analysis yields the porous feature of MCM-41 materials, while information about morphology of the particles is obtained from the SEM studies. <sup>29</sup>Si NMR spectroscopy is employed to probe the attachment of the alkyl chains on the mesoporous MCM-41 silica material. <sup>13</sup>C NMR and variable temperature FTIR studies are used to examine the conformational state and the mobility of the attached alkyl chains. The chromatographic performances of these C<sub>18</sub> alkyl modified MCM-41 stationary phases are tested with a mixture of alkyl benzenes. The results are compared with those for commercially available C<sub>18</sub> alkyl modified Prontosil silica, and are discussed in detail.

## 4.2 Sample Preparation

### 4.2.1 Chemicals

Commercially available Prontosil (200-5-Si; 5  $\mu\text{m}$ ) was delivered by Bischoff Chromatography (Leonberg, Germany). The silylating agent *n*-octadecyltrimethoxysilane (purity of 90 %) used for the surface modification, cetyltrimethylammonium bromide (CTAB) and sodium hydroxide (NaOH) were purchased from Aldrich Chemical Company (Sigma-Aldrich Chemie, Steinheim, Germany). Alkylbenzenes used for the chromatography were purchased from different companies: Benzene (>99 %), ethylbenzene (>98 %) and butylbenzene (99 %) from Fluka, Germany and toluene (99.8 %), pentylbenzene and hexylbenzene (>97 %) from Merck, Germany. All solvents used in the HPLC experiments were of HPLC grade (LiChrosolv, Merck, Germany). Reagent grade toluene was distilled two times before use.

### 4.2.2 Synthesis of MCM-41 Silica Material

According to the pseudomorphic synthesis, the Prontosil silica was stirred in an alkaline solution of cetyltrimethylammonium bromide (CTAB) to produce the MCM-41 type ordered mesoporous spheres [33]. The reactants, with molar composition of  $\text{SiO}_2$ : NaOH: CTAB:  $\text{H}_2\text{O}$  = 1: 0.25: 0.1: 20 were slowly mixed under stirring. The reaction mixture was stirred at 400 rpm for another 30 min at room temperature. Afterwards, the mixture was transferred to an autoclave and kept at 363 K for 40 h. The as-synthesized MCM-41 material was filtered and dried overnight at 353 K. After heating the sample at a rate of 1 K  $\text{min}^{-1}$ , the surfactant was removed by calcination in air at 823 K for 5 h.

### 4.2.3 Reaction of Silylating Agents with MCM-41 Silica Material

According to the previous reports it was assumed that only 4  $\mu\text{mol m}^{-2}$  of the hydroxyl groups are present on the MCM-41 silica surface after calcination at 823 K, while about 8  $\mu\text{mol m}^{-2}$  of hydroxyl groups are discussed for conventional amorphous silica gels [134]. *n*-Octadecylsilyl groups were attached to the calcined MCM-41 spherical silica with *n*-octadecyltrimethoxysilane by the following methods.

### a) Direct Grafting Method

About 2.0 g of calcined MCM-41 silica was preevacuated at 378 K for 4 h. The activated MCM-41 silica was suspended in toluene (20 ml) and heated to 333 K. In this method, we used a two-fold excess (8  $\mu\text{mol}$  of silane per  $\text{m}^2$  of calcined MCM-41 silica surface area) of *n*-octadecyltrimethoxysilane.

### b) Surface Polymerization Method

About 2.0 g of calcined MCM-41 silica was preevacuated at 378 K for 4 h. The resulting dry powders were equilibrated with humid air at room temperature for 6 h [52-53]. In this surface polymerization method, silanization is carried out on surfaces with a monolayer surface coverage of water using an apparatus similar to that described by Wirth and Fatunmbi [53]. The humidified MCM-41 silica materials were suspended in toluene (50 ml) and heated to 333 K. A two and three-fold excess (8 and 12  $\mu\text{mol}$  of silane per  $\text{m}^2$  of calcined MCM-41 silica surface area) of the *n*-octadecyltrimethoxysilane in toluene (150 ml) were added to the above suspension. These mixtures were placed in rotavapor at 333 K for 3 and 4 days, respectively. The resulting MCM-41 silica spheres from both the preparation methods were filtered (G4 filter) and washed with toluene, followed by acetone, ethanol, ethanol/water (1:1, v:v.), water, ethanol, acetone, and pentane to rinse away any residual chemicals. The octadecyl ( $\text{C}_{18}$ ) surface modified MCM-41 silica was dried overnight in an oven at 353 K and stored in airtight bottles.

## 4.3 Results and Discussion

### 4.3.1 Synthesis and Surface Modification of MCM-41 Silica Material

Prontosil MCM-41 silica spheres were prepared by the pseudomorphic transformation of the amorphous Prontosil silica spheres. The resulting MCM-41 spheres have a trimodal pore size distribution: primary mesopores (2.7 nm), secondary mesopores (3.7 nm) and a wide pore size distribution including the parent silica pore diameter (16.8 nm) which is discussed in detail in the next section. A similar distribution in pore size while using Prontosil as silica source was observed with significant amount of secondary and larger mesopores [57,135]. It was found that the presence of secondary mesoporosity depends on the pore volume of the parent silica, and materials with uniform mesoporosity can be

prepared by carrying out the reaction for longer time, depending on the actual silica source [22,57,135].

*n*-Octadecyltrimethoxysilane was used as silylating agent to prepare the samples DA, SP1 and SP2 presented in this study (listed in Table 4.1). C<sub>18</sub> alkyl chains were attached on the calcined Prontosil MCM-41 silica spheres by direct attachment, and after humidification (surface polymerization) to obtain materials with varying degrees of hydrophobic character. The octadecyl modified MCM-41 silica spheres prepared after the surface polymerization method results in a higher grafting density or surface coverage when compared to the directly grafted spheres. In this method, the adsorbed water molecules on these spheres promote more binding to the surface along with cross-linking of neighbouring silanes to attain more surface coverage. As mentioned earlier, alkyl modified mesoporous silica spheres exhibit a high mechanical stability compared to the unmodified material [136].

Sample DA was prepared by attachment of C<sub>18</sub> alkyl chains directly, samples SP1 and SP2 were prepared after the humidification of the calcined MCM-41 silica spheres. The attachment and cross-linking of the silanes are higher in the case of surface polymerized samples SP1 and SP2 than the DA sample as reflected by the surface coverage (Table 4.2) and <sup>29</sup>Si NMR studies (Section 4.3.5) of these materials. The main drawback of this reaction is the production of alcohol as by-product which may adsorb or react with the substrate to form methoxy-derivatized surfaces (discussed in Section 4.3.6, <sup>13</sup>C NMR studies) [137].

The surface coverage for the present systems was found be lower when compared to alkyl modified normal silica gels [100,135], and it affects the alkyl chain conformational behaviour which is explained in detail in Sections 4.3.6 (<sup>13</sup>C NMR) and 4.3.7 (FTIR). This is a consequence of the lesser amount of surface silanol groups especially on the calcined MCM-41 materials, and also of the relatively smaller diameter of the primary mesopores of calcined MCM-41 silica which creates difficulties in coating the interior of the mesopores. In addition, pore blocking at the entrance of the mesopores by the longer C<sub>18</sub> chains (cross-sectional area is 20 Å<sup>2</sup> and length is 23 Å) prevents the chains to diffuse inside the pores [57,135].

Table 4.1: Details of octadecyl (C<sub>18</sub>) modified MCM-41 silica spheres

Material code	Amount of Methoxy Silane	Reaction Duration	Octadecyl (C <sub>18</sub> ) modified MCM-41 silica
SP2	3 fold	4 days	MCM-calcined-Surface polymerization
SP1	2 fold	3 days	MCM-calcined-Surface polymerization
DA	2 fold	3 days	MCM-calcined-Direct attachment

### 4.3.2 Nitrogen Sorption Studies

Nitrogen sorption isotherms of the calcined MCM-41 silica are typical of reversible IV type isotherms and are shown in Figure 4.1 (left). The textural properties of these MCM-41 spheres are summarized in Table 4.2. The strong rise of the BET curve around the relative pressure of  $p/p_0 = 0.3$  for unmodified MCM-41 silica stems from the capillary condensation in the mesopores which is typical for MCM-41 materials. A hysteresis is observed in the sorption curves between about  $p/p_0 = 0.45$  and 1.0, which is attributed to the presence of mesopores with the larger diameters. A similar finding was already reported from earlier studies which explains that the larger mesopores are connected to the exterior of the particles by the structured porosity, and hence the desorption occurs in these pores via a cavitation process [75]. An additional step in the desorption curve at about  $p/p_0 = 0.45$  is found for the MCM-41 samples prepared using Prontosil silica source which refers to the presence of secondary mesopores [75,138]. Parental pores and pores with even larger pore diameters are present in smaller amounts, which is observed at a relative pressure of about  $p/p_0 = 0.92$  in the isotherm [25,138-139].

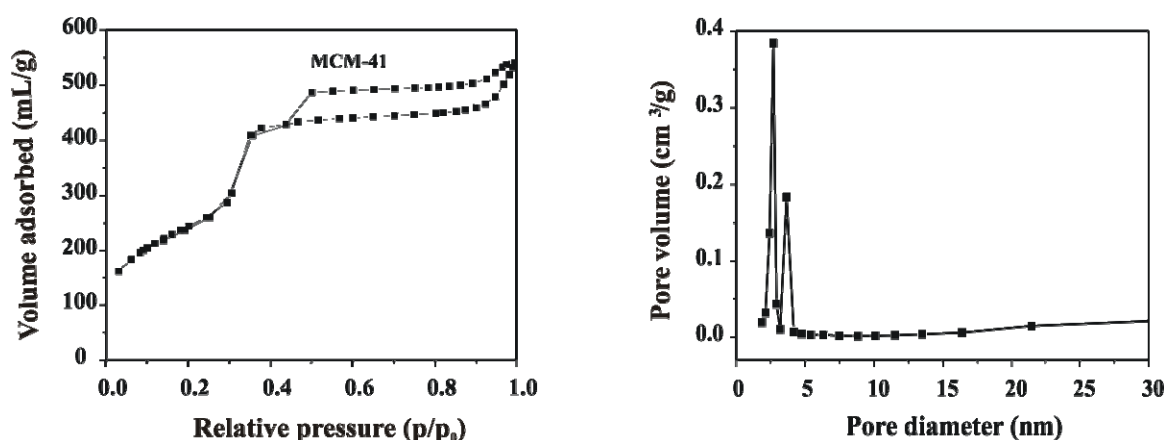


Figure 4.1: BET isotherm (left) and BJH pore size distribution (right) of calcined Prontosil MCM-41 silica spheres.

The respective BJH analysis provides the pore diameters of the calcined MCM-41 spheres, shown in Figure 4.1 (right) by the pore size distribution plot with primary and secondary mesopores with diameters of 2.7 nm and 3.7 nm, respectively. Moreover, wider parental silica pores of diameter 16.8 nm (centered pore diameter value since the pore size distribution is very broad, 3–20 nm) are also present and their presence is confirmed by a broad peak in Figure 4.1 (right). Thus the calcined MCM-41 spheres exhibit a trimodal pore distribution which is due to the incomplete pseudomorphic transformation of amorphous silica spheres into MCM-41 silica spheres, as mentioned earlier. Here, the dissolution of the primary nanoparticles and their reprecipitation into micelle-templated silica lead to the fusion of the primary nanoparticles into larger nanoparticles. This results in intraparticle pores inside the spheres identified as larger pores than the parental pores by nitrogen sorption measurements [22]. MCM-41 spheres with uniform mesopores are synthesized with longer reaction times with different sources of silica, and the details are discussed in the next chapter. The optimum conditions (duration, temperature, etc.) for complete pseudomorphic transformation, however, are also found to strongly depend on the silica source [22].

Prontosil MCM-41 silica spheres surface modified with octadecyl ( $C_{18}$ ) chains (DA, SP1 and SP2) again exhibit similar isotherms as shown in Figure 4.2, as discussed above for the unmodified MCM-41 sample with trimodal pore distribution. However, the plateau value is lowered for all the samples with increase in surface coverage, in agreement with former observations [140]. Hence a lower amount of nitrogen is adsorbed which introduces a significant reduction in surface area and total pore volume, as also found for non-spherical MCM-41 materials [141], and which correlates with the increase in surface coverage of these materials (Table 4.2). After the surface modification of the MCM-41 spheres, the first bend in the isotherm is shifted towards the lower pressure region which results in smaller pore diameters, confirmed by the pore size distribution analysis (Table 4.2). A low-pressure hysteresis below the relative pressure of 0.3 is observed for all the surface modified materials in which the desorption curves lie above the respective adsorption curves. A similar hysteresis was found in the earlier studies for the attachment of  $C_8$  and  $C_{18}$  chains, and may result from very weak interactions between nitrogen and the long aliphatic chains [25,135-136].

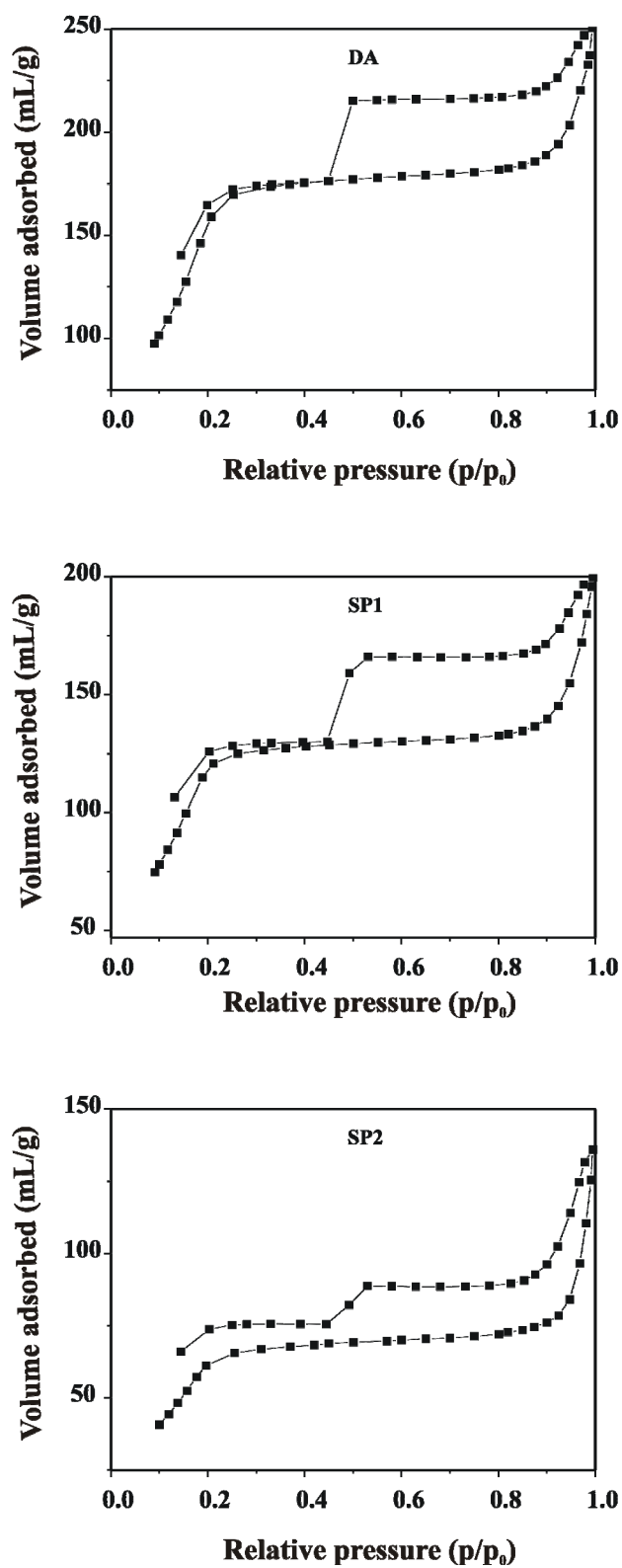


Figure 4.2: BET isotherms of octadecyl (C<sub>18</sub>) modified Prontosil MCM-41 silica spheres.

The cross-sectional area of a C<sub>18</sub> ligand is about 20 Å<sup>2</sup>. Therefore, these larger C<sub>18</sub> ligands are not able to diffuse deeply into the pores. Hence the octadecyl chains are attached to MCM-41 spheres mainly near the entrance of the primary mesopores and cross-link with the neighboring silanes. There is a greater reduction of the surface area and the total pore volume for surface polymerized samples, especially for sample SP2, and this may be caused by a pore blocking effect due to more attachment of C<sub>18</sub> alkyl chains on the surface (due to surface polymerization) which hinder the other chains to diffuse into the mesopores as described in former studies [138,142]. It should be noted that the reduction in surface area and pore volume are in accordance with their increase in surface coverage of the surface modified MCM-41 materials, as given in Table 4.2.

Table 4.2 Textural features of Prontosil silica, MCM-41 silica and octadecyl (C<sub>18</sub>) modified MCM-41 silica materials.

Material code	a <sub>0</sub> (nm)	S <sub>BET</sub> (m <sup>2</sup> /g)	V <sub>p</sub> (ml/g)	D <sub>pore</sub> (nm)	% C	Surface coverage (μmol/m <sup>2</sup> )
Prontosil	-	137	0.81	16.8	-	-
MCM-41	4.6	744	0.82	2.7, 3.7	-	-
SP2	5.4	225	0.19	2.1, 3.6	22.70	1.61
SP1	4.7	521	0.30	2.0, 3.7	17.45	1.10
DA	5.1	571	0.39	2.1, 3.7	15.70	0.96

(a<sub>0</sub>: Unit-cell parameter which is calculated for the primary mesopores, S<sub>BET</sub>: BET surface area, V<sub>p</sub>: total pore volume, D<sub>pore</sub>: pore diameter, % C: weight percent of carbon in the samples, SC: surface coverage of chemically bonded ligands.)

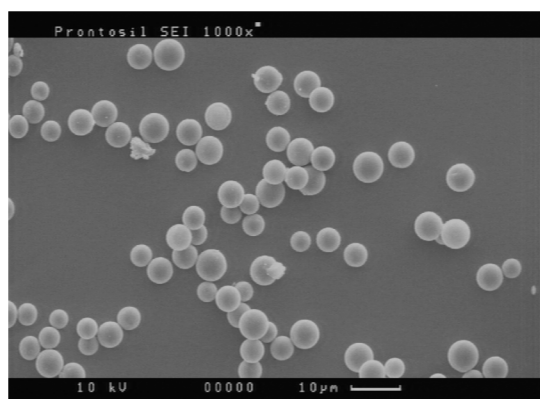
The given pore diameters were derived from the BJH method which is known to underestimate the pore diameter up to 25 % for pores smaller than 100 Å. Hence, for the present samples, the real pore diameters are about 0.7-0.9 nm larger than the reported values in Table 4.2. These “corrected values” are in agreement with the reported values from the studies on the pseudomorphic MCM-41 spheres and their grafted analogues [25,143].

### 4.3.3 Scanning Electron Microscopy

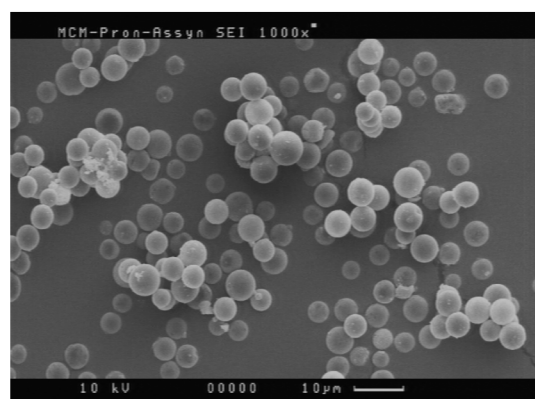
SEM pictures of the spheres of Prontosil silica, MCM-41 silica and octadecyl (C<sub>18</sub>) modified MCM-41 samples are shown in Figure 4.3. The spherical morphology of the Prontosil silica particles is preserved during the pseudomorphic synthesis of the MCM-41



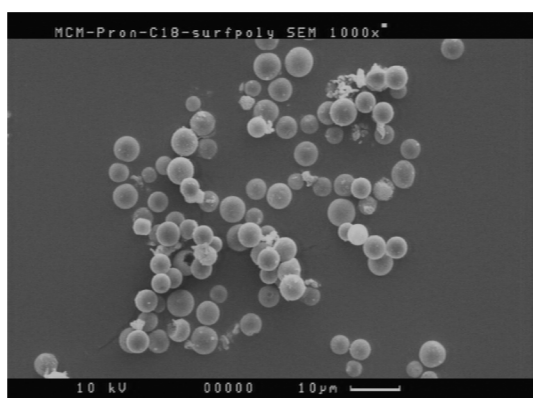
spheres and it is clearly indicated by their SEM pictures. It should be noted that the silica spheres of commercial Prontosil is not completely monodisperse in distribution, and the dispersity of the spheres is retained during the pseudomorphic transformation. Thus, the particle diameter and the particle size distribution are preserved. In addition, there is no evidence for agglomeration of the MCM-41 silica spheres. Similarly, the spherical morphology is retained after the surface modification of MCM-41 silica.



**Prontosil silica**



**MCM-41 silica**



**Octadecyl (C<sub>18</sub>) modified MCM-41 silica**

Figure 4.3: SEM micrographs for silica spheres of Prontosil, MCM-41 and octadecyl (C<sub>18</sub>) modified MCM-41.

#### 4.3.4 Small Angle X-ray Diffraction

Figure 4.4 shows the XRD pattern of the calcined MCM-41 silica spheres synthesized from Prontosil as silica source. Three broader reflection peaks [indexed as (100), (110) and (200)] are present for the Prontosil MCM-41 silica in which the (110) and (200) reflections appear as partially overlapped peaks. It was shown that a broader XRD pattern of MCM-41 silica originates from a distortion of the hexagonal symmetry of second- and

higher-order neighbor pores around a central pore for the spherical MCM-41 silica [19]. Hence, the broader Bragg reflections of the Prontosil samples point to a long-range distortion of the hexagonal arrangement of the mesopores [57,135]. The secondary mesopores present in these materials cause a further broadening of the XRD pattern. Nevertheless, the XRD pattern clearly demonstrates that the calcined sample is of MCM-41 type with the hexagonal pore arrangement.

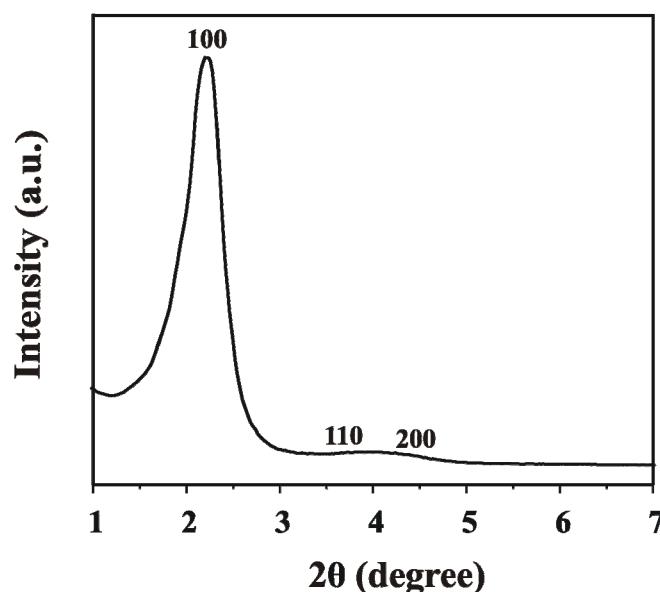


Figure 4.4: XRD pattern of Prontosil MCM-41 silica spheres.

XRD pattern of the octadecyl ( $C_{18}$ ) modified Prontosil MCM-41 silica spheres are presented in Figure 4.5. The Bragg reflection (100) shows as a broad peak along with lesser intensity for (110) and (200) reflections. Thus, there is a decrease in ordered porosity of these octadecyl modified MCM-41 spheres [57,144]. This behavior is usually observed during the surface modification of mesoporous material in which the structural order does not extend over a long range [144]. The intensity of the Bragg reflections is decreasing with increase in surface coverage of the samples. The attachment of more alkyl chains on these MCM-41 materials results in the decrease in ordered porosity of these spheres. Moreover, the unit-cell parameters for all the MCM-41 samples are reported in Table 4.2.

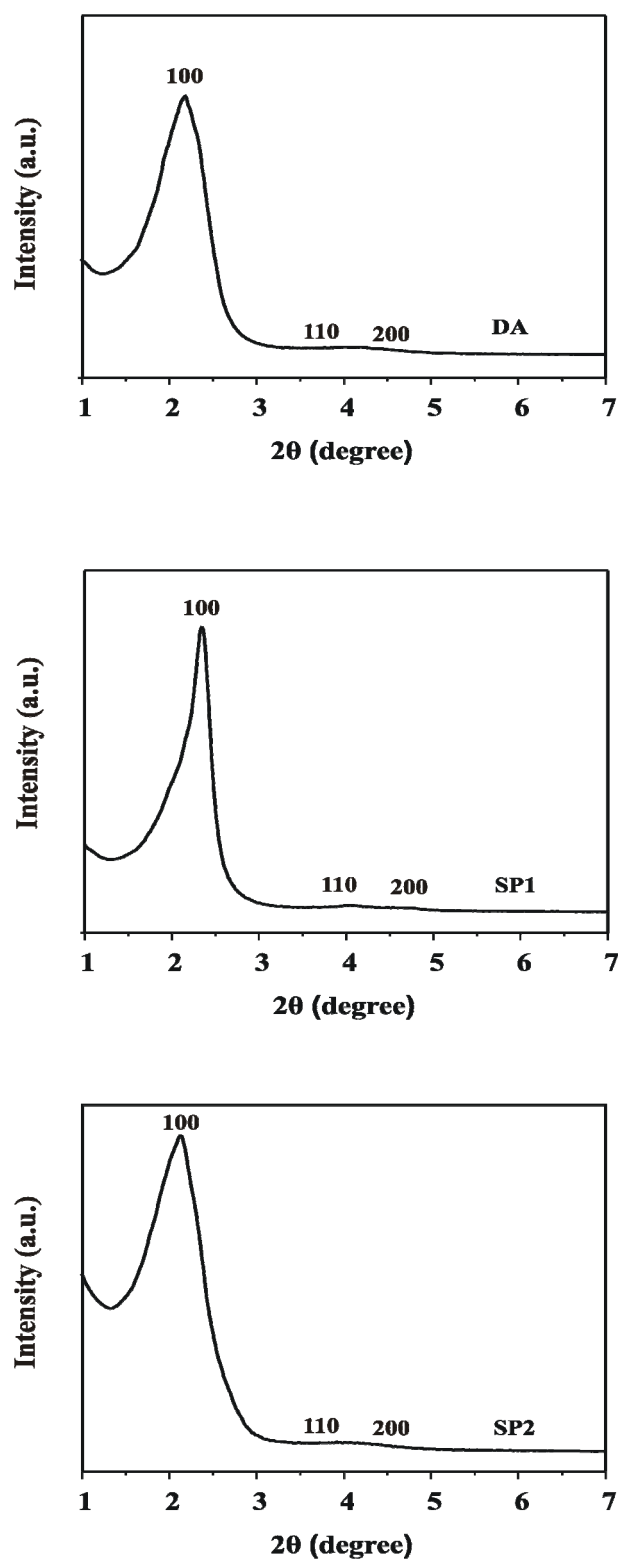


Figure 4.5: XRD patterns of octadecyl ( $C_{18}$ ) modified Prontosil MCM-41 silica spheres.

### 4.3.5 $^{29}\text{Si}$ NMR Spectroscopy

$^{29}\text{Si}$  MAS NMR spectroscopy is a suitable technique for the examination of the surface species, amount of alkyl chain attachment and degree of cross-linking of the alkyl silanes. The signals around -91, -100 and -109 ppm reflect surface silanol groups, i.e.,  $\text{Q}^2$  and  $\text{Q}^3$  units, and interior, completely condensed  $\text{Q}^4$  units, respectively ( $\text{Q}^n$  units =  $\text{Si}(\text{OSi})_n(\text{OH})_{4-n}$ , with  $n = 1$  to 4) [95,97].  $^{29}\text{Si}$  CP/MAS NMR spectra of the unmodified and octadecyl ( $\text{C}_{18}$ ) modified MCM-41 silica samples (DA, SP1 and SP2) are shown in Figure 4.6, and the chemical shift values are reported in Table 4.3. The comparison of the  $^{29}\text{Si}$  NMR spectrum of the calcined unmodified MCM-41 sample with those of the surface modified samples reveals a significant reduction of the  $\text{Q}^3$  peak intensity and increase in  $\text{Q}^4$  intensity upon surface modification. Also a significant reduction of the  $\text{Q}^2$  signal was observed, in accordance with the increase in surface coverage.

The attachment and cross-linking of the alkyl chains on the MCM-41 silica surface is identified from the  $\text{T}^n$  group signals ( $\text{T}^n = \text{RSi}(\text{OSi})_n(\text{OH})_{3-n}$ , with  $n = 1, 2, 3$ ) between -45 ppm and -70 ppm [54], which refer to  $\text{T}^1$  and  $\text{T}^2$  groups with partial, and  $\text{T}^3$  groups with complete cross-linking at the chemical shift values given in Table 4.3. The presence of  $\text{T}^1$  and  $\text{T}^2$  species in all these samples indicates an incomplete hydrolysis of the methoxy groups which is in agreement with the  $^{13}\text{C}$  NMR data (see Section 4.3.6), while the  $\text{T}^3$  groups are completely absent in these samples. Since the silanol groups are isolated in the calcined MCM-41 spheres, the majority of monolayers of water molecules are not able to bridge between the two existing hydroxyl groups. This results in the above mentioned incomplete hydrolysis of the methoxy species, and less efficient cross-linking of the alkyl chains on the surface and with the neighboring alkyl chains, respectively. It is reflected in the presence of  $\text{Q}^3$  signals in the surface modified samples, thus indicating the inner mesopores are not coated completely with the longer  $\text{C}_{18}$  chains due to the smaller diameter of mesopores and pore blocking by the chains at the entrance of the mesopores.

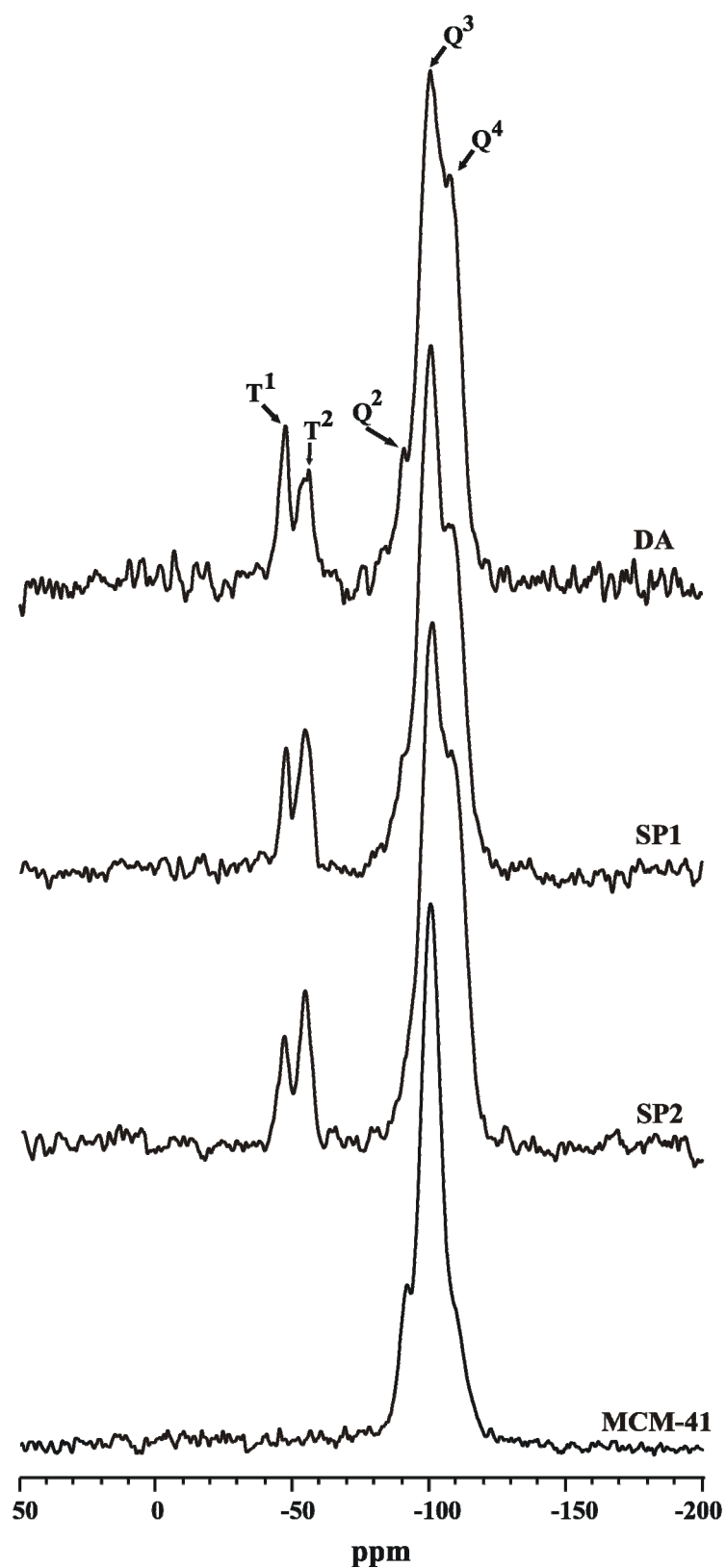


Figure 4.6:  $^{29}\text{Si}$  CP/MAS NMR spectra of octadecyl ( $\text{C}_{18}$ ) modified MCM-41 silica with *n*-octadecyltrimethoxysilane.

The relative intensities of the T<sup>n</sup> group signals for the samples studied here are in accordance with the increase in surface coverage of the samples. For instance, the intensity of T<sup>1</sup> species follows the order DA>SP1>SP2 while the reverse order was observed for the T<sup>2</sup> intensities, i.e., SP2>SP1>DA (see Figure 4.6). The increase in intensity of the T<sup>n</sup> group signals for the surface polymerized samples is due to the presence of monolayer coverage of water which provides more alkyl chain attachment on the surface and also additional cross-linking of the silanes when compared to the direct octadecyl (C<sub>18</sub>) modified MCM-41 silica, DA.

Table 4.3: <sup>13</sup>C and <sup>29</sup>Si chemical shifts for octadecyl (C<sub>18</sub>) modified MCM-41 silica spheres.

Material code	<sup>29</sup> Si chemical shift (ppm)					<sup>13</sup> C chemical shift (ppm)				
	Q <sup>4</sup>	Q <sup>3</sup>	Q <sup>2</sup>	T <sup>2</sup>	T <sup>1</sup>	OCH <sub>3</sub>	C-3, C-16	C-4 – C-15	C-2, C-17	C-1, C-18
MCM-41	-109.8	-101.2	-91.0	-	-	-	-	-	-	-
SP2	-107.8	-100.8	-90.4	-54.0	-46.5	50.3	32.7	30.5	23.2	14.0
SP1	-108.0	-100.5	-90.2	-54.4	-47.5	50.0	32.5	30.3	23.1	13.5
DA	-107.8	-100.9	-90.9	-56.1	-47.5	50.0	32.5	30.2	23.0	13.4

#### 4.3.6 <sup>13</sup>C NMR Spectroscopy

<sup>13</sup>C NMR spectroscopy was employed to examine the conformational order of the attached alkyl chains and to acquire further information about the attachment of the MCM-41 silica surface. Figure 4.7 depicts the <sup>13</sup>C CP/MAS NMR spectra of the C<sub>18</sub> modified MCM-41 silica samples (DA, SP1 and SP2) and the chemical shift values are reported in Table 4.3. The <sup>13</sup>C resonances of carbons C-1 and C-18 appear at 13–14 ppm [97,145]. The peak around 23 ppm represents carbons C-2 and C-17 of the alkyl chains while the signal at about 32.5 ppm represents carbons C-3 and C-16.

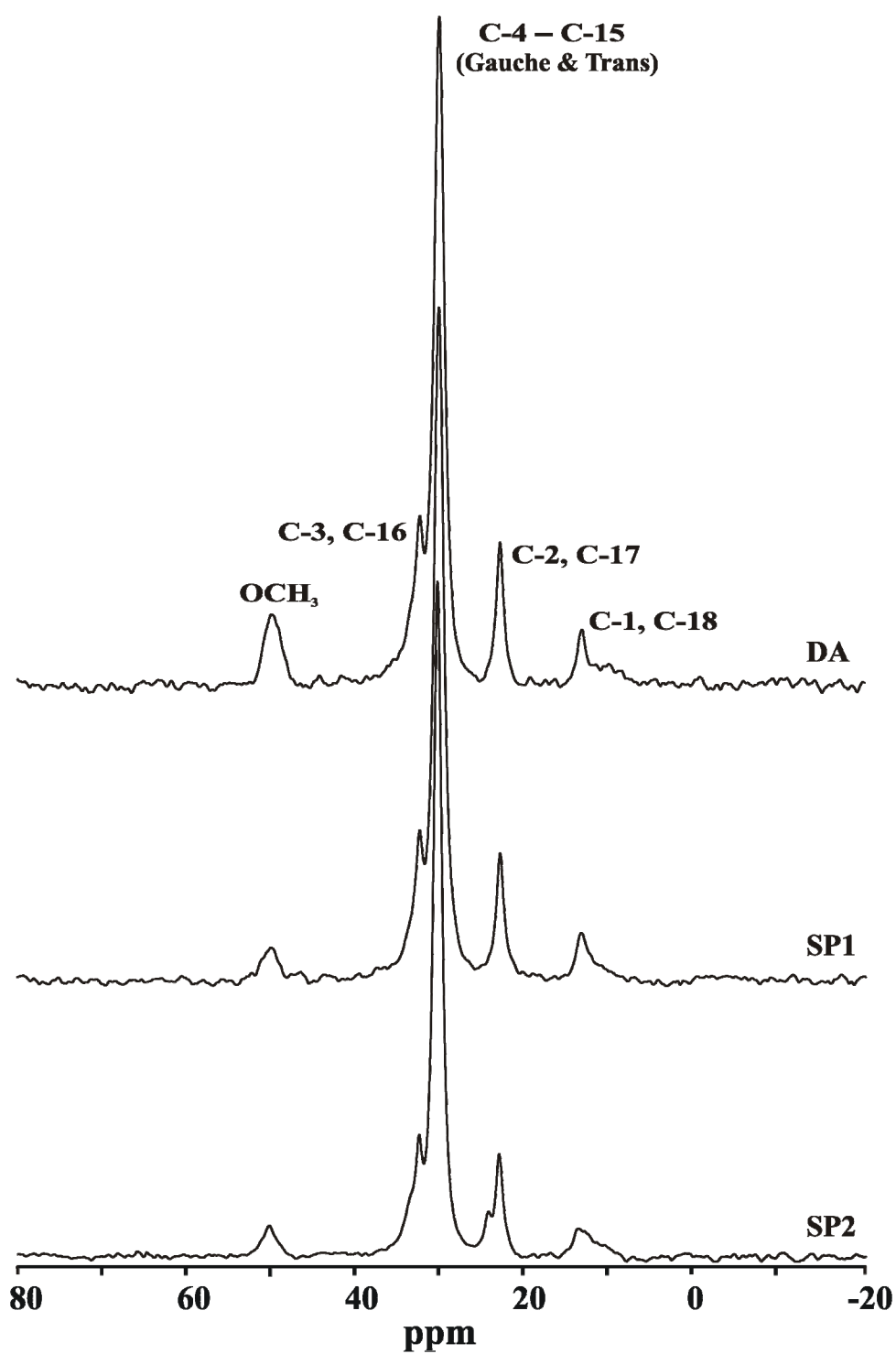


Figure 4.7:  $^{13}\text{C}$  CP/MAS NMR spectra of octadecyl ( $\text{C}_{18}$ ) modified MCM-41 silica with *n*-octadecyltrimethoxysilane.

The differences in the alkyl chain conformational order are accessed qualitatively by comparing the  $^{13}\text{C}$  NMR resonances from the inner methylene segments C-4 to C-15, which may exist as “crystalline-like” trans and “solution-like” gauche conformations [117,145]. The signals at around 30 ppm found in the present work point to  $\text{C}_{18}$  chains in the gauche state (more mobile part) with low conformational chain order.  $\text{C}_{18}$  chains with a high degree of chain ordering (trans conformers) which is the less mobile part, are characterized by  $^{13}\text{C}$  resonance at about 32 ppm [117,145] and obviously do not occur in the present samples. The low conformational order for the present samples points to a large spatial freedom and high chain mobility, in agreement with the low surface coverage. Such correlations between the alkyl chain conformational disorder and the surface coverage are well known and were discussed earlier during  $^{13}\text{C}$  NMR studies on other alkyl chain modified silica materials [100,145].

The additional  $^{13}\text{C}$  resonance at around 50 ppm can be assigned to methoxy groups bound to silicon. This signal can be explained either by non-reacted methoxy groups of the alkylsilane, or more likely, by the presence of methoxy groups which are released during the hydrolysis of the trifunctional silanes and which are subsequently bound to the surface silanol groups [146]. The degree of the intensity of the 50 ppm peak decreases with increase in surface coverage of the samples. This implies that a high amount of cross-linking occurs for the higher surface coverage samples especially for the surface polymerized MCM-41 silicas as proved by the  $^{29}\text{Si}$  NMR spectra. It should be kept in mind that the signal also results from the methoxy derivatized surfaces. The presence of these remaining methoxy groups might be explained by the small amount of accessible surface silanol groups along with a minor probability for closely spaced silanol groups at which all three functional groups of an octadecylsilane molecule can bind. This explains the effective loose packing of chains and higher conformational disorder of the alkyl chains which is further elaborated in the next section by a variable temperature FTIR study.

#### 4.3.7 FTIR Spectroscopy

FTIR spectroscopy is used to provide information about the conformational state of the attached alkyl chains. In general, the conformational properties of attached alkyl chains can be studied by several conformation-sensitive vibrational bands [110-111]. Among these, the symmetric and antisymmetric  $\text{CH}_2$  stretching bands ( $2800\text{-}3000\text{ cm}^{-1}$ ) are the



most intense signals, and in the majority of cases are easily accessible. The CH<sub>2</sub> stretching modes can be utilized to discuss the evolution of conformational order in the octadecyl (C<sub>18</sub>) modified MCM-41 materials. Variable temperature FTIR spectra for samples SP1, SP2 and DA in the temperature range between 193 K and 353 K are depicted in Figure 4.8. The influence of temperature on the alkyl chain mobility and on their conformational order is clearly visible from the changes of the CH<sub>2</sub> symmetric and antisymmetric stretching band positions. It is observed that the conformational order successively decreases with increasing temperature, as expressed by a shift towards higher wavenumbers. In addition, a broadening of IR bands with increasing temperature implies the presence of conformationally disordered octadecyl chains which gain additional mobility after raising the sample temperature. The analysis of the conformational order in a temperature range from 193 to 353 K is important because during chromatographic separations, the shape selectivity can be affected by column temperature, especially for certain classes of solutes with rigid and well-defined molecular shapes [22].

Figure 4.8 reveals that the absorption band maxima shift towards higher wavenumbers with increasing sample temperature. For all samples, the overall change in the CH<sub>2</sub> symmetric and antisymmetric stretching band position is approximately 2.5 cm<sup>-1</sup> and 4 cm<sup>-1</sup>, respectively, over the temperature range used here. The shift in the band position occurs uniformly with temperature, which is consistent with an absence of a phase transition for these stationary phase materials. There is a slight increase in CH<sub>2</sub> stretching bandwidths at higher temperatures due to the higher alkyl chain mobility. Both these observations demonstrate that the tethered alkyl chains are conformationally more disordered with increasing temperature. The conformational order follows the sequence, SP2>SP1>DA. The samples under this study also show that the conformational order increases with increase in surface coverage of the octadecyl (C<sub>18</sub>) modified samples, similar to our earlier studies on alkyl modified MCM-41 silica spheres. However, the conformational order of these systems is lower when compared to the alkyl modified silica gels which can be related to the lower surface coverage [97]. These results are in agreement with similar variable temperature FTIR studies on other octadecyl (C<sub>18</sub>) modified MCM-41 silica spheres [57].

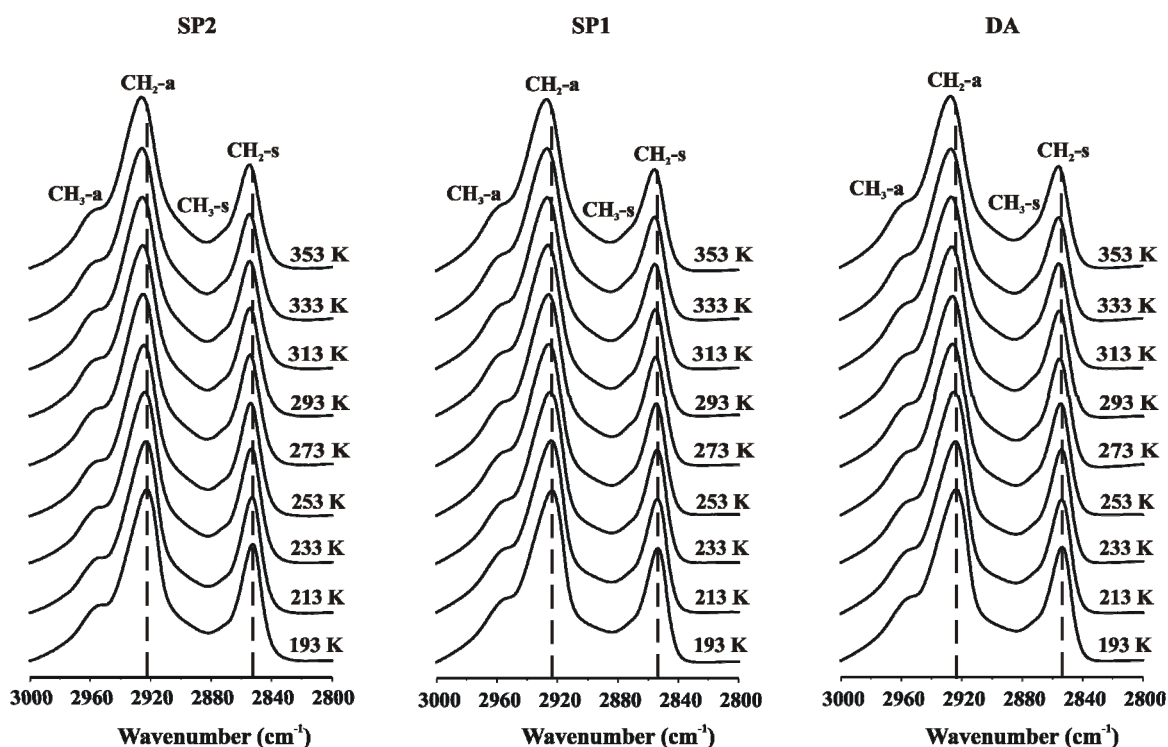


Figure 4.8: Temperature dependence of the antisymmetric and symmetric  $\text{CH}_2$  stretching band spectra of octadecyl ( $\text{C}_{18}$ ) chains attached on sample SP2, SP1 and DA samples.

#### 4.3.8 HPLC Measurements

In the present work, two surface modified MCM-41 materials (DA and SP1) were slurry-packed into an HPLC column in order to separate a mixture of five alkylbenzenes – Toluene (C1), Ethylbenzene (C2), Propylbenzene (C3), Butylbenzene (C4), Pentylbenzene (C5) and Hexylbenzene (C6) – under controlled conditions (i.e., mobile phase, flow and temperature). This mixture was also separated using a commercial Prontosil column (CP), which is octadecyl ( $\text{C}_{18}$ ) modified Prontosil silica. All the separations were performed with the detection at 210 nm. The methylene selectivity in this separation follows the order from C1-C6 in all the columns that were employed.

Figure 4.9 shows the separation of the alkylbenzenes in the columns DA, SP1 and CP with a mobile phase composition of methanol/water-80/20. The separation was effective for all the analytes with elution at different retention times which followed the order  $\text{SP1} > \text{DA} > \text{CP}$ . It is observed that the increase in surface coverage plays a role in better retention of the solutes in these columns. In the columns DA and SP1, the surface coverage of SP1 is slightly higher and the retention is greater in SP1 than in DA. As the

alkylbenzenes are hydrophobic analytes, the retention was determined by interaction with the alkyl chains and also with the available larger surface area. The retention time during the separation of these analytes was very short in column CP when compared to the columns DA and SP1. This implies that these spherical MCMs are more suitable for the better separation of poorly retained analytes with higher retention times as compared to normal silica stationary phases. This is due to the interaction of these analytes with the higher surface areas leading to higher retention times. Thus, spherical mesoporous MCM-41 silica possess better chromatographic performance than normal silica stationary phases, and this can be attributed to their high surface area, well-defined pore size and uniform particle size.

The separation of alkylbenzenes provides information about the retention of analytes which depend on their interactions with the available surface area and also with the surface coverage of octadecyl (C<sub>18</sub>) modified MCM-41 columns when compared to the commercial Prontosil column, CP.

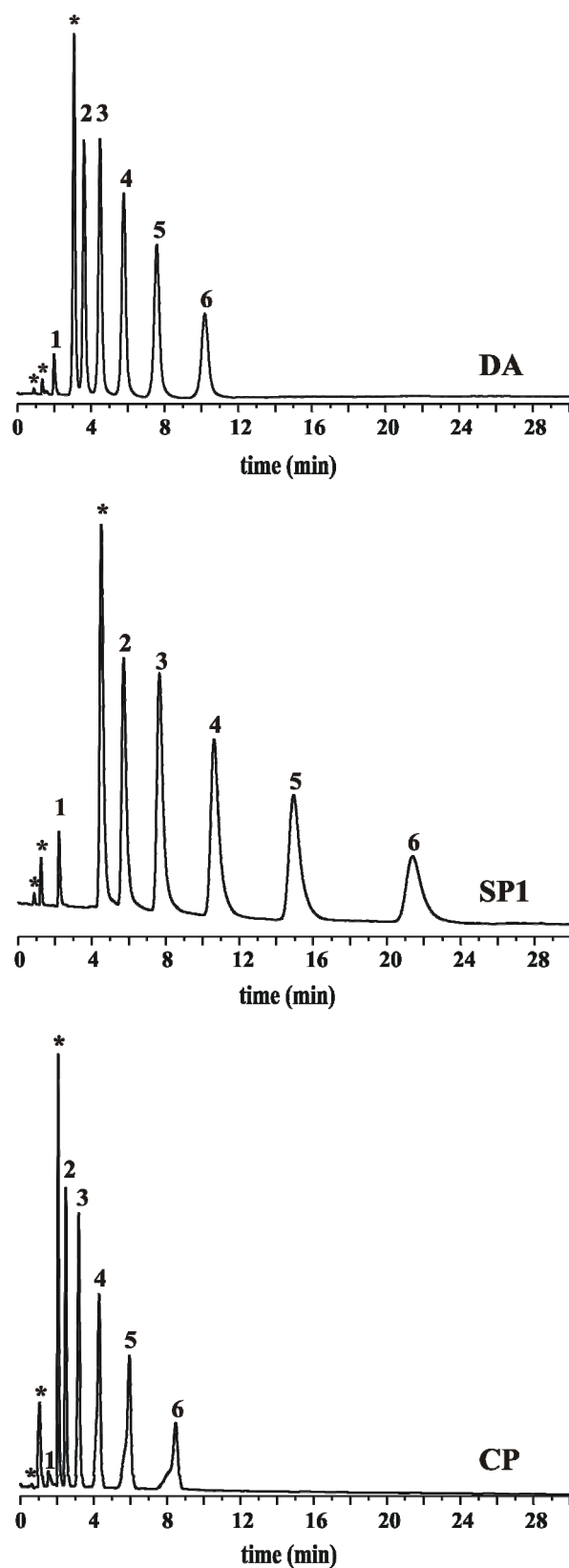


Figure 4.9: Separation of alkylbenzenes (1 Toluene, 2 Ethylbenzene, 3 Propylbenzene, 4 Butylbenzene, 5 Pentylbenzene, and 6 Hexylbenzene) using DA, SP1 and CP stationary phases using a mobile phase composition of water/methanol = 80/20 v/v. \* denotes isomeric impurity.

#### **4.4 Concluding Remarks**

MCM-41 silica spheres with trimodal pore size distribution were prepared via the pseudomorphic route using commercial Prontosil silica spheres. Surface modification of the MCM-41 silica material was made by using octadecyltrifunctional silane via direct grafting and surface polymerization methods. The surface polymerization method is found to give higher surface coverages as compared to the direct grafting method. Nitrogen sorption and XRD experiments showed that the mesoporosity and pore symmetry of the material is retained after surface modification. The chromatographic performance of two samples, one prepared by direct grafting and the other by the surface polymerization method was tested. A better separation performance with longer elution times was found for the MCM-41 sample prepared by surface polymerization method. This is due to the higher surface coverage of the material prepared by surface polymerization method and hence the conformational order of attached octadecyl (C<sub>18</sub>) chains, which is found to increase with increasing surface coverage. These results are found to be better as compared to the commercial Prontosil silica column and this can be attributed to their high surface area, well-defined pore size and uniform particle size.



## Chapter 5

# Synthesis and Surface Modification of MCM-41 Silica Materials with Shorter Alkyl Chains Using the Surface Polymerization Method

### 5.1 Introduction

Surface modification offers a great opportunity to adjust both the pore diameter and surface properties of MCM-41 type organic-inorganic hybrid materials which results in materials of improved hydrothermal and mechanical stability. Therefore, MCM-41 silica, surface modified with organic ligands, are promising systems with engineered properties and attractive for advanced applications. In this chapter, after optimization of the reaction conditions highly ordered MCM-41 silica spheres with uniform mesopores are prepared by the pseudomorphic transformation route using Kromasil silica. Previously, MCM-41 materials with trimodal pore size distribution have been prepared using Prontosil silica and the resulting materials were surface modified with octadecyl ( $C_{18}$ ) chains using both direct grafting and the surface polymerization methods. As the materials prepared using the surface polymerization showed higher surface coverages, we follow this method in the present contribution. The molecular length of the silylating reagent is very crucial for the surface coverage with organic components. The effect of alkyl chain length and functionality of the alkyl ligands during surface modification is probed by using alkylsilanes of two different alkyl chain lengths and functionalities, butyl and octylsilanes ( $CH_3(CH_2)_nSiR_3$ , with  $n=3$  and  $7$ ;  $R=OCH_3$ ). The shorter chains are able to bind to the interior mesopore walls while on the other hand, because of steric hindrance, longer chains primarily bind to the outer surface and only few chains are attached within the mesopores, leaving a large fraction of non-reacted surface silanol groups which are considered to lead to surface hydrophilicity [147]. These residual silanol groups are weakly acidic, and cause peak tailing for basic solutes which reduces the resolution and

column efficiency in chromatographic applications. Endcapping of these silanols, for instance, by hexamethyldisilazane (HMDS) overcomes this problem and provides a better performance during chromatographic separation.

The various MCM-41 materials before and after surface modification are comprehensively characterized by nitrogen sorption experiments, small angle X-ray diffraction (XRD), scanning electron microscopy (SEM), FTIR, solid-state  $^{13}\text{C}$  and  $^{29}\text{Si}$  NMR spectroscopy as well as HPLC.

## 5.2 Sample Preparation

### 5.2.1 Chemicals

Commercially available silica, Kromasil (300 Å; 5 μm) was obtained by Akzo-Nobel (Bohus, Sweden). Silanes, *n*-octyltrimethoxysilane, *n*-octyldimethylmethoxysilane, *n*-butyl trimethoxysilane and *n*-butyldimethylmethoxysilane (purity: 97%), used for the surface modification, 1,1,1,3,3,3-hexamethyldisilazane (HMDS; purity: 97%), cetyltrimethylammonium bromide (CTAB) and sodium hydroxide (NaOH) were obtained from Aldrich Chemical Company (Sigma-Aldrich Chemie, Steinheim, Germany). Reagent grade toluene was distilled two times before use and stored over molecular sieves.

### 5.2.2 Synthesis of MCM-41 Silica Material

Mesoporous MCM-41 silica spheres were prepared by using Kromasil as silica source and following the pseudomorphic transformation route. Kromasil silica was stirred in an alkaline solution of cetyltrimethylammonium bromide (CTAB) with the molar composition of  $\text{SiO}_2:\text{NaOH}:\text{CTAB}:\text{H}_2\text{O} = 1:0.25:0.1:20$ . After slowly mixing of the components, the reaction mixture was stirred at 400 rpm for 30 min at room temperature. Afterwards, the mixture was transferred to an autoclave and kept at 388 K for six days. The as-synthesized MCM-41 material was filtered and dried overnight at 353 K. After heating the sample at a rate of  $1 \text{ K min}^{-1}$ , the surfactant was removed by calcination in air at 823 K for 5 h.



### 5.2.3 Reaction of Silylating Agents with MCM-41 Silica Material

Schuster et al. [134] reported that only  $4 \mu\text{mol m}^{-2}$  of the hydroxyl groups are present on the MCM-41 silica surface after calcination at 823 K, while about  $8 \mu\text{mol m}^{-2}$  of hydroxyl groups are discussed for conventional amorphous silica gels. Surface modification of calcined MCM-41 silica material with alkylsilanes was carried out by following the surface polymerization method. Here, about 1 g of calcined MCM-41 silica was preevacuated at 378 K for 4 h and allowed to cool to ambient temperature. The resulting dry powder was equilibrated with humid air at room temperature for 6 h [52-53] which gives a water layer on the silica surface. Afterwards, the humidified MCM-41 silica was suspended in toluene (200 ml) and heated to 343 K. A three-fold excess ( $12 \mu\text{mol}$  of silane per  $\text{m}^2$  of calcined MCM-41 silica surface area) of the corresponding silanes in toluene (50 ml) was then added. This mixture was placed in a rotavapor for three days at 333 K. For the MCM-41 materials modified with octylsilanes, part of the material was used to endcap the remaining silanol groups with HMDS. This was done by adding a two-fold excess of HMDS to the reaction mixture which afterwards was kept at 343 K for one day. The resulting MCM-41 silica material was filtered (G4 filter) and washed with toluene, followed by acetone, ethanol, ethanol/water (1:1, v:v.), water, ethanol, acetone, and pentane to remove any residual chemicals. The surface modified MCM-41 silica was dried overnight in an oven at 353 K and stored in airtight bottles.

## 5.3 Results and Discussion

### 5.3.1 Synthesis and Surface Modification of MCM-41 Silica Material

The pseudomorphic transformation route was applied for the preparation of MCM-41 silica. To improve the quality of the resulting mesoporous material, the reaction time was varied. The remaining pores of the parent silica, as deduced from the corresponding nitrogen sorption isotherms, demonstrated that for reaction times less than six days only incomplete transformation can be achieved (data not shown). Both the nitrogen sorption and the XRD data proved complete transformation of Kromasil silica spheres into MCM-41 silica spheres, with high order and uniform mesopores after six days of reaction time.

Surface modification of MCM-41 silica material was carried out with octyl and butyl groups using the surface polymerization method, and the resulting materials with their

material codes are shown in Table 5.1. Octyl groups were attached on the calcined MCM-41 silica spheres by reaction with *n*-octyltrimethoxysilane (M-C8T) and *n*-octyldimethylmethoxysilane (M-C8M). The percentage of carbon obtained from the elemental analysis for samples M-C8T and M-C8M are 8.5 and 1.5, respectively (see Table 5.1). The respective surface coverage for the material surface modified with the monofunctional silane was very low ( $0.19 \mu\text{mol m}^{-2}$ ), because only one functionality is available for attachment to the silica surface, and no additional cross-linking of the silanes can take place. Trifunctional octylsilane provided much higher surface coverage ( $1.32 \mu\text{mol m}^{-2}$ ) because apart from binding to the surface silanol groups cross-linking reactions with neighbouring silane chains can occur. Hence, in this case a better chain packing with higher surface coverage, good thermal and enhanced chemical stability can be achieved.

In the same way, butylsilanes were attached on the calcined MCM-41 silica spheres by reaction with *n*-butyltrimethoxysilane (M-C4T) and *n*-butyldimethylmethoxysilane (M-C4M). The percentages of carbon obtained from the elemental analysis for these samples, M-C4T and M-C4M were 5.5 and 1.9, leading to surface coverages of 1.6 and  $0.5 \mu\text{mol m}^{-2}$ , respectively. These surface coverage values are significantly higher than those reported above for the octylsilane modified materials.

Most likely, for samples M-C8T and M-C8M, the longer octyl chains remain on the outer silica surface and near the entrance of the mesopores, which prevents other molecules from diffusion into the pores. In this case, a large number of surface silanol groups remain at the interior mesopore walls. Endcapping with HMDS was done to obtain materials with enhanced hydrophobicity. Samples M-C8TE and M-C8ME are the endcapped materials derived from samples M-C8T and M-C8M, respectively. Inspection of Table 5.1 reveals a substantial increase of the carbon content and thus for the surface coverage after endcapping with HMDS. This effect is particularly pronounced for sample M-C8ME, which in the initial step was surface modified with the monofunctional alkylsilane.

Table 5.1: Surface modified MCM-41 silica materials and their material codes.

Material code	Surface modified MCM-41 silica materials
M-C4T	MCM-41 modified with <i>n</i> -butyltrimethoxysilane
M-C8T	MCM-41 modified with <i>n</i> -octyltrimethoxysilane
M-C8TE	MCM-41 modified with <i>n</i> -octyltrimethoxysilane and endcapped with HMDS
M-C4M	MCM-41 modified with <i>n</i> -butyldimethylmethoxysilane
M-C8M	MCM-41 modified with <i>n</i> -octyldimethylmethoxysilane
M-C8ME	MCM-41 modified with <i>n</i> -octyldimethylmethoxysilane and endcapped with HMDS

### 5.3.2 Nitrogen Sorption Studies

Nitrogen sorption experiments were used to determine the textural properties and surface features of mesoporous materials in terms of surface area, pore size, pore size distribution and porosity. The nitrogen sorption isotherms for the unmodified and surface modified MCM-41 materials are shown in Figures 5.1 and 5.2.

The textural properties are summarized in Table 5.2. The overall appearance of the BET isotherms is very similar and typical for the group of reversible type IV isotherms. The strong rise of the BET curve for the unmodified MCM-41 sample above a relative pressure of  $p/p_0 = 0.3$  stems from capillary condensation in the mesopores, and is characteristic for a mesoporous structure. Surface modification leaves the overall appearance of these type IV isotherms practically unchanged, indicating that the textural characteristics are not altered by surface modification with butyl- and octylsilanes. For the surface modified samples, the steep adsorption steps are shifted towards lower pressure, and the adsorption plateau values, reflecting the total silica surface area, are lowered.

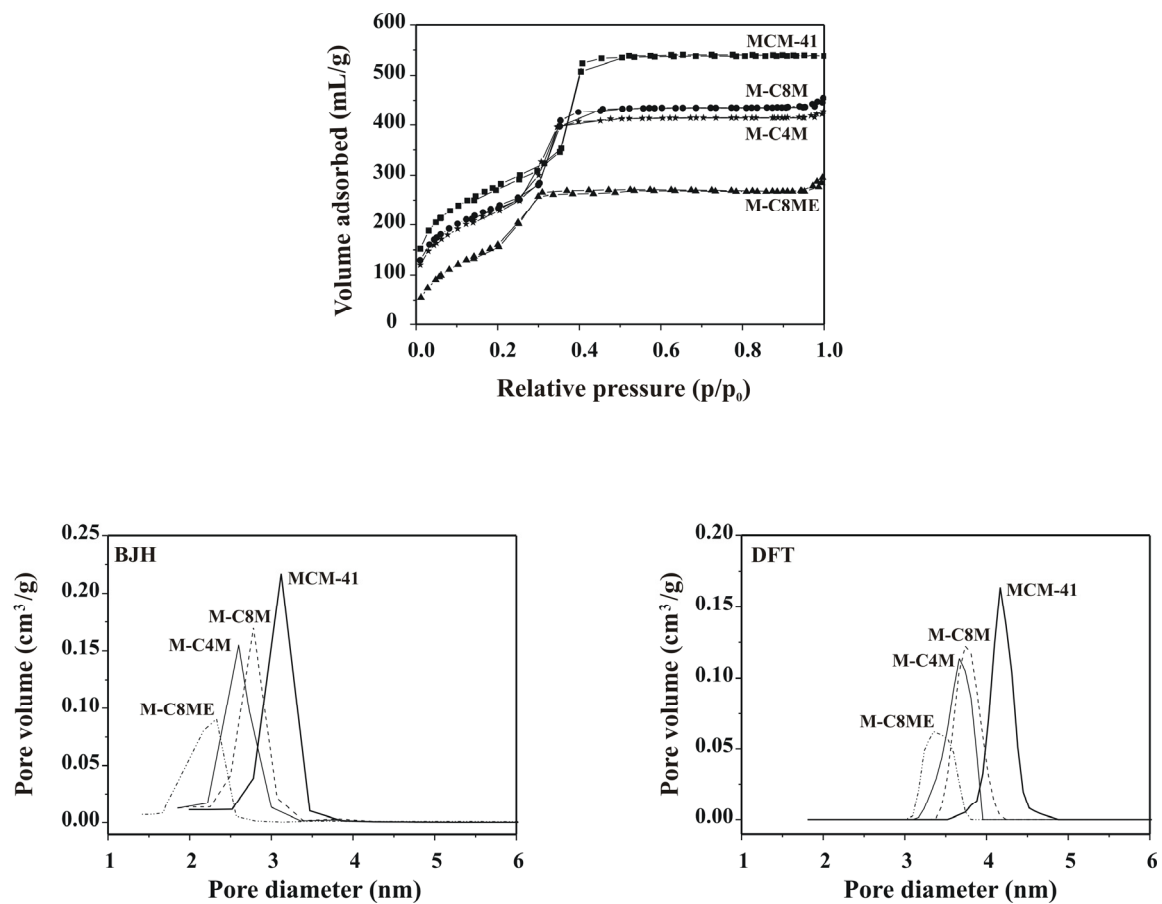


Figure 5.1: Nitrogen sorption isotherms (top), BJH pore size distributions (bottom left) and DFT pore size distributions (bottom right) for MCM-41 materials before and after surface modification with trifunctional silanes.

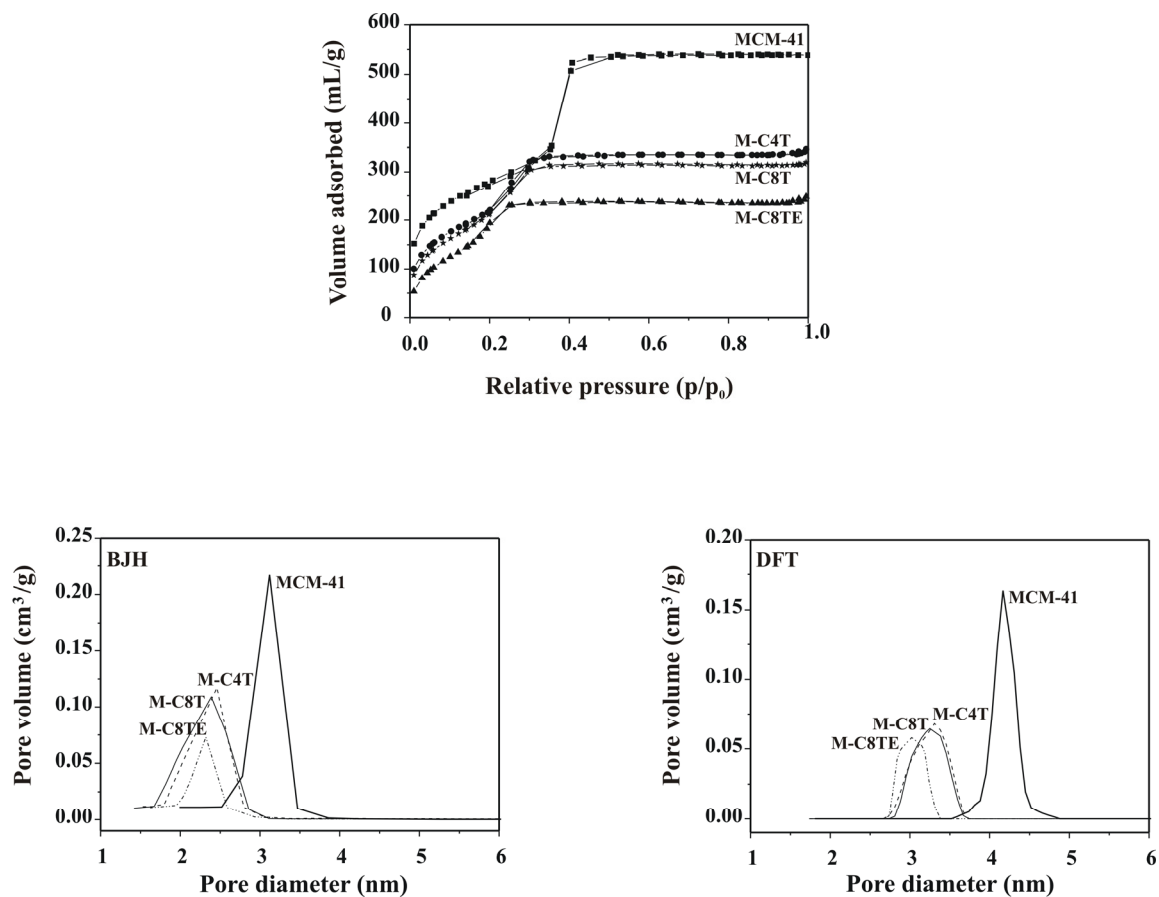


Figure 5.2: Nitrogen sorption isotherms (top), BJH pore size distributions (bottom left) and DFT pore size distributions (bottom right) for MCM-41 materials before and after surface modification with monofunctional silanes.

The pore size distribution represents another important structural quantity of porous materials. In this context, the BJH method is commonly employed. However, this classical method does not provide a correct description of the sorption and phase behaviour of fluids in narrow mesopores, with widths  $< 100 \text{ \AA}$ , and leads to an underestimation of the pore diameters [79]. Rather, in this case a density functional theory (DFT) based analysis has demonstrated to be the most accurate method for pore size and pore size distribution determination [69]. This approach takes into account the details of the fluid-fluid interactions and the adsorption potential, which depends on the strength of fluid-wall interactions and the pore geometry. It is based on a combination of statistical mechanical calculations and experimental observations for macroporous silica, zeolites as well as mesoporous MCM-41 silica. It has been shown that with the DFT analysis reliable results for the pores size in MCM-41 materials (both for unmodified and surface modified samples) can be obtained [136].

Inspection of Table 5.2, Figures 5.1 and 5.2 reveals that the derived surface area, pore diameter from the DFT analysis and pore volume of the basic MCM-41 material is in good agreement with the literature data [22-23,33,136]. It is also seen that the BJH method underestimates the pore diameter substantially, as mentioned earlier. Furthermore, a significant reduction in surface area, total pore volume and pore diameter of the MCM-41 samples upon alkyl chain attachment is observed. The actual values depend on the chain length of the alkylsilane and, in particular, on its functionality, and thus on the surface coverage.

The MCM-41 samples which were surface modified with the trifunctional alkylsilanes exhibit a stronger reduction in surface area, pore size and total pore volume than those from surface modified with monofunctional silanes. In general, the pore size distribution is broadened after surface modification which reflects a non-uniformity of the surface modified MCM-41 channels. The strongest reduction in surface area and pore volume is observed for the two samples which were endcapped with HMDS. Here, the sample from treatment with the monofunctional alkylsilane, M-C8ME, exhibits a larger effect, which is explainable by the low surface coverage of the parent M-C8M samples. From the substantial reduction of these surface quantities, it is clear that smaller trimethylsilyl groups can deeply penetrate into channels resulting in a better surface coverage with enhanced surface hydrophobicity.

Table 5.2: Nitrogen sorption parameters for MCM-41 materials before and after surface modification.

Material code	$S_{\text{BET}}$ ( $\text{m}^2/\text{g}$ )	$V_{\text{p}}$ ( $\text{ml}/\text{g}$ )	BJH $D_{\text{pore}}$ (nm)	DFT $D_{\text{pore}}$ (nm)	% C	SC ( $\mu\text{mol}/\text{m}^2$ )
MCM-41	845	0.83	3.10	4.2	-	-
M-C4T	684	0.53	2.46	3.3	5.5	1.69
M-C8T	667	0.49	2.39	3.2	8.5	1.32
M-C8TE	616	0.37	2.32	3.0	11.9	2.06
M-C4M	705	0.65	2.60	3.6	1.9	0.50
M-C8M	721	0.69	2.78	3.7	1.5	0.19
M-C8ME	528	0.44	2.30	3.4	9.2	1.40

( $S_{\text{BET}}$ : BET surface area,  $V_{\text{p}}$ : total pore volume,  $D_{\text{pore}}$ : pore diameter, % C: weight percent of carbon in the samples, SC: surface coverage of chemically bonded ligands.)

### 5.3.3 Scanning Electron Microscopy

SEM pictures of the spheres of Kromasil silica and calcined MCM-41 silica are shown in Figure 5.3. The pictures clearly demonstrate that the spherical morphology of the silica particles is retained during the pseudomorphic synthesis of the MCM-41 spheres. It should be noted that the silica spheres of commercial Kromasil are not completely monodisperse in diameter, and the size distribution is preserved during the pseudomorphic transformation. Moreover, agglomeration of the MCM-41 silica spheres is not observed. It should be mentioned that in the MCM-41 product (Figure 4.3, right) additional undefined material is observed on the beads. This seems to be a general phenomenon of the pseudomorphic transformation, which so far has not been examined in further detail.

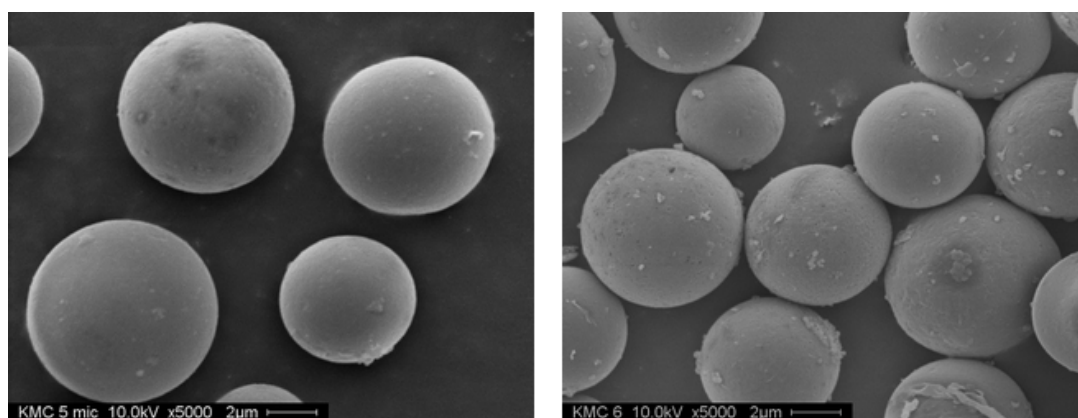


Figure 5.3: SEM micrographs for Kromasil silica (left) and MCM-41 silica (right).

### 5.3.4 Small Angle X-ray Diffraction

Figure 5.4 depicts the XRD pattern obtained for the calcined MCM-41 material obtained from the pseudomorphic route and for surface modified MCM-41 samples. Calcined MCM-41 silica shows three Bragg peaks at low angles, a strong (100) as well as the (110) and (200) reflections of lower intensity, which characterize the highly ordered hexagonal pore structure in the sample. The surface-modified materials exhibit almost identical XRD pattern which clearly indicates that the basic MCM-41 pore structure remains unchanged after surface modification. In the case of the endcapped materials, the (110) and (200) reflections become weaker and are broadened. This observation points to a lower long-range order because of (unordered) additional scattering material inside the pores.

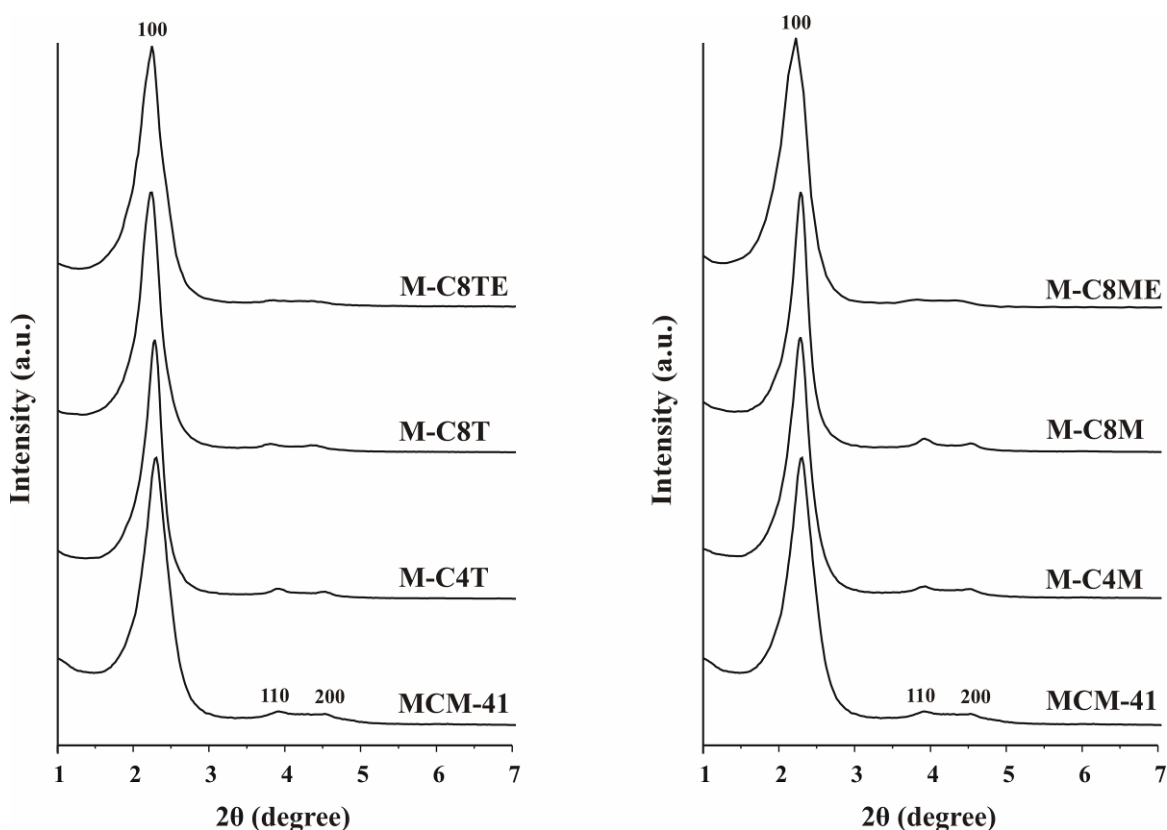


Figure 5.4: XRD patterns for MCM-41 materials before and after surface modification with trifunctional silanes (left), and monofunctional silanes (right).



### 5.3.5 $^{29}\text{Si}$ NMR Spectroscopy

$^{29}\text{Si}$  NMR spectroscopy was employed for the determination of the surface species, amount of alkyl chain attachment and degree of cross linking of the attached alkylsilanes.  $^{29}\text{Si}$  CP/MAS NMR spectra of the unmodified and modified MCM-41 samples are shown in Figure 5.5, and the  $^{29}\text{Si}$  chemical shifts are reported in Table 5.3. The  $^{29}\text{Si}$  resonances around -92, -102 and -110 ppm originate from the structural units of the MCM-41 support and reflect surface silanol groups, i.e.,  $\text{Q}^2$  and  $\text{Q}^3$  units, and interior, completely condensed  $\text{Q}^4$  units, respectively ( $\text{Q}^n = \text{Si}(\text{OSi})_n(\text{OH})_{4-n}$ , with  $n=1$  to 4) [95,97]. After attachment of the butyl or octyl silanes, the intensities of  $\text{Q}^2$  and  $\text{Q}^3$  units, bearing surface hydroxyl groups, are significantly reduced, while the intensity for the  $\text{Q}^4$  units increases. This trend continues for the endcapped samples which exhibit an additional considerable growth for the  $\text{Q}^4$  signal intensity.

The  $\text{Q}^3$  signal intensity for the samples modified with monofunctional alkylsilanes is found to be higher than for those obtained from trifunctional alkylsilanes, which is consistent with the lower surface coverage. This can be related to the lower reactivity of the former silylation reagent due to the lower probability (only one reactive group available) to react with surface silanols. Further reasons might be the bulky methyl groups of the monofunctional alkylsilane, which provide a steric hindrance for the binding of other alkylsilane chains in close vicinity to a surface-bound alkylsilane, and the lack of cross-linking reactions due to the presence of a single reactive group.

For the endcapped materials, an additional peak at about 13 ppm [ $\text{M} = \text{R}_3\text{Si}(\text{OSi}-)$ ] is found arising from the trimethylsilyl groups of the endcapping reagent. For sample, M-C8ME (derived from the monofunctional alkylsilane) this peak also contains a small signal component from the attached monofunctional alkylsilane chains of the first surface modification step. Hence, for sample M-C4M this latter signal is clearly visible in Figure 5.5, while for sample M-C8M, due to the low surface coverage, the respective resonance is relatively weak.

Table 5.3:  $^{29}\text{Si}$  chemical shifts for MCM-41 materials before and after surface modification.

Material code	$^{29}\text{Si}$ Chemical Shift (ppm)						
	Q <sup>2</sup>	Q <sup>3</sup>	Q <sup>4</sup>	T <sup>1</sup>	T <sup>2</sup>	T <sup>3</sup>	M
MCM-41	-93.0	-102.5	-111.8	-	-	-	-
M-C4T	-92.2	-102.9	-110.0	-49.8	-57.9	-68.2	-
M-C8T	-92.4	-102.3	-110.0	-49.3	-56.9	-65.8	-
M-C8TE	-	-102.7	-110.4	-50.5	-57.5	-66.7	12.7
M-C4M	-92.9	-102.4	-111.3	-	-	-	13.3
M-C8M	-92.7	-102.2	-110.6	-	-	-	13.1
M-C8ME	-	-102.4	-109.7	-	-	-	12.6

The presence of T<sup>1</sup>, T<sup>2</sup> and T<sup>3</sup> peaks (at about -49 ppm, -57 ppm and -66 ppm) for the MCM-41 samples treated with trifunctional alkylsilanes clearly prove the attachment and cross-linking of these chains at the MCM-41 silica surface ( $\text{T}^n = \text{RSi}(\text{OSi})_n(\text{OH})_{3-n}$ ,  $n=1, 2, 3$ ) [54]. They refer to trifunctional groups without (T<sup>1</sup>), with partial (T<sup>2</sup>) and complete cross-linking (T<sup>3</sup>). For sample M-C4T, the intensity of T<sup>1</sup> and T<sup>2</sup> peaks is higher as compared to sample M-C8T which is in agreement with the findings for the surface coverage.

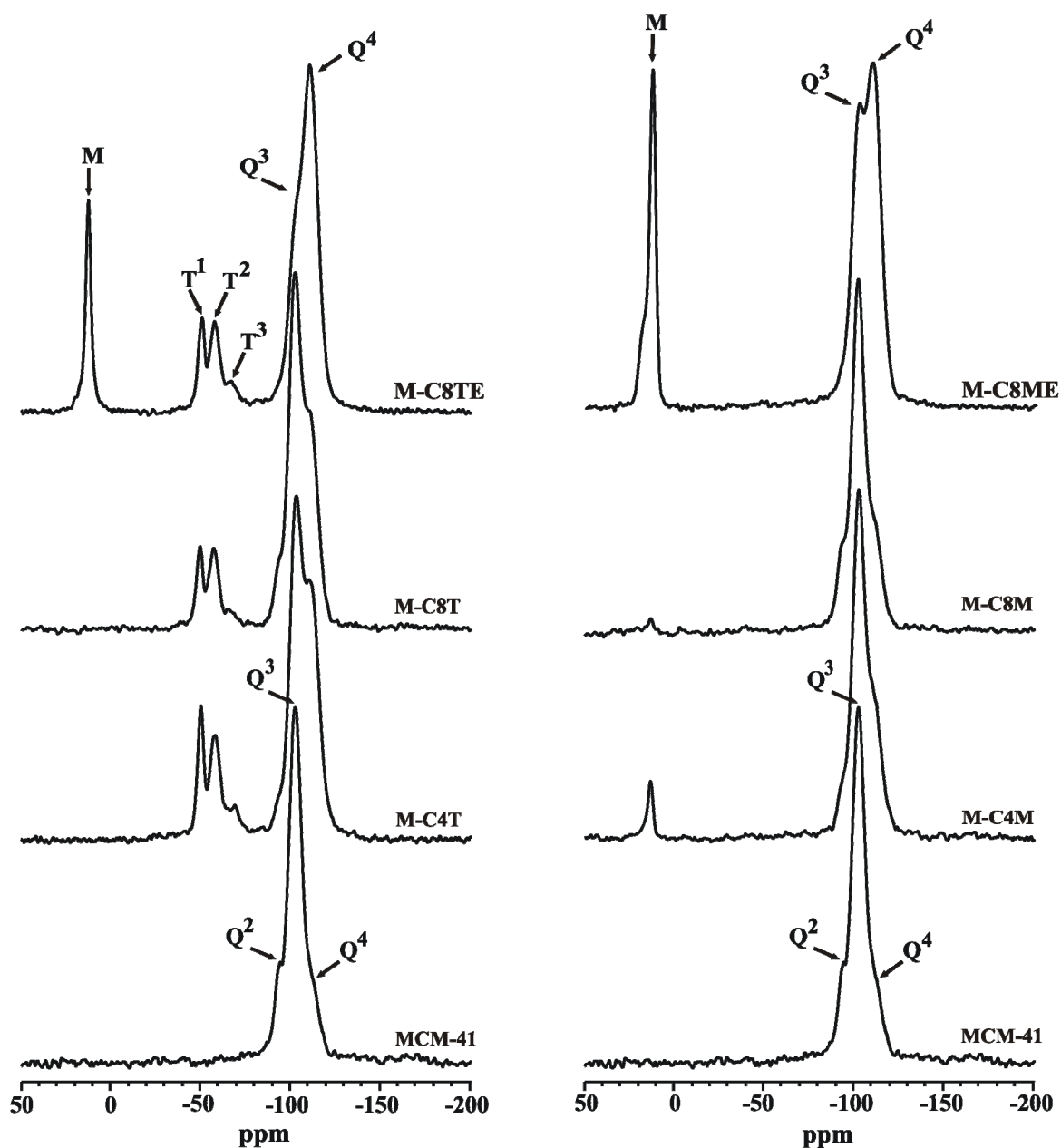


Figure 5.5:  $^{29}\text{Si}$  CP/MAS NMR spectra of MCM-41 materials before and after surface modification with trifunctional silanes (left), and monofunctional silanes (right).

All  $^{29}\text{Si}$  NMR spectra discussed so far were recorded under  $^{29}\text{Si}\{\text{H}\}$  cross polarization conditions to increase the signal-to-noise ratio. Cross-polarization experiments, however, do not give the correct signal intensities, and provide enhanced intensities for the resonances of those  $^{29}\text{Si}$  nuclei with adjacent protons. Therefore, single pulse  $^{29}\text{Si}$  NMR spectra, given in Figure 5.6, were recorded to determine the relative amount of silanols on the silica surface, and to compare the amounts before and after surface modification. The  $^{29}\text{Si}$  chemical shifts of the various species and their relative intensities obtained by spectral deconvolution are reported in Table 5.4.

Table 5.4: Spectral parameters from deconvolution of  $^{29}\text{Si}$  single pulse spectra (chemical shifts ( $\delta$ ), line widths (FWHM) and relative intensities (I)).

Material code	$\text{Q}^2$			$\text{Q}^3$			$\text{Q}^4$			$\text{T}^1$	$\text{T}^2$	$\text{M}$
	$\delta$ (ppm)	FWHM (Hz)	I (%)	$\delta$ (ppm)	FWHM (Hz)	I (%)	$\delta$ (ppm)	FWHM (Hz)	I (%)	$\delta$ (ppm)	$\delta$ (ppm)	$\delta$ (ppm)
MCM-41	-92.7	330	1	-102.0	986	44	-110.0	787	55	-	-	-
M-C4T	-	-	-	-101.9	724	22	-111.2	778	78	-50.2	-57.9	-
M-C8T	-	-	-	-101.7	680	24	-111.0	790	76	-50.6	-57.5	-
M-C8TE	-	-	-	-	-	-	-110.0	-	100	-51.1	-58.0	12.7
M-C4M	-	-	-	-102.0	673	28	-111.3	737	72	-	-	-
M-C8M	-	-	-	-102.2	760	32	-110.8	713	68	-	-	-
M-C8ME	-	-	-	-	-	-	-110.3	-	100	-	-	12.4

The derived intensities for the  $\text{Q}^3$  and  $\text{Q}^4$  species, as given in Table 5.4, support the expected structural changes by surface modification with the alkylsilanes. Hence, the relative amount of the  $\text{Q}^3$  species decreases, while - due to the formation of new Si-O-Si units - the amount of  $\text{Q}^4$  species increases. In general, the derived signal intensities are in complete agreement with the surface coverage data, given in Table 5.2. That is, an increasing surface coverage is accompanied by an intensity reduction of the  $\text{Q}^3$  units along with an intensity rise of the  $\text{Q}^4$  group resonance. Single pulse  $^{29}\text{Si}$  NMR spectra also show the presence of cross-linking of the chains. However, the intensity of the  $\text{T}^3$  peaks is very low.

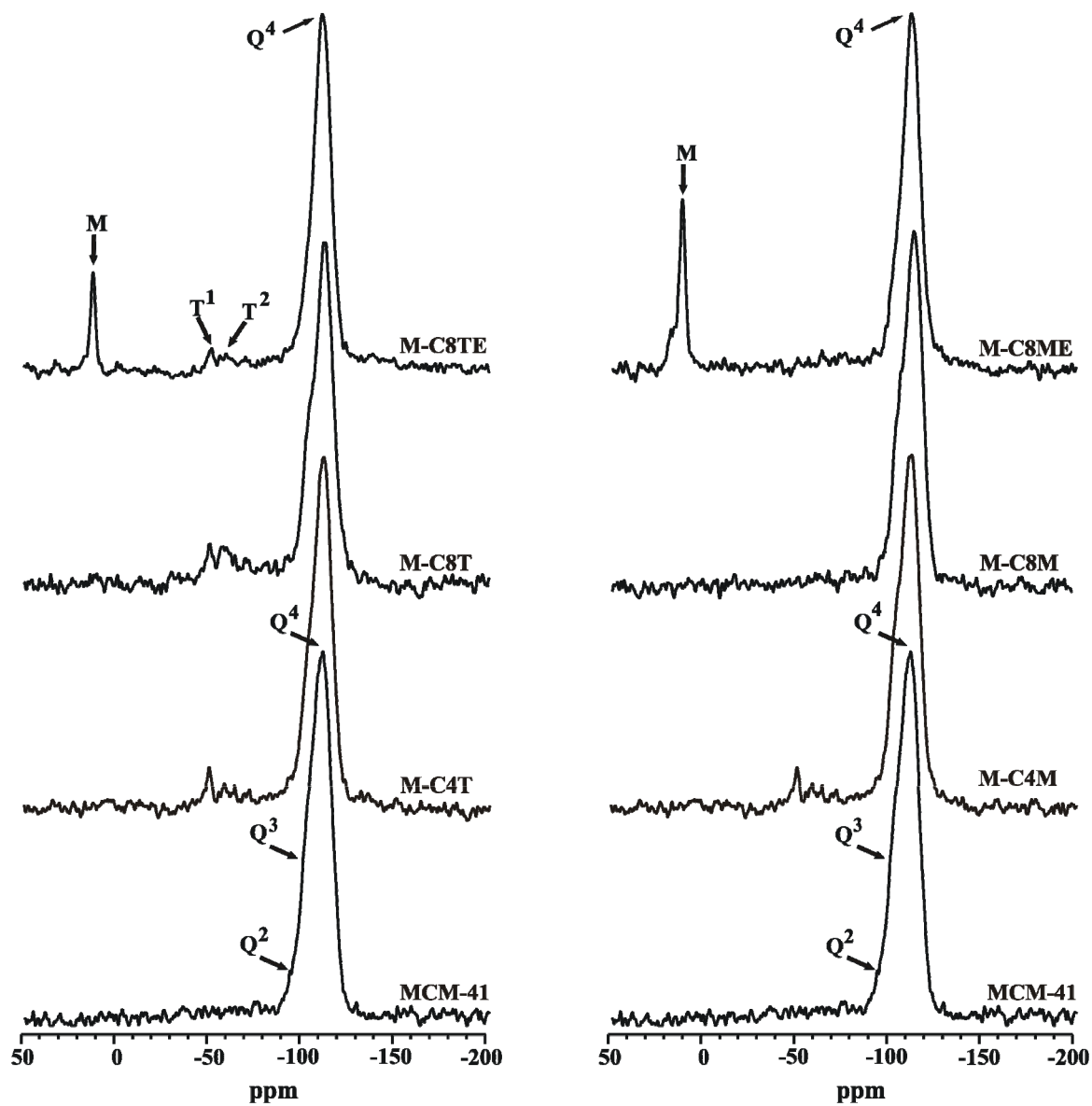


Figure 5.6:  $^{29}\text{Si}$  single pulse NMR spectra of MCM-41 materials before and after surface modification with trifunctional silanes (left) and monofunctional silanes (right).

### 5.3.6 $^{13}\text{C}$ NMR Spectroscopy

$^{13}\text{C}$  NMR spectroscopy was used to study the organic components after attaching alkylsilanes to the MCM-41 silica surface. For alkylsilanes with longer alkyl chains (i.e., with 10 or more methylene segments), the  $^{13}\text{C}$  resonances of the inner methylene groups can be used to get qualitative information about the chain conformational order.

Figure 5.7 depicts experimental  $^{13}\text{C}$  CP/MAS NMR spectra for the present MCM-41 materials after surface modification. The signals can be assigned on the basis of solution NMR data for the respective alkylsilanes [148-149]. The  $^{13}\text{C}$  chemical shifts of the various species are reported in Table 5.5, and are in good agreement with these literature values.

As can be seen, the signal-to-noise ratio varies with the actual sample which again reflects the differences in surface coverage. For the MCM-41 samples, surface modified with trifunctional silanes, carbon C-1 resonates at about 13 ppm, while for those obtained from monofunctional silanes the respective  $^{13}\text{C}$  NMR signal occurs at about 17 ppm.

For the samples modified with trifunctional silanes, an additional peak around 50 ppm shows up, which can be assigned to methoxy groups bound to silicon. This signal could be explained either by non-reacted methoxy groups of the alkylsilanes. Another, more likely explanation is the presence of methoxy groups which were released during the hydrolysis of the trifunctional silanes, and which are subsequently bound to the surface silanol groups [146].

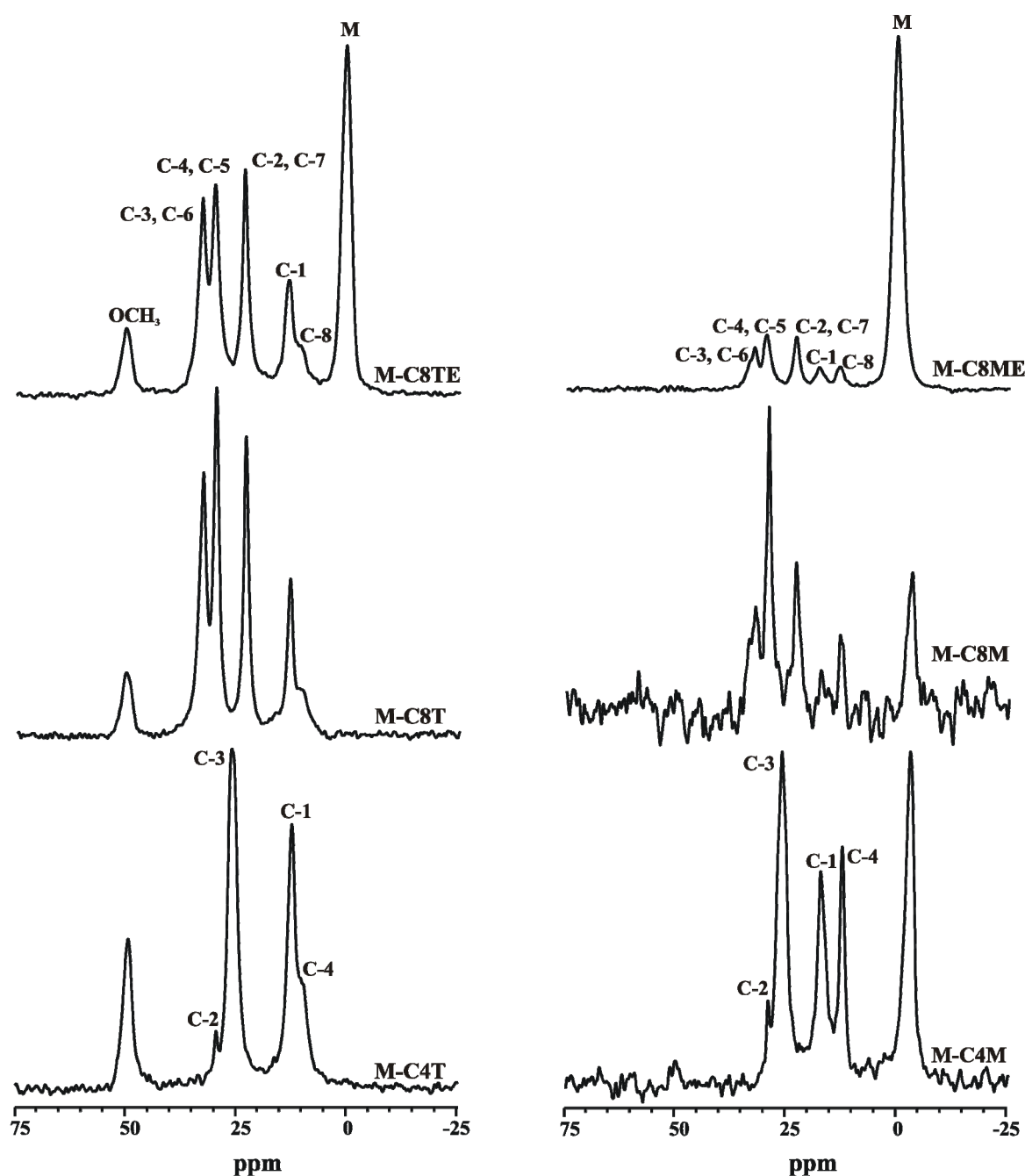


Figure 5.7:  $^{13}\text{C}$  CP/MAS NMR spectra of MCM-41 materials after surface modification with trifunctional silanes (left), and monofunctional silanes (right).

The trimethylsilyl groups after endcapping with HMDS resonate at about 0.4 ppm and 0.1 ppm for sample M-C8TE and M-C8ME, respectively. In the latter case, this signal also contains a spectral component from the methyl groups of the attached dimethyloctylsilane. For samples M-C8M and M-C4M (i.e., without endcapping), these methyl groups bound to the silicon atom of the alkylsilane resonate at about -3.0 ppm.

Table 5.5:  $^{13}\text{C}$  chemical shifts and assignment of surface modified MCM-41 materials.

Sample	Carbon position	$^{13}\text{C}$ shift (ppm)
M-C4T	OCH <sub>3</sub>	49.3
	C-4	10.5
	C-1	12.7
	C-3	25.8
	C-2	29.6
M-C8T	OCH <sub>3</sub>	50.2
	C-8	11.0
	C-1	13.2
	C-2, C-7	23.2
	C-4, C-5	29.9
	C-3, C-6	32.8
M-C8TE	OCH <sub>3</sub>	50.3
	Si(CH <sub>3</sub> ) <sub>3</sub>	0.4
	C-8	11.0
	C-1	13.5
	C-2, C-7	23.4
	C-4, C-5	30.1
	C-3, C-6	33.0
M-C4M	Si(CH <sub>3</sub> ) <sub>2</sub> R	-3.5
	C-4	12.7
	C-1	17.0
	C-3	25.7
	C-2	29.1
M-C8M	Si(CH <sub>3</sub> ) <sub>2</sub> R	-3.1
	C-8	13.2
	C-1	17.3
	C-2, C-7	23.1
	C-4, C-5	29.2
	C-3, C-6	32.2
M-C8ME	Si(CH <sub>3</sub> ) <sub>2</sub> R, Si(CH <sub>3</sub> ) <sub>3</sub>	0.1
	C-8	13.1
	C-1	17.9
	C-2, C-7	23.0
	C-4, C-5	29.8
	C-3, C-6	32.5

### 5.3.7 FTIR Measurements

For the examination of the conformational properties of attached alkyl chains several conformation-sensitive vibrational bands can be exploited [110-111]. Among these, the symmetric and antisymmetric CH<sub>2</sub> stretching bands (2800-3000 cm<sup>-1</sup>) are the most



intense signals, and in the majority of cases are easily accessible. Their positions as a function of external parameters, like temperature, pressure or sample constitution, can be used for a qualitative discussion of the conformational order in the aliphatic chains. Hence, changes in the positions of these bands are directly related to the alteration of the *trans/gauche* ratios. A band shift towards lower wavenumbers reflects an increase in conformational order (i.e., higher amount of *trans* conformers and reduced mobility), while a shift towards higher wavenumbers points to an increasing conformational disorder with a higher amount of *gauche* conformers and thus enhanced chain flexibility. Similar information can in principle be derived from the bandwidths, although the respective alterations are typically less pronounced [105].

Variable temperature FTIR studies were performed for the present surface modified MCM-41 materials in a temperature range between 193 K and 353 K. Representative FTIR spectra, covering the region of the CH<sub>2</sub> and CH<sub>3</sub> stretching bands, are shown in Figures 5.8 and 5.9. The bands are assigned according to previous reports [108,150-155]. The CH<sub>3</sub> groups exhibit antisymmetric (CH<sub>3</sub>-a) and symmetric (CH<sub>3</sub>-s) stretching modes near 2962 cm<sup>-1</sup> and 2872 cm<sup>-1</sup> while for the CH<sub>2</sub> groups these modes occur near 2927 cm<sup>-1</sup> (CH<sub>2</sub>-a) and 2857 cm<sup>-1</sup> (CH<sub>2</sub>-s), respectively. It is interesting to note that for sample M-C4T (see Figure 5.8) the symmetric CH<sub>2</sub> band is split into two bands at 2866 cm<sup>-1</sup> and 2854 cm<sup>-1</sup> at 193 K. According to Fox and Martin [154-155], this split can arise from coupling between the two methylenes. A similar split-up of this IR band has also been reported earlier for conventional silica modified with butylsilanes [99,156-157]. At higher temperatures, the splitting of bands becomes successively smaller and finally a single band at about 2858 cm<sup>-1</sup> is observed showing an increasing conformational disorder with increasing temperature.

For sample M-C8T, at 193 K the antisymmetric and symmetric CH<sub>2</sub> stretching bands are visible at 2931 cm<sup>-1</sup> and 2859 cm<sup>-1</sup>, respectively. Upon temperature increase, these peaks are slightly shifted towards higher wavenumbers to reach at 353 K values of 2932 cm<sup>-1</sup> and 2860 cm<sup>-1</sup>, respectively. Such shifts for the CH<sub>2</sub> stretching bands are well documented for many materials [97,100,105]. They point to an increase in conformational disorder and enhanced chain mobility [158]. In addition, a broadening of the IR bands is registered with increasing sample temperature which also can be attributed to the enhanced chain flexibility. It is seen that the IR spectra for sample M-C8TE closely resemble those for sample M-C8T. The only difference is the higher intensity of the CH<sub>3</sub>

stretching modes in the M-C8TE spectra due to the additional methyl groups in the endcapped material.

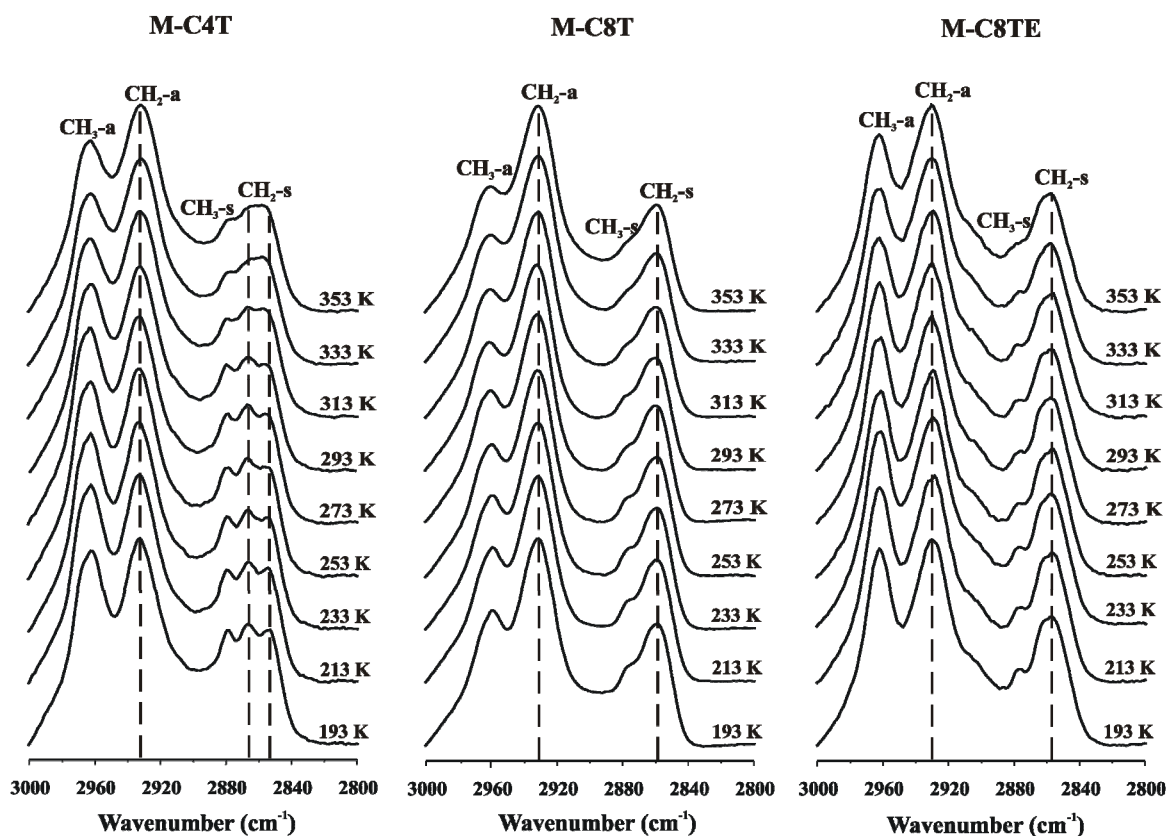


Figure 5.8: Variable temperature FTIR spectra of MCM-41 samples surface modified with trifunctional alkylsilanes.

Figure 5.9 shows the FTIR spectra of MCM-41 materials surface modified with monofunctional chains. Here, two methyl groups are bound to the silicon atom in the alkyl chains which explains the higher relative intensity of the antisymmetric  $\text{CH}_3$  stretching bands. For sample M-C4M, a split-up of the symmetric  $\text{CH}_2$  band, as discussed above for sample M-C4T, is not observable. Sample M-C8M shows the antisymmetric  $\text{CH}_2$  stretching band at  $2927\text{ cm}^{-1}$  and the symmetric  $\text{CH}_2$  stretching band at  $2856\text{ cm}^{-1}$  with a slight shift towards larger wavenumbers upon increasing the sample temperature. The same behaviour is found for sample M-C8ME. For MCM-41 samples surface modified with the monofunctional alkylsilanes, the  $\text{CH}_2$  stretching bands appear at slightly lower wavenumbers as compared to the trifunctional materials which is attributed to the lower conformational order of the monofunctional chains.

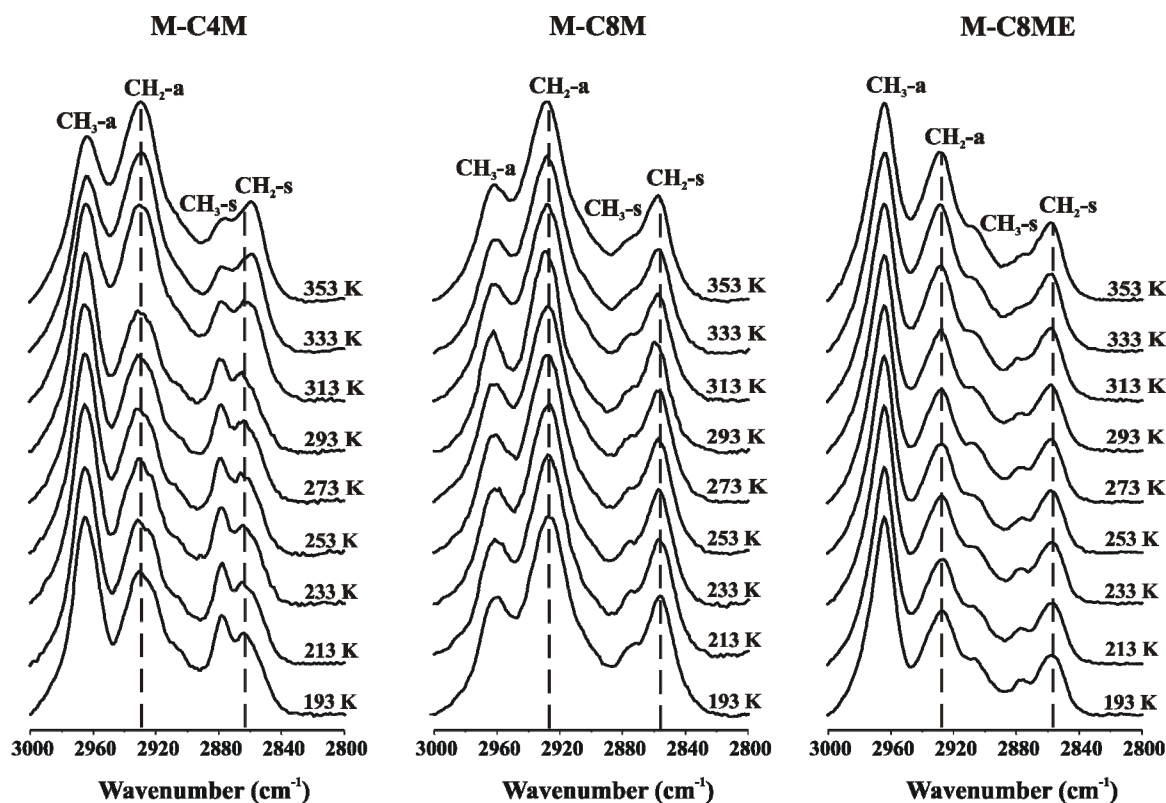


Figure 5.9: Variable temperature FTIR spectra of MCM-41 samples surface modified with monofunctional alkylsilanes.

### 5.3.8 HPLC Measurements

The most widely used method of modern liquid chromatography is reversed-phase liquid chromatography with alkyl-bonded stationary phases. In reversed-phase chromatography, the separation mechanism is dependent upon interactions between the analyte components, the mobile phase and the surface of the solid stationary phase. RPLC typically uses a polar mobile phase, such as a mixture of methanol or acetonitrile with water. Water-acetonitrile mixtures demonstrated good chromatographic efficiencies for aromatic analyte mixtures. The mechanism of separation is primarily attributed to solvophobic or hydrophobic interactions. Silica is the most frequently used stationary material, and is characterized by a good versatility, high column efficiency and mechanical stability, and possesses an easily controllable particle size and porosity. Chromatographic silica materials are available from both spherically and irregularly shaped particles. Spherical particles are superior due to the ease and reproducibility with which the particles can be packed into the columns [159].

It has been shown that spherical mesoporous MCM-41 silica possess an even better chromatographic performance than normal silica stationary phases which can be attributed to their high surface area, well-defined pore size and uniform particle size [6,160].

The MCM-41 silica surface contains both silanols (Si–OH) and siloxane units (Si–O–Si). Siloxane units are hydrophobic, and it has been shown that they have very little to do with solute retention [161]. Silanol groups are considered to be the strong adsorption sites, and they are hydrophilic in nature. During surface modification, the silanols react with the alkylsilane groups. However, for steric and reactivity reasons, the surface modification might not be complete and residual silanols remain on the silica surface [107]. The non-reacted silanol groups are weakly acidic, and their presence causes difficulties when analyzing basic compounds, as found, for instance, in biomedical, pharmaceutical, and environmental compounds. To remove the effect of these residual silanols, endcapping may be carried out by using small, highly reactive silylation reagents, like HMDS.

In the present work, the basic MCM-41 material and the surface modified MCM-41 silica spheres were slurry-packed into an HPLC column in order to separate a test mixture, NIST SRM 870, which consists of five organic components (uracil, toluene, ethylbenzene, quinizarin and amitriptyline; see Figure 5.10) under controlled conditions, i.e., mobile phase, flow, and temperature. This procedure provides an objective and standardised evaluation of the behaviour of a chromatographic packing [162].

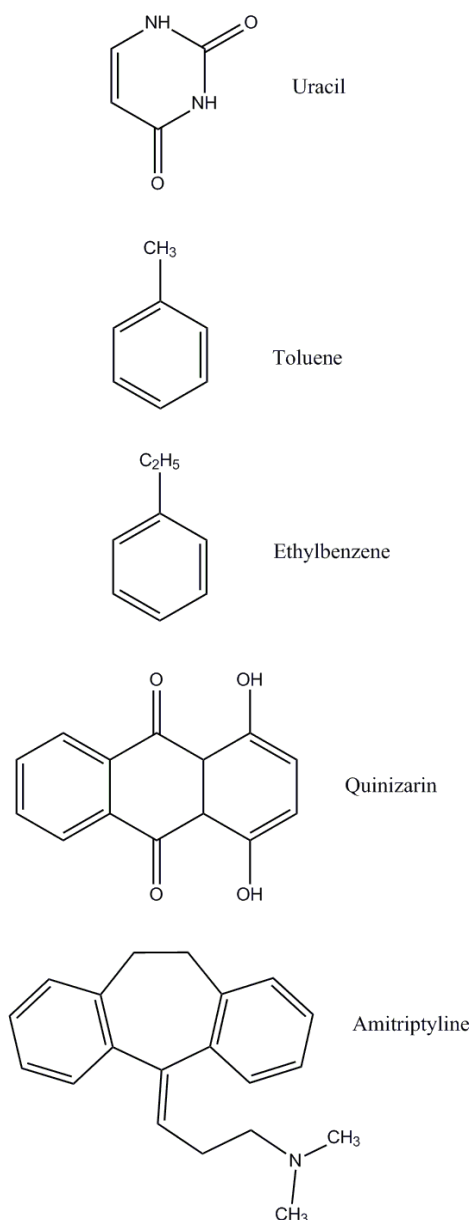


Figure 5.10: Chemical structures of components in test mixture SRM 870.

After some test runs, an optimum mobile phase was assigned as 50 % acetonitrile and 50 % water (v/v), and the optimum flow rate was determined to 1.0 ml/min. The eluent time of organic components under the optimum separation conditions follows the order: uracil < toluene < ethylbenzene < quinizarin < amitriptyline. As expected, for reversed-phase chromatography, the more polar compounds elute faster than the less polar molecules [19]. In the present case, uracil, the most polar component, elutes first.

Figure 5.11 shows the separation chromatograms of the aforementioned test mixture by using the surface modified MCM-41 silica columns. In the majority of the cases, well-separated peaks for uracil, toluene, ethylbenzene, quinizarin, and amitriptyline can be

observed. In contrast, the HPLC performance of the column packed with unmodified MCM-41 spheres was found to be very poor.

Surface coverage and alkyl chain lengths are the main factors which affect the chromatographic performance of the stationary phases. Hence, the test mixture is well separated with good peak shapes for the stationary phases with higher surface coverage for the alkylsilanes. It is seen that generally the alkylsilanes with shorter chains give better peak shapes, in agreement with the findings from other studies [163]. Endcapping also improves the peak shapes and the chromatographic performance. However, like the trend for longer alkylsilane chains, the increasing hydrophobicity of the surface, in general, also increases the elution time. Materials with low surface coverages often yield tailing peaks for basic analytes because of their interaction with residual silanols. At higher surface coverage, only a small number of silanols remains, and symmetric peak shapes are observed [164].

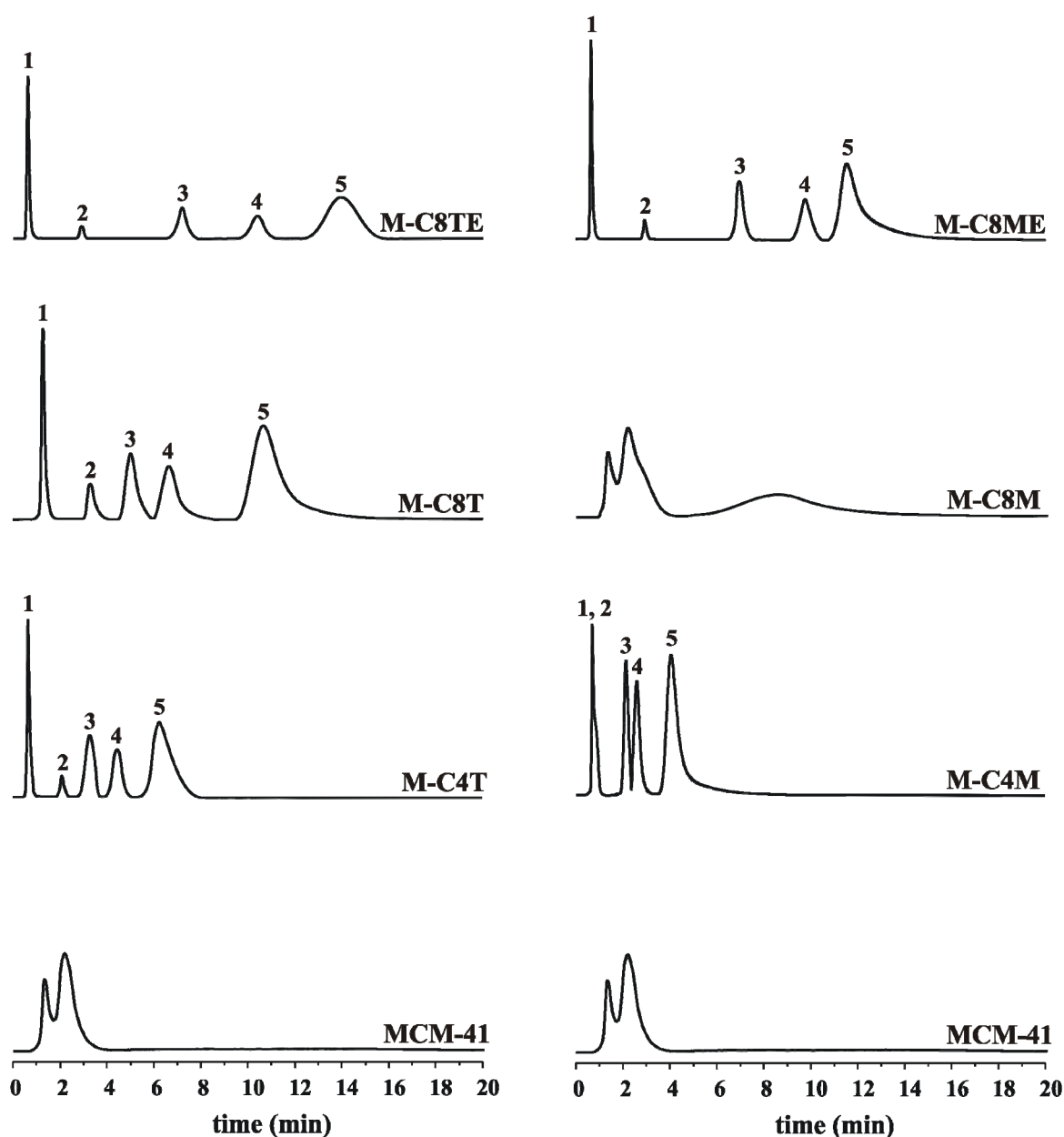


Figure 5.11: HPLC diagrams for test mixture SRM 870 mixture: uracil (1), toluene (2), ethylbenzene (3), quinizarin (4) and amitriptyline (5) using a acetonitrile/water mixture (50/50, v/v) as the mobile phase at flow rate of 1.0 ml/min at 254 nm for MCM-41 materials before and after surface modification.

## 5.4 Concluding Remarks

The main goal of the present study is to combine the pseudomorphic transformation route for MCM-41 synthesis and the surface modification technique to obtain new materials with improved HPLC performance. Surface modification of the MCM-41 silica spheres was made by using alkylsilanes of different alkyl chain lengths and functionalities. The

investigations showed that the mesoporosity and pore symmetry of the material is retained after surface modification, as derived from nitrogen sorption and XRD experiments. It was found that trifunctional silanes provide higher surface coverage because of their higher reactivity and the possibility for cross-linking. For the alkylsilanes with shorter chain lengths higher surface coverages were found, as they can also bind to the interior of the mesopores. The chromatographic performance of all samples was tested. A better separation performance was found for the MCM-41 samples with higher surface coverage. For the materials modified with shorter alkylsilanes sharper peaks of better symmetry were observed. A further improvement of the chromatographic separation performance could be achieved by subsequent endcapping with HMDS. Here, the increased hydrophobicity yielded longer elution times. In summary, these studies have demonstrated that such mesoporous silica materials possess a great potential for chromatographic applications.



## **Chapter 6**

# **Structural Characterization of Alkyl Bonded MCM-41 Silica Materials Prepared by the Supercritical Fluid Method**

### **6.1 Introduction**

A comprehensive study is conducted on alkyl bonded mesoporous MCM-41 silica materials prepared using supercritical carbon dioxide (sc-CO<sub>2</sub>) as a bonding medium. The higher surface coverages of resulting materials as compared with organic solvent produced bonded phases are attributed to greater accessibility of the silica silanols in sc-CO<sub>2</sub>. The variation in pore dimensions depends on the nature of bonded alkyl chains. Supercritical carbon dioxide (sc-CO<sub>2</sub>) has been demonstrated to be an effective reaction medium for the generation of chromatographic stationary phases [59]. Supercritical CO<sub>2</sub> has certain properties that make it an attractive solvent compared with traditional organic solvents. It is non-flammable, more environmentally friendly, and considerably less hazardous than most organic solvents. In the present work, we provide a systematic report on the sc-CO<sub>2</sub> surface modification of mesoporous MCM-41 materials for the preparation of alkyl bonded phases. Their surface coverages are compared with organic solvent produced bonded phases using surface polymerization method (described in Chapter 5). The pore dimensions can be progressively decreased by using alkyl chains of different lengths and functionalities. MCM-41 silica materials are surface modified by mono- and trifunctional butyl- (C<sub>4</sub>) and octylsilanes (C<sub>8</sub>). Because of steric hindrance, the longer chains primarily bind only to the outer surface and only few chains are attached to the mesopores, leaving a large fraction of unreacted surface silanol groups which are considered to lead to surface hydrophilicity [147]. These residual silanol groups are weakly acidic, and cause peak tailing for basic solutes which reduces the resolution and

column efficiency in chromatographic applications. These remaining silanol groups are endcapped using hexamethyldisilazane (HMDS).

The resulting materials are characterized before and after surface modification using various characterization techniques. The specific surface area is calculated using the BET method while information about pore diameter is obtained by DFT calculations. The degree of organization is investigated by XRD, and SEM analysis gives information about morphology of the material. Solid-state  $^{29}\text{Si}$  and  $^{13}\text{C}$  NMR spectroscopies are employed to probe the attachment of the alkyl chains on MCM-41 materials. The conformational state and mobility of bonded alkyl chains are examined using Fourier transform infrared (FTIR) spectroscopy.

## 6.2 Sample Preparation

### 6.2.1 Chemicals

Commercially available silica, Kromasil (300 Å; 5 μm) was obtained by Akzo-Nobel (Bohus, Sweden). Silanes, *n*-octyltrimethoxysilane, *n*-octyldimethylmethoxysilane, *n*-butyltrimethoxysilane and *n*-butyldimethylmethoxysilane (purity: 97 %), used for the surface modification, 1,1,1,3,3,3-hexamethyldisilazane (HMDS; purity: 97 %), cetyltrimethylammonium bromide (CTAB) and sodium hydroxide (NaOH) were obtained from Aldrich Chemical Company (Sigma-Aldrich Chemie, Steinheim, Germany). The CO<sub>2</sub> used in this research was obtained from Irish Oxygen (Cork, Ireland) with purity of 99.9% and a moisture content of <50 ppmv.

### 6.2.2 Reaction of Silylating Agents with MCM-41 Silica Material

Mesoporous MCM-41 silica spheres were prepared by using Kromasil as silica source and following the pseudomorphic transformation route as described in Chapter 5.

Reactions in sc-CO<sub>2</sub> were carried out using an Isco model 260D syringe pump with an external 25 ml stainless steel reaction cell with 0.625" sapphire windows at either end of the reaction cell, all of which were obtained from Thartech Inc. (USA). The temperature of the reaction cell was controlled using a Horst heating tape (1m in length) connected to a Horst temperature controller, which made contact with the reaction cell via a thermocouple. These were obtained from Sigma–Aldrich. Agitation was achieved by stirring with a Teflon coated magnetic stirrer bar in the reaction cell and a magnetic stirrer

plate underneath the cell. The magnetic stirrer plate without heating (Midi-MR 1 digital IKAMAG) was purchased from Ika Werke Gmbh & Co. KG (Germany).

For reactions in sc-CO<sub>2</sub>, unmodified MCM-41 silica material along with the chosen alkyl silane reagent and a magnetic stirrer bar were added to the stainless steel reaction cell. The quantity of alkyl silane reagent used was generally a three-fold excess (12 μmol of silane per m<sup>2</sup> of calcined MCM-41 silica surface area). The temperature of the reaction cell was raised beyond the critical temperature of CO<sub>2</sub> (31.1 °C) above which CO<sub>2</sub> becomes supercritical, once above the critical pressure (73.8 bar). Once the temperature was established, the reaction chamber was filled with CO<sub>2</sub> to establish a pressure of 414 bar which is above the critical pressure for CO<sub>2</sub> (73.8 bar). Supercritical reactions were carried out at 100 °C and 414 bar. The magnetic stirrer plate was switched on, ensuring agitation of the contents of the cell (600 rpm), which was visually verified by looking through the sapphire windows at either end of the reaction cell. Following the reaction time of 3 h, the magnetic stirrer was switched off so as to allow the contents of the cell to settle for several minutes, after which the cell mixture was subjected to dynamic extraction. During this extraction period, the pressure and temperature of the reaction cell were maintained and almost 120 ml of fresh CO<sub>2</sub> was flushed through the cell. After this time, the cell was then depressurized and the surface modified MCM-41 silica offloaded as a free flowing white powder.

In case of the C<sub>8</sub> materials, the remaining silanol groups were endcapped using HMDS. To produce C<sub>8</sub> endcapped materials, after the three hours reaction time, as described above, a two-fold excess of HMDS was added to the reaction mixture. The system was again pressurised to 414 bar and the temperature raised to 100 °C. The endcapping reaction was allowed to proceed for three hours, before recovering the endcapped sc-C<sub>8</sub> materials.

## 6.3 Results and Discussion

### 6.3.1 Synthesis and Surface Modification of MCM-41 Silica Materials

MCM-41 silica spheres were prepared using pseudomorphic transformation route, as described in Chapter 5. Surface modification of MCM-41 silica material was carried out with octyl and butyl groups using the supercritical fluid method, and the resulting materials with their material codes are listed in Table 6.1. Octyl groups were attached on the calcined MCM-41 silica spheres by reaction with *n*-octyltrimethoxysilane and

*n*-octyldimethylmethoxysilane. Endcapping with HMDS was done to obtain materials with enhanced hydrophobicity. The percentage of carbon obtained from the elemental analysis for samples prepared by supercritical fluid method M-C8TE-a and M-C8ME-a are 12.45 and 11.33, respectively (see Table 6.2). These values are higher as compared to materials prepared by surface polymerization method (Chapter 5), M-C8TE-b is 11.9 and M-C8ME-b is 9.2 (see Table 6.2). The respective surface coverage for the materials surface modified with the monofunctional silanes was relatively low, since for attachment to the silica surface only one functionality is available, and no additional cross-linking of the silanes can take place. Trifunctional octylsilane provided much higher surface coverage because apart from binding to the surface silanol groups cross-linking reactions with neighbouring silane chains can occur. Hence, in this case a better chain packing with higher surface coverage, good thermal and enhanced chemical stability can be achieved.

In the same way, butylsilanes were attached on the calcined MCM-41 silica spheres by reaction with *n*-butyltrimethoxysilane and *n*-butyldimethylmethoxysilane. The percentages of carbon obtained from the elemental analysis for these samples prepared by supercritical fluid method M-C4T-a and M-C4M-a are 6.42 and 4.32, respectively, while for samples prepared by surface polymerization method, values of 5.50 (M-C4T-b) and 1.90 (M-C4M-b) are obtained (see Table 6.2). Hence, the samples prepared by the supercritical fluid method are found to have higher percentage of carbon, and therefore higher surface coverages. This is because the silica silanols which are inaccessible in organic solvents are accessible in sc-CO<sub>2</sub> which can be attributed to the unique properties of the supercritical fluid, such as gas-like diffusivities and liquid-like solubilities, as demonstrated by McCool and Tripp [60].

Table 6.1: Surface modified MCM-41 silica materials using supercritical fluid and surface polymerization methods and their material codes.

Material code	Surface modified MCM-41 silica materials
Supercritical fluid method	
M-C4T-a	MCM-41 modified with <i>n</i> -butyltrimethoxysilane
M-C8TE-a	MCM-41 modified with <i>n</i> -octyltrimethoxysilane and endcapped with HMDS
M-C4M-a	MCM-41 modified with <i>n</i> -butyldimethylmethoxysilane
M-C8ME-a	MCM-41 modified with <i>n</i> -octyldimethylmethoxysilane and endcapped with HMDS
Surface polymerization method	
M-C4T-b	MCM-41 modified with <i>n</i> -butyltrimethoxysilane
M-C8TE-b	MCM-41 modified with <i>n</i> -octyltrimethoxysilane and endcapped with HMDS
M-C4M-b	MCM-41 modified with <i>n</i> -butyldimethylmethoxysilane
M-C8ME-b	MCM-41 modified with <i>n</i> -octyldimethylmethoxysilane and endcapped with HMDS

### 6.3.2 Nitrogen Sorption Studies

Nitrogen sorption experiments were used to determine the textural properties and surface features of mesoporous materials in terms of surface area, pore size, pore size distribution and porosity. The nitrogen sorption isotherms for the unmodified and surface modified MCM-41 materials are shown in Figures 6.1 and 6.2.

The textural properties are summarized in the Table 6.2 along with the textural properties of alkyl bonded materials prepared by organic solvent. The overall appearance of all BET isotherms is very similar and typical for the group of reversible IV type isotherms. The strong rise of the BET curve for the unmodified MCM-41 sample above a relative pressure of  $p/p_0 = 0.3$  stems from the capillary condensation in the mesopores and is characteristic for a mesoporous structure. Surface modification leaves the overall appearance of these type IV isotherms practically unchanged, indicating that the textural characteristics are not altered by surface modification with butyl- and octylsilanes. For the surface modified samples, the steep adsorption steps are shifted towards lower pressures, and the adsorption plateau values, reflecting the total silica surface area, are lowered.

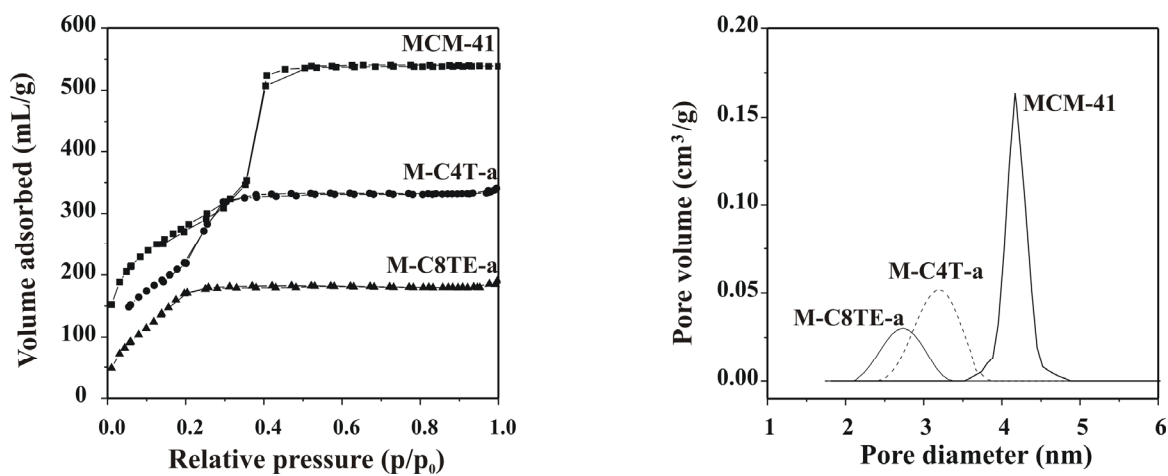


Figure 6.1: Nitrogen sorption isotherms (left) and DFT pore size distributions (right) for unmodified and surface modified MCM-41 materials with trifunctional silanes.

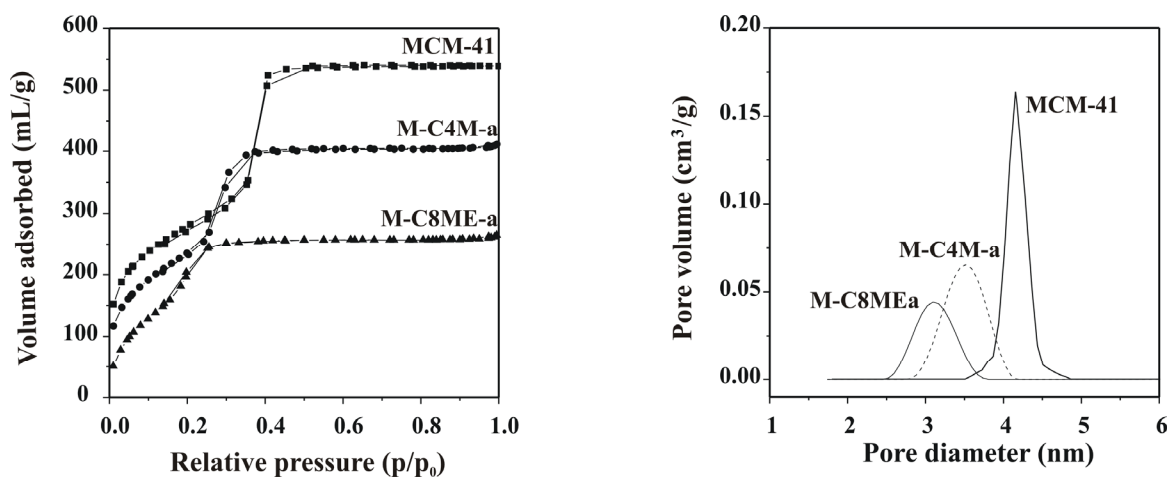


Figure 6.2: Nitrogen sorption isotherms (left) and DFT pore size distributions (right) for unmodified and surface modified MCM-41 materials with monofunctional silanes.

The pore size distribution is based on density functional theory (DFT) [69]. The pore-filling pressures were determined as a function of the pore size from sorption isotherms on MCM-41 materials. The variation of the pore fluid density with pressure and pore size has been accounted for by DFT calculations. Inspection of Table 6.2 and Figures 6.1 and 6.2 reveal that the derived values for surface area, pore diameter and pore volume of the basic MCM-41 material are in good agreement with the literature data [22-23,33,136]. There is a reduction in surface area, total pore volume and pore diameter of the MCM-41 samples upon alkyl chain attachment. The actual values depend on the nature of the alkylsilane, i.e., alkyl chain length and its functionality, and thus on the surface coverage. In case of endcapped materials the smaller trimethylsilyl groups can deeply penetrate into channels to provide better surface coverage with enhanced surface hydrophobicity.

Table 6.2: Nitrogen sorption parameters for unmodified and surface modified MCM-41 materials using supercritical fluid and surface polymerization methods.

Material code	$S_{\text{BET}}$ ( $\text{m}^2/\text{g}$ )	$V_{\text{p}}$ ( $\text{ml}/\text{g}$ )	DFT $D_{\text{pore}}$ ( $\text{nm}$ )	% C	SC ( $\mu\text{mol}/\text{m}^2$ )
Supercritical fluid method					
MCM-41	845	0.83	4.20	-	-
M-C4T-a	680	0.52	3.20	6.42	2.07
M-C8TE-a	610	0.28	2.74	12.45	2.20
M-C4M-a	726	0.63	3.52	4.32	1.22
M-C8ME-a	678	0.40	3.10	11.33	1.83
Surface polymerization method					
MCM-41	845	0.83	4.20	-	-
M-C4T-b	684	0.53	3.30	5.50	1.69
M-C8TE-b	616	0.37	3.00	11.90	2.06
M-C4M-b	705	0.65	3.60	1.90	0.50
M-C8ME-b	528	0.44	3.40	9.20	1.40

### 6.3.3 Scanning Electron Microscopy

SEM pictures of the spheres of Kromasil silica and calcined MCM-41 silica samples have been shown in Chapter 5 (see Figure 5.3).

### 6.3.4 Small Angle X-ray Diffraction

Figure 6.3 shows the XRD pattern obtained for the calcined MCM-41 and surface modified MCM-41 materials using supercritical fluid method. Calcined MCM-41 silica shows three Bragg reflections at low angles, a strong (100) reflection and the (110) and (200) reflections of lower intensity which characterize the highly ordered hexagonal pore structure in MCM-41. The surface-modified materials exhibit almost identical XRD pattern which clearly indicates that the basic MCM-41 pore structure remains unchanged by the surface modification step.

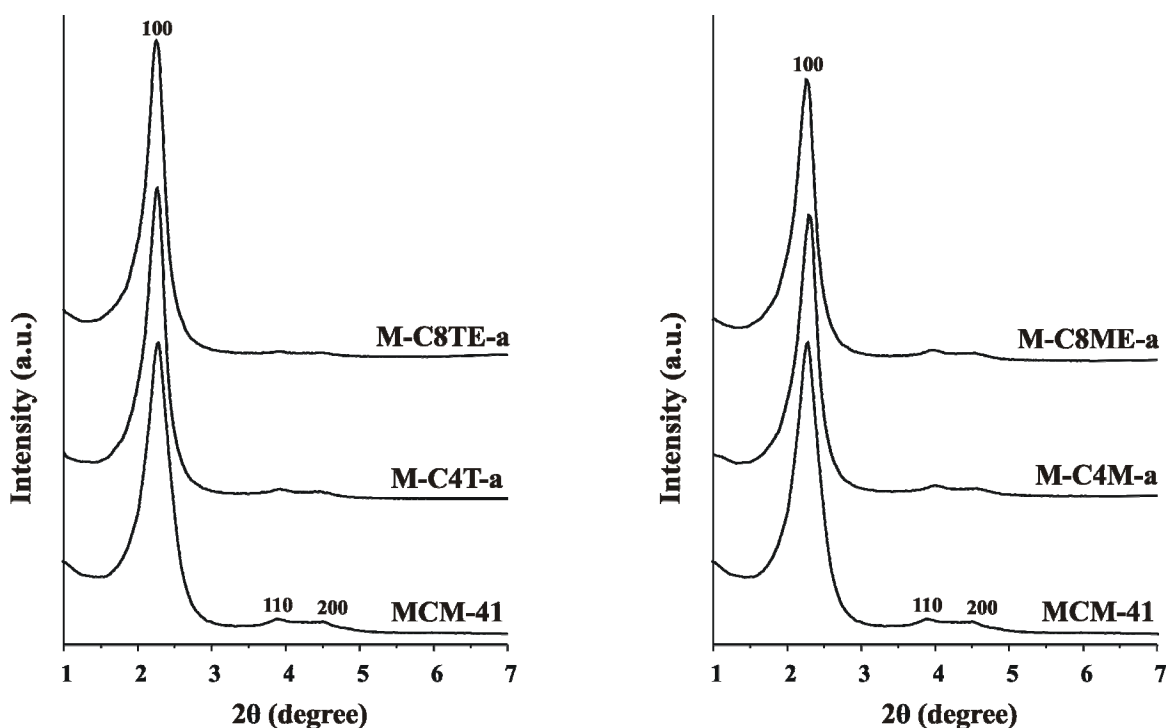


Figure 6.3: XRD patterns for the unmodified and surface modified MCM-41 materials with trifunctional silanes (left) and monofunctional silanes (right).

### 6.3.5 $^{29}\text{Si}$ NMR Spectroscopy

$^{29}\text{Si}$  NMR spectroscopy was employed for the determination of the surface species, amount of alkyl chain attachment and degree of cross linking of the attached alkylsilanes. The  $^{29}\text{Si}$  CP/MAS NMR spectra of the unmodified and surface modified MCM-41



samples are shown in Figure 6.4. The  $^{29}\text{Si}$  chemical shifts of the various species are reported in Table 6.3. The  $^{29}\text{Si}$  resonance around -92, -102 and -110 ppm originate from the structural units of the MCM-41 support and reflect surface silanol groups,  $\text{Q}^2$ ,  $\text{Q}^3$  and  $\text{Q}^4$  groups, respectively ( $\text{Q}^n$  units =  $\text{Si}(\text{OSi})_n(\text{OH})_{4-n}$ , with  $n = 1$  to 4) [95,97]. After attachment of the  $\text{C}_4$  or  $\text{C}_8$  alkylsilanes, the intensities of  $\text{Q}^2$  and  $\text{Q}^3$  groups, bearing surface hydroxyl groups, are significantly reduced, while the  $\text{Q}^4$  intensity increases.

The  $\text{Q}^3$  intensity for the samples surface modified with the monofunctional alkylsilanes is found to be higher than for those obtained from the trifunctional alkylsilanes, which is consistent with the lower surface coverage. This can be related to the lower reactivity and hence lower probability of monofunctional chains to react with surface silanol groups. Further reasons might be the bulky methyl groups of the monofunctional alkylsilane, which provide a sterical hindrance for the binding of other alkylsilane chains in the vicinity of an already surface-attached alkylsilane, and the lack of cross-linking reactions since only a single reactive group is present.

In the case of materials surface modified with octyl silanes and subsequent endcapping, an additional peak at about 13 ppm ( $\text{R}_3\text{SiOSi}=\text{M}$  group) is found due to the trimethylsilyl groups from the endcapping reaction. For the MCM-41 sample surface modified with octyl monofunctional silane, this peak also contains a finite intensity from the attached monofunctional alkylsilane chains. For instance, for sample M-C4M-a this latter signal is clearly visible in Figure 6.4, while for sample M-C8M-a, due to the low surface coverage, the respective resonance is relatively weak.

Table 6.3:  $^{29}\text{Si}$  CP/MAS chemical shift values for unmodified and surface modified MCM-41 materials.

Material code	$^{29}\text{Si}$ Chemical Shift (ppm)						
	$\text{Q}^2$	$\text{Q}^3$	$\text{Q}^4$	$\text{T}^1$	$\text{T}^2$	$\text{T}^3$	M
MCM-41	-93.0	-102.5	-111.8	-	-	-	-
M-C4T-a	-91.8	-101.8	-109.3	-49.1	-56.9	-67.6	-
M-C8TE-a	-90.4	-101.3	-109.5	-49.8	-57.5	-66.1	13.9
M-C4M-a	-90.8	-101.8	-111.3	-	-	-	13.6
M-C8ME-a	-91.5	-101.5	-109.1	-	-	-	13.9

The presence of  $\text{T}^1$ ,  $\text{T}^2$  and  $\text{T}^3$  peaks (at about -49 ppm, -57 ppm and -66 ppm) prove the attachment and cross-linking of the chains on the MCM-41 silica surface ( $\text{T}^n = \text{RSi}(\text{OSi})_n(\text{OH})_{3-n}$  with  $n = 1, 2, 3$ ) [54]. They refer to trifunctional groups without

cross-linking ( $T^1$ ), with partial cross-linking ( $T^2$ ) and complete cross-linking ( $T^3$ ). For sample M-C4T-a, the intensity of  $T^1$  and  $T^2$  peaks is higher while the intensity of  $T^3$  is lower as compared to sample M-C8TE-a, showing incomplete cross-linking.

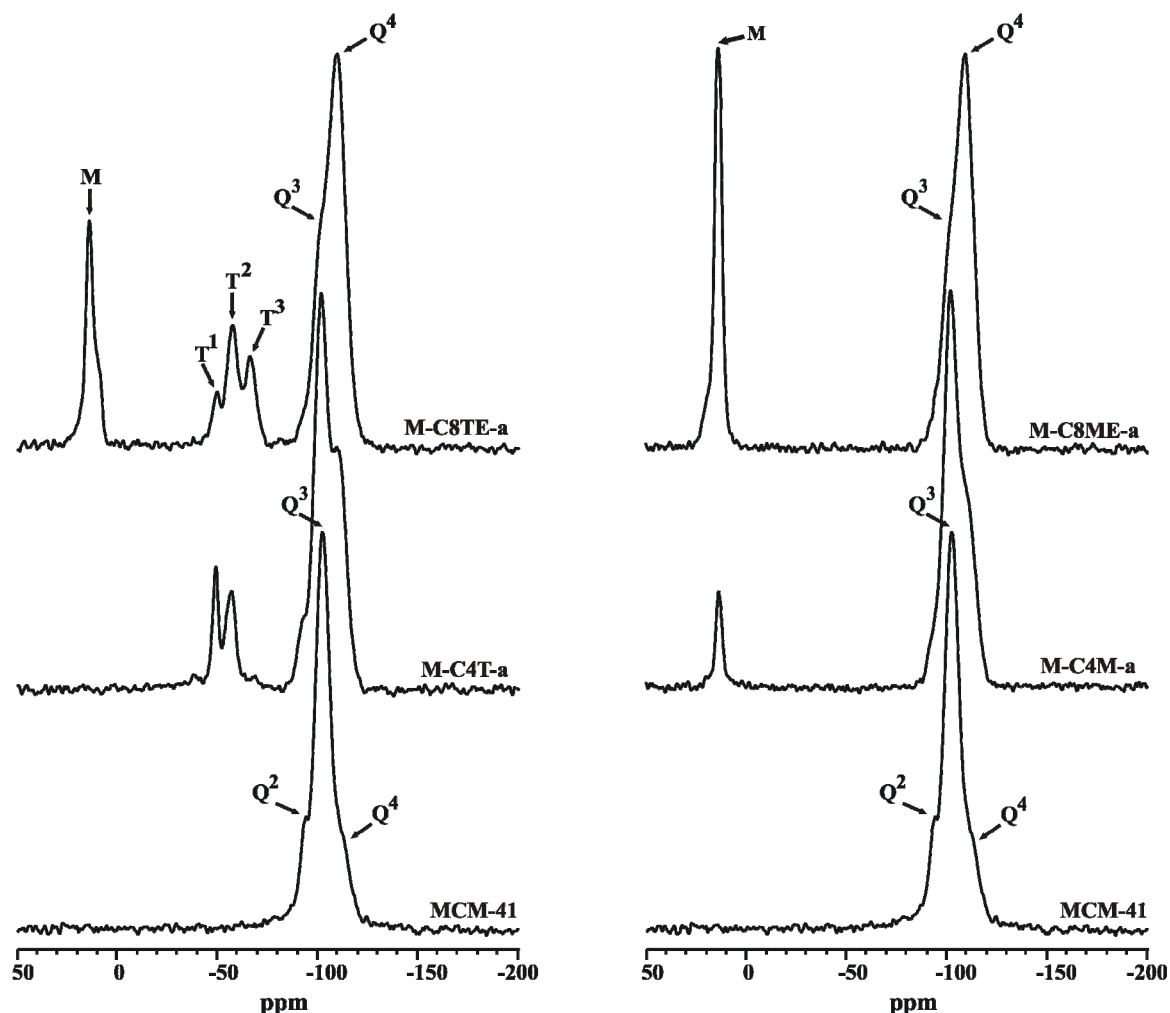


Figure 6.4:  $^{29}\text{Si}$  CP/MAS NMR spectra of unmodified and surface modified MCM-41 materials with trifunctional silanes (left) and monofunctional silanes (right).

When these results are compared with MCM-41 materials which are prepared using surface polymerization method (Chapter 5), the  $Q^3$  intensity is found to be lower while the  $Q^4$  intensity is higher for materials prepared using supercritical fluid method. Also the intensity of the  $T^2$  and  $T^3$  peaks is increasing in case of the trifunctional samples and this indicates the higher surface coverages of the MCM-41 materials prepared by supercritical fluid method.

### 6.3.6 $^{13}\text{C}$ NMR spectroscopy

$^{13}\text{C}$  NMR spectroscopy was used to study the organic components after attaching the alkylsilanes to the MCM-41 silica surface. For alkylsilanes with longer alkyl chains (i.e., with 10 or more methylene segments), the  $^{13}\text{C}$  resonances of the inner methylene groups can be used to get qualitative information about the chain conformational order.

Figure 6.5 depicts experimental  $^{13}\text{C}$  CP/ MAS NMR spectra for the present MCM-41 materials after surface modification. The various signals can be assigned on the basis of solution NMR data for the respective alkylsilanes [15-16]. The  $^{13}\text{C}$  chemical shifts of the various species are reported in Table 6.4 and they are in agreement with the literature values.

Table 6.4:  $^{13}\text{C}$  chemical shifts and assignment of surface modified MCM-41 materials.

Sample	Carbon position	$^{13}\text{C}$ shift (ppm)
M-C4T-a	OCH <sub>3</sub>	49.8
	C-4	10.1
	C-1	12.7
	C-3	25.9
	C-2	29.7
M-C8TE-a	OCH <sub>3</sub>	50.0
	Si(CH <sub>3</sub> ) <sub>3</sub>	0.7
	C-1, C-8	13.0
	C-2, C-7	23.1
	C-4, C-5	30.0
	C-3, C-6	32.7
M-C4M-a	Si(CH <sub>3</sub> ) <sub>2</sub> R	-2.0
	C-4	12.9
	C-1	17.8
	C-3	26.3
	C-2	29.7
M-C8ME-a	Si(CH <sub>3</sub> ) <sub>2</sub> R, Si(CH <sub>3</sub> ) <sub>3</sub>	0.3
	C-8	13.6
	C-1	18.0
	C-2, C-7	23.2
	C-4, C-5	30.0
	C-3, C-6	32.6

As can be seen, the signal-to-noise ratio varies with the actual sample which again reflects the changes in surface coverage. For the MCM-41 samples, surface modified with the trifunctional silane, carbon C-1 resonates at about 13 ppm, while for those obtained

from monofunctional silanes, the respective  $^{13}\text{C}$  NMR signal occurs at about 18 ppm. The low field shift of this resonance can be attributed to the electronic effects from the methyl groups bound to the silicon atom.

For the samples surface modified with trifunctional silanes, there is an additional peak around 50 ppm which may stem from non-reacted methoxy groups. The presence of non-reacted methoxy groups could be explained by the small amount of accessible surface silanol groups along with a minor probability for closely spaced silanol groups at which all three functional groups of silane molecule can bind. Another, more likely explanation is the presence of methoxy groups which were released during the hydrolysis of the trifunctional silanes and which are subsequently bound to the surface silanol groups in a type of endcapping reaction [146].

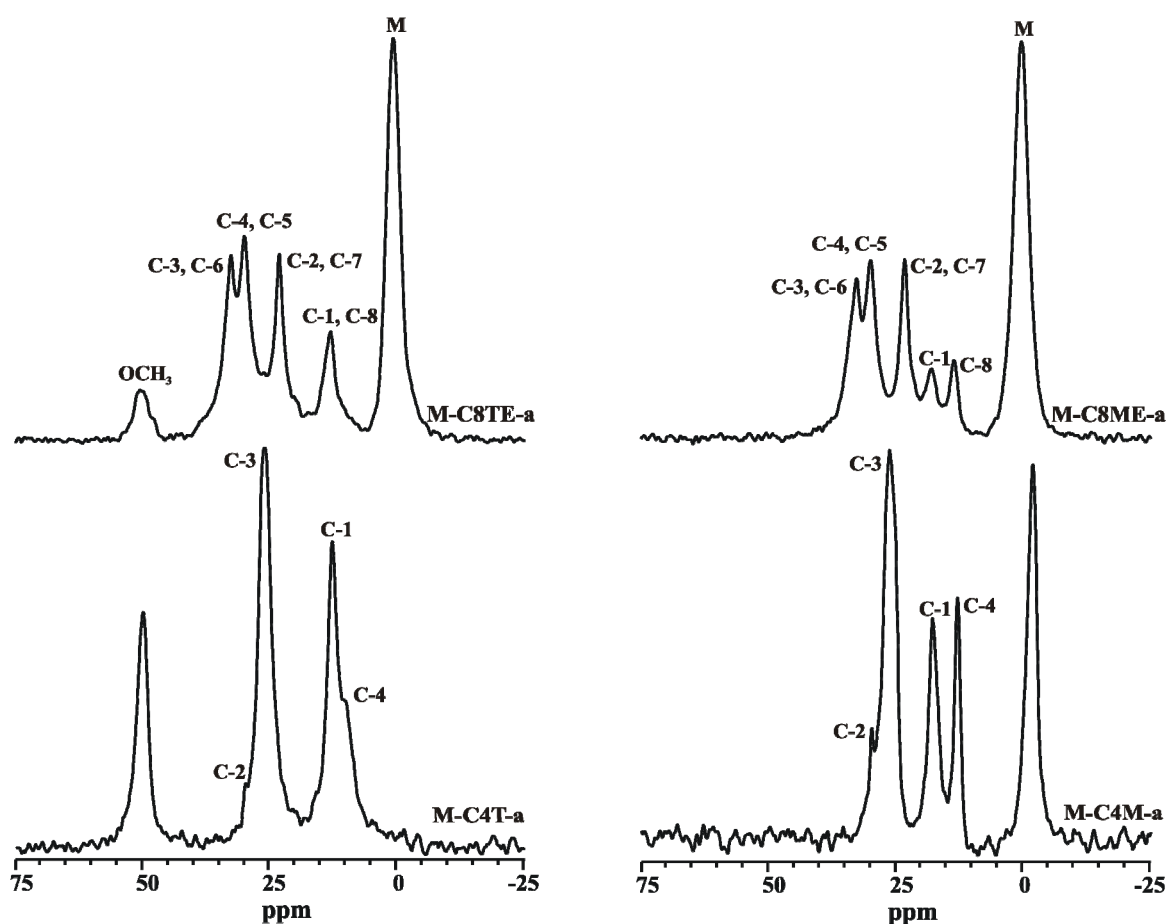


Figure 6.5:  $^{13}\text{C}$  CP/MAS NMR spectra of unmodified and surface modified MCM-41 materials with trifunctional silanes (left) and monofunctional silanes (right).

The trimethylsilyl groups after endcapping with HMDS resonate at about 0.7 ppm and 0.3 ppm for sample M-C8TE-a and M-C8ME-a, respectively. In the latter case, this

signal also contains a spectral component from the methyl groups of the attached dimethyloctylsilane.

The signal-to-noise ratio is increasing for the MCM-41 materials prepared by supercritical fluid method as compared to those materials prepared using surface polymerization method (Chapter 5), and this reflects the increase in surface coverage for the MCM-41 materials prepared by the supercritical fluid method.

### 6.3.7 FTIR Measurements

FTIR measurements were carried out for evaluation of the conformational properties of the attached alkyl chains on MCM-41 silica materials. For this reason, several conformation-sensitive vibrational bands [110-111] are considered to be important. Among these, the symmetric and antisymmetric  $\text{CH}_2$  stretching bands ( $2800\text{-}3000\text{ cm}^{-1}$ ) are the most intense signals and in the majority of cases are easily accessible. Their positions as a function of external parameters, like temperature, pressure or sample constitution, can be used for a qualitative discussion of the conformational order in the aliphatic chains. Hence, changes in the positions of these bands are directly related to the alteration of the *trans/gauche* ratios in the alkyl chain. A band shift towards lower wavenumbers generally reflects an increase in conformational order (i.e., higher amount of *trans* conformers and reduced mobility), while a shift towards higher wavenumbers is an indication for increasing conformational disorder with a higher amount of *gauche* conformers and thus enhanced chain flexibility. Similar information can in principle be derived from the bandwidths, although their changes are typically less pronounced [105].

Variable temperature FTIR studies were performed for the present surface modified MCM-41 materials in a temperature range between 193 K and 353 K. Representative FTIR spectra covering the region of the  $\text{CH}_2$  and  $\text{CH}_3$  stretching bands are shown in Figures 6.6 and 6.7.

The bands are assigned according to previously reported literature [108,150-153,155]. The  $\text{CH}_3$  groups possess antisymmetric and symmetric stretching modes near  $2962\text{ cm}^{-1}$  and  $2872\text{ cm}^{-1}$  while for the  $\text{CH}_2$  groups these modes occur near  $2927\text{ cm}^{-1}$  and  $2857\text{ cm}^{-1}$ , respectively. For the sample modified with butyl trifunctional chain, M-C4T-a (see Figure 6.6) the symmetric  $\text{CH}_2$  band is split into two bands at  $2866\text{ cm}^{-1}$  and  $2852\text{ cm}^{-1}$  at 193 K. A similar split-up of this IR band has also been reported earlier [99,156]. At higher temperatures, the splitting of bands becomes successively smaller and finally a

band at about  $2859\text{ cm}^{-1}$  is observed showing an increasing conformational disorder with increasing temperature. For sample M-C4M-a, a similar split-up of the symmetric  $\text{CH}_2$  band as discussed above cannot be observed.

For sample M-C8TE-a, at 193 K the antisymmetric and symmetric  $\text{CH}_2$  stretching bands are visible at  $2930\text{ cm}^{-1}$  and  $2858\text{ cm}^{-1}$ , respectively. Upon temperature increase, these peaks are shifted to  $2931\text{ cm}^{-1}$  and  $2859\text{ cm}^{-1}$ , respectively. Such shifts for the  $\text{CH}_2$  stretching are well documented for many materials [97,100,105]. They point to an increase in conformational disorder and enhanced chain mobility [158]. In addition, a broadening of the IR bands is registered with increasing sample temperature which again can be attributed to the enhanced chain flexibility.

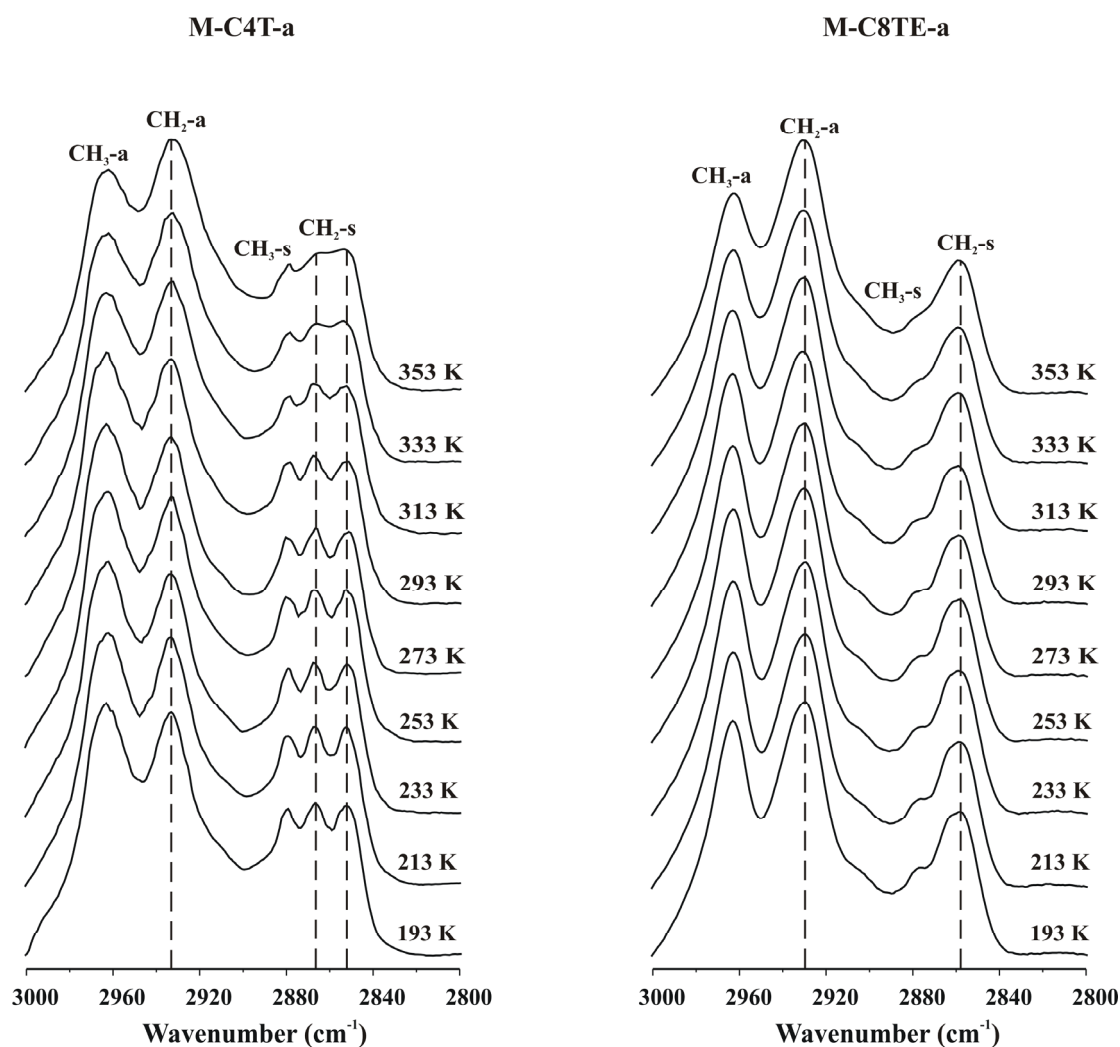


Figure 6.6: Temperature dependence of the antisymmetric and symmetric  $\text{CH}_2$  stretching band spectra of trifunctional chains attached on MCM-41.

Figure 6.7 shows the FTIR spectra of MCM-41 materials surface modified with monofunctional chains. Here, two methyl groups are bound to the silicon atom of the alkyl chains which explains the higher relative intensity of the antisymmetric  $\text{CH}_3$  stretching bands as compared to materials surface modified with trifunctional chains. Sample M-C8ME-a shows the antisymmetric  $\text{CH}_2$  stretching band at  $2925\text{ cm}^{-1}$  and the symmetric  $\text{CH}_2$  stretching band at  $2855\text{ cm}^{-1}$  with a slight shift towards larger wavenumbers at  $2927\text{ cm}^{-1}$  and  $2856\text{ cm}^{-1}$ , respectively, with increasing sample temperature.

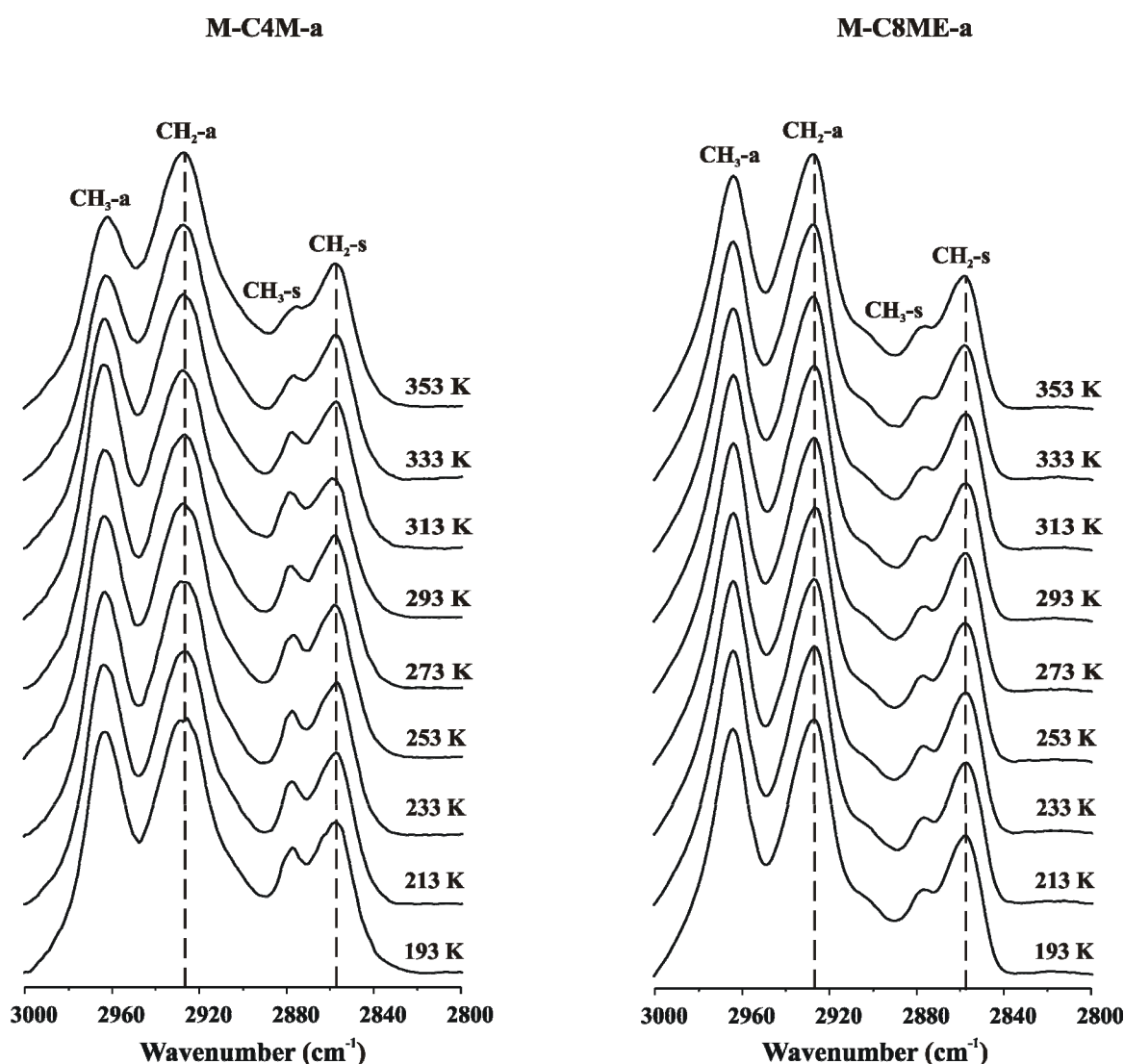


Figure 6.7: Temperature dependence of the antisymmetric and symmetric  $\text{CH}_2$  stretching band spectra of monofunctional chains attached on MCM-41.

The comparison with the results for MCM-41 materials surface modified by using the surface polymerization method (Chapter 5) shows that for the present samples the

bands occur at lower wave numbers reflecting an increase in conformational order. The increase in conformational order is in agreement with the increase in surface coverage, and these results are similar to earlier FTIR studies on alkyl modified MCM-41 silica spheres [57].

## 6.4 Concluding Remarks

Surface modification of MCM-41 silica material was carried out using supercritical carbon dioxide (sc-CO<sub>2</sub>) as the reaction medium. The surface coverages of the resulting materials are found to be higher than the organic solvent based materials which were prepared using surface polymerization method, and this is attributed to the greater accessibility of silanols in sc-CO<sub>2</sub>. The resulting materials were characterized using nitrogen sorption analysis, XRD, SEM analysis, <sup>29</sup>Si and <sup>13</sup>C NMR spectroscopies. A qualitative study of the conformational order was made by the analysis of the symmetric and antisymmetric CH<sub>2</sub> stretching bands in FTIR.



## Chapter 7

# Synthesis and Characterization of Surface Modified SBA-15 Silica Materials and Their Application in Chromatography

### 7.1 Introduction

Hexagonally ordered SBA-15 mesoporous silica spheres with large uniform pore diameters (almost double as compared to MCM-41 materials) are obtained using the triblock copolymer, Pluronic P123, as template with a cosurfactant cetyltrimethylammonium bromide (CTAB) and the cosolvent ethanol in acidic media. By surface modification with organic groups, the mesoporous SBA-15 silica spheres can be used as a stationary phase in HPLC to separate both small aromatic molecules as well as biomolecules such as proteins. A series of surface modified SBA-15 silica materials is prepared using mono- and trifunctional alkyl chains of various lengths which will improve hydrothermal and mechanical stability of the material to make it suitable stationary phase for high performance liquid chromatography. In the present context, we report on a systematic study of the C<sub>4</sub>, C<sub>8</sub> and C<sub>18</sub> alkyl modified SBA-15 materials which are prepared using the surface polymerization method with tri- and monofunctional silanes. In the case of materials modified with C<sub>8</sub> and C<sub>18</sub> alkyl chains, endcapping of remaining silanol groups is done with hexamethyldisilazane (HMDS) to improve their chromatographic performance.

Several technologies, such as element analysis, nitrogen sorption analysis, small angle X-ray diffraction, scanning electron microscopy (SEM), FTIR, solid-state <sup>29</sup>Si and <sup>13</sup>C NMR spectroscopy are employed to characterize the SBA-15 materials before and after surface modification with alkyl chains. Nitrogen sorption analysis is performed to calculate specific surface area, pore volume and pore size distribution (PSD). The

application of surface modified SBA-15 silica materials as stationary phase is tested by means of a suitable test mixture.

## 7.2 Sample Preparation

### 7.2.1 Chemicals

All materials were used as received without further purification: Pluronic (P123,  $M_w=5800$ , BASF), cetyltrimethylammonium bromide (CTAB, Aldrich), tetraethyl orthosilicate (TEOS, 98%, ACROS), hydrochloric acid (HCl, 37%, Fluka), ethanol (100%, Fluka), the alkoxy silanes: *n*-octadecyltrimethoxysilane, *n*-octadecyldimethylmethoxysilane, *n*-octyltrimethoxysilane, *n*-octyldimethylmethoxysilane, *n*-butyltrimethoxysilane and *n*-butyldimethylmethoxysilane (97%, Aldrich) and 1,1,1,3,3,3-hexamethyldisilazane (HMDS, 97%, Aldrich). Reagent grade toluene was distilled two times before the use and stored in molecular sieves.

### 7.2.2 Synthesis and Surface Modification of SBA-15 Silica material

SBA-15 mesoporous silica spheres were synthesized using the triblock copolymer, Pluronic P123 ( $\text{EO}_{20}\text{PO}_{70}\text{EO}_{20}$ ), as a structure directing agent. 2.0 g of Pluronic P123 was dissolved by stirring in a solution of 10 ml of ethanol, 15 ml of water and 30 ml of 2 M HCl. Then 0.2 g of CTAB was added followed by dropwise addition of 5.0 g of tetraethyl orthosilicate (TEOS) while stirring. This mixture was well stirred for 1 h and was transferred to an autoclave for 5 h at 353 K. Loosely cross-linked SBA-15 particles precipitated during this reaction time period at 353 K. The silica framework was further crosslinked by heating the reaction mixture for 15 h at 393 K. This as-synthesized SBA-15 material was filtered and dried overnight. After heating the sample at a rate of  $1 \text{ K min}^{-1}$ , the surfactant was removed by calcination in air at 823 K for 5 h.

Surface modification of the calcined SBA-15 silica material with mono- and trifunctional chains of different lengths ( $\text{C}_4$ ,  $\text{C}_8$  and  $\text{C}_{18}$ ) was carried out by using the surface polymerization method. About 1.0 g sample of calcined SBA-15 silica was preevacuated at 378 K for 4 h and allowed to cool to ambient temperature. The resulting dry powders were equilibrated with humid air at room temperature for 6 h which gives a water layer on the silica surface [52-53]. Afterwards, the humidified SBA-15 silica were suspended in 200 ml of toluene and heated to 343 K. The corresponding silane was added

in 50 ml of toluene and then added to the above suspension. This mixture was placed in a rotavapor for three days at 333 K. For the SBA-15 materials surface modified with octyl ( $C_8$ ) and octadecylsilanes ( $C_{18}$ ), a part of the material was used to endcap the remaining silanol groups with HMDS. The resulting SBA-15 silica spheres were filtered (G4 filter) and washed with toluene, followed by acetone, ethanol, ethanol/water (1:1, v:v.), water, ethanol, acetone, and pentane to rinse away any residual chemicals. The surface modified SBA-15 silica was dried overnight in an oven at 353 K and stored in airtight bottles.

## 7.3 Results and Discussion

### 7.3.1 Synthesis and Surface Modification of SBA-15 Silica material

Well-ordered hexagonal SBA-15 mesoporous silica spheres were synthesized using commercially available block-copolymer surfactant in strong acid media. At first, we prepared a sample by heating the reaction mixture to 393 K for 20 h which showed only irregular morphologies (see Figure 7.1 (A)). In order to get spherical particles, we divided the reaction in two steps. In the first step, we heated the reaction mixture at 353 K for 5 h and the resulting SBA-15 material exhibited the perfect spherical morphology (see Figure 7.1 (B)), but the pore diameter and pore volume were too low ( $D_{\text{pore}} = 4.67$  nm,  $V_p = 0.90$  mlg<sup>-1</sup> and  $S_{\text{BET}}$  is 885 m<sup>2</sup>g<sup>-1</sup>). These SBA-15 microspheres were further heated at 393 K for more 15 h, and it was indicated that this second heating step at 393 K had no considerable effect on the macroscopic morphology and size, (see Figure 7.1 (C)). However, there is a decrease in surface area accompanied by an increase in pore dimensions ( $D_{\text{pore}} = 10.10$  nm,  $V_p = 1.52$  mlg<sup>-1</sup> and  $S_{\text{BET}}$  is 735 m<sup>2</sup>g<sup>-1</sup>) of the SBA-15 material.

Alkyl groups ( $C_4$ ,  $C_8$  and  $C_{18}$ ) were attached on the calcined SBA-15 silica spheres by reaction with the corresponding silanes. The resulting materials are denoted as S-CxT or S-CxM, where  $x = 4, 8$  and  $18$  and T stands for trifunctional while M for monofunctional chains. The endcapped materials are denoted by S-CxTE or S-CxME where  $x = 8$  and  $18$  (see Table 7.1). The percentage of carbon obtained from the elemental analysis for samples S-C18T and S-C18M are 12.92 and 1.67, respectively (see Table 7.2). The surface coverage calculated for the material surface modified with monofunctional silane is relatively low (0.11  $\mu\text{mol m}^{-2}$ ), since the monofunctional silanes can be only attached to the silica surface by reaction of the methoxy group with a surface silanol group. This method therefore yields only moderate surface coverages since further

cross-linking of the silanes is not possible. On the other hand, trifunctional silane provided much higher surface coverage ( $1.05 \mu\text{mol m}^{-2}$ ) because the trifunctional silanes can bind directly to the surface silanol groups and are able to undergo cross-linking reactions with neighbouring silane chains. Hence, the latter assemblies typically exhibit a better chain packing with higher surface coverage, good thermal and enhanced chemical stability. Similarly, in the case of the S-C8T material, the percentage of carbon is 9.42 ( $1.73 \mu\text{mol m}^{-2}$ ) while in material S-C8M it is 2.90 ( $0.57 \mu\text{mol m}^{-2}$ ). Similarly, for the material S-C4T, the percentage of carbon is 6.61 ( $3.75 \mu\text{mol m}^{-2}$ ) and for S-C4M it is 5.50 ( $2.57 \mu\text{mol m}^{-2}$ ). Hence, it is clearly indicated that shorter chains provide higher surface coverages, and this can be explained by their greater affinity to incorporate inside the channels of the materials as compared to the longer ones. The longer ones are assumed to bind mostly on the surface of the SBA-15 materials, and only a few are able to go inside the channels of the material because of steric hinderance. Therefore, endcapping was carried out for the SBA-15 materials which were surface modified with  $C_8$  and  $C_{18}$  alkyl chains. In general, a substantial increase of the carbon content and thus for the surface coverage could be observed after endcapping.

Table 7.1: Surface modified SBA-15 silica materials and their material codes.

<b>Material code</b>	<b>Surface modified SBA-15 silica materials</b>
S-C4T	SBA-15 modified with <i>n</i> -butyltrimethoxysilane
S-C8T	SBA-15 modified with <i>n</i> -octyltrimethoxysilane
S-C8TE	SBA-15 modified with <i>n</i> -octyltrimethoxysilane and endcapped with HMDS
S-C18T	SBA-15 modified with <i>n</i> -octadecyltrimethoxysilane
S-C18TE	SBA-15 modified with <i>n</i> -octadecyltrimethoxysilane and endcapped with HMDS
S-C4M	SBA-15 modified with <i>n</i> -butyldimethylmethoxysilane
S-C8M	SBA-15 modified with <i>n</i> -octyldimethylmethoxysilane
S-C8ME	SBA-15 modified with <i>n</i> -octyldimethylmethoxysilane and endcapped with HMDS
S-C18M	SBA-15 modified with <i>n</i> -octadecyldimethylmethoxysilane
S-C18ME	SBA-15 modified with <i>n</i> -octadecyldimethylmethoxysilane and endcapped with HMDS

### 7.3.2 Scanning Electron Microscopy

SEM pictures of the spheres of mesoporous SBA-15 materials are shown in Figure 7.1. Figure 7.1 (A) refers to the SBA-15 material obtained by directly heating the reaction mixture to 393 K having irregular morphology. The spherical morphology of the SBA-15 sample prepared at 353 K is shown in Figure 7.1 (B), and Figure 7.1 (C) represents the sample prepared using two heating steps. This picture clearly demonstrates that the spherical morphology of the silica particles is retained during the second heating step.

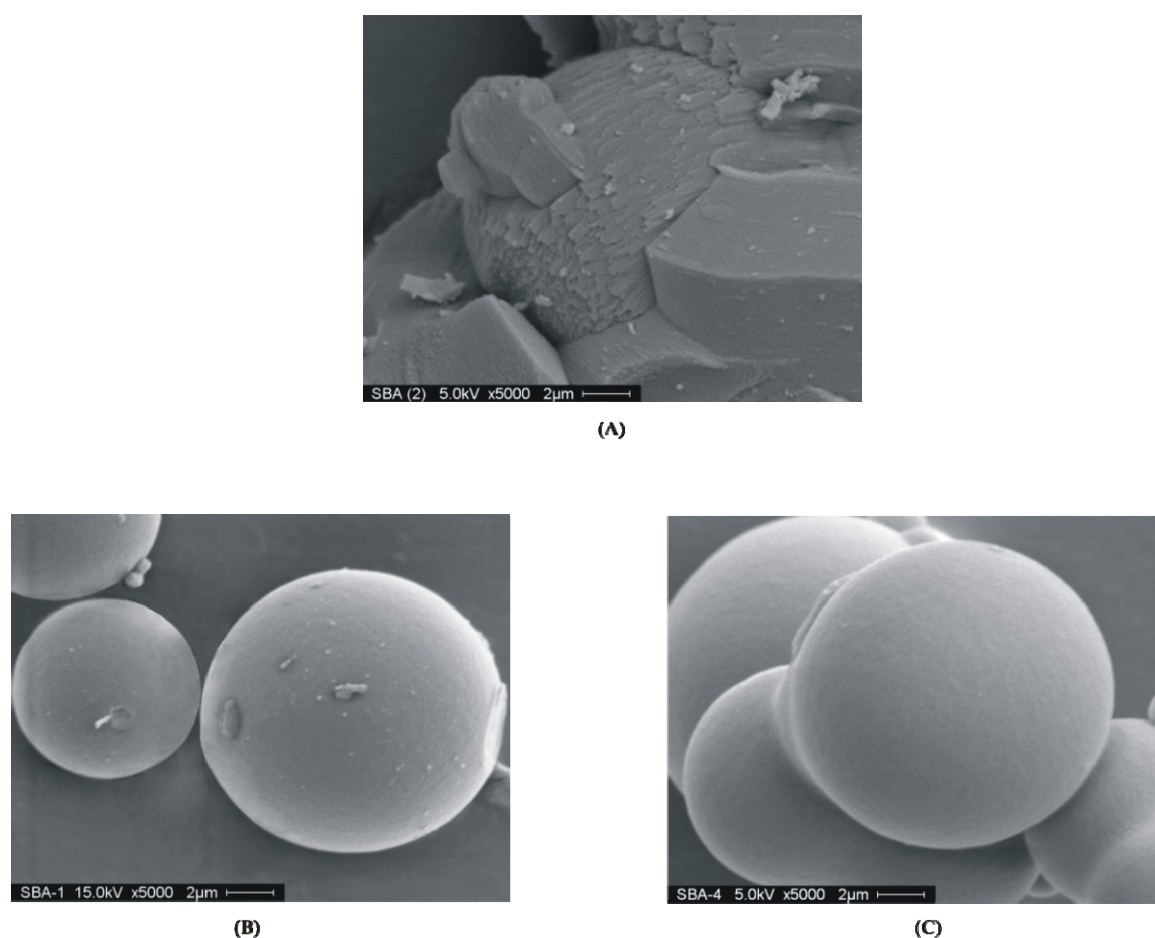


Figure 7.1: SEM micrographs for SBA-15 materials prepared by directly heating to 393 K (A), prepared at 353 K (B) and prepared at 353 K followed by second heating step at 393 K (C).

### 7.3.3 Nitrogen Sorption Studies

Nitrogen sorption isotherms of SBA-15 materials have been used to obtain information about the mesoporosity. Table 7.2 presents all the nitrogen sorption parameters. Nitrogen sorption isotherms are shown in Figure 7.2 (top) and Figure 7.2 (bottom) shows DFT pore size distributions for unmodified SBA-15 and the materials surface modified with

trifunctional alkylsilanes. Figure 7.3 shows nitrogen sorption isotherms and DFT pore size distributions for the corresponding monofunctional chains. A typical irreversible IV type isotherm with a H1 hysteresis loop, as defined by IUPAC [4], is observed. The isotherm exhibits a sharp inflection in the  $p/p_0$  range from 0.60 to 0.80 characteristic of capillary condensation within uniform pores. The  $p/p_0$  position of the inflection points is clearly related to the diameter in the mesopore range and the sharpness of the step indicates the uniformity of the mesopore size distribution. The overall trend of nitrogen sorption isotherms from the surface modified SBA-15 materials is similar to that of the unmodified SBA-15 material while there is a notable shift of the hysteresis position towards lower  $p/p_0$  values and a decrease is observed in overall nitrogen adsorption volume as the surface coverage of the material increases. This indicates that the attached alkyl chains are located inside the mesoporous channels, and hence reduce the pore dimension of the parent SBA-15 silica material. The SBA-15 samples which were surface modified with the trifunctional alkylsilanes exhibit a stronger reduction in surface area, pore diameter and total pore volume than those from modification with monofunctional silanes.

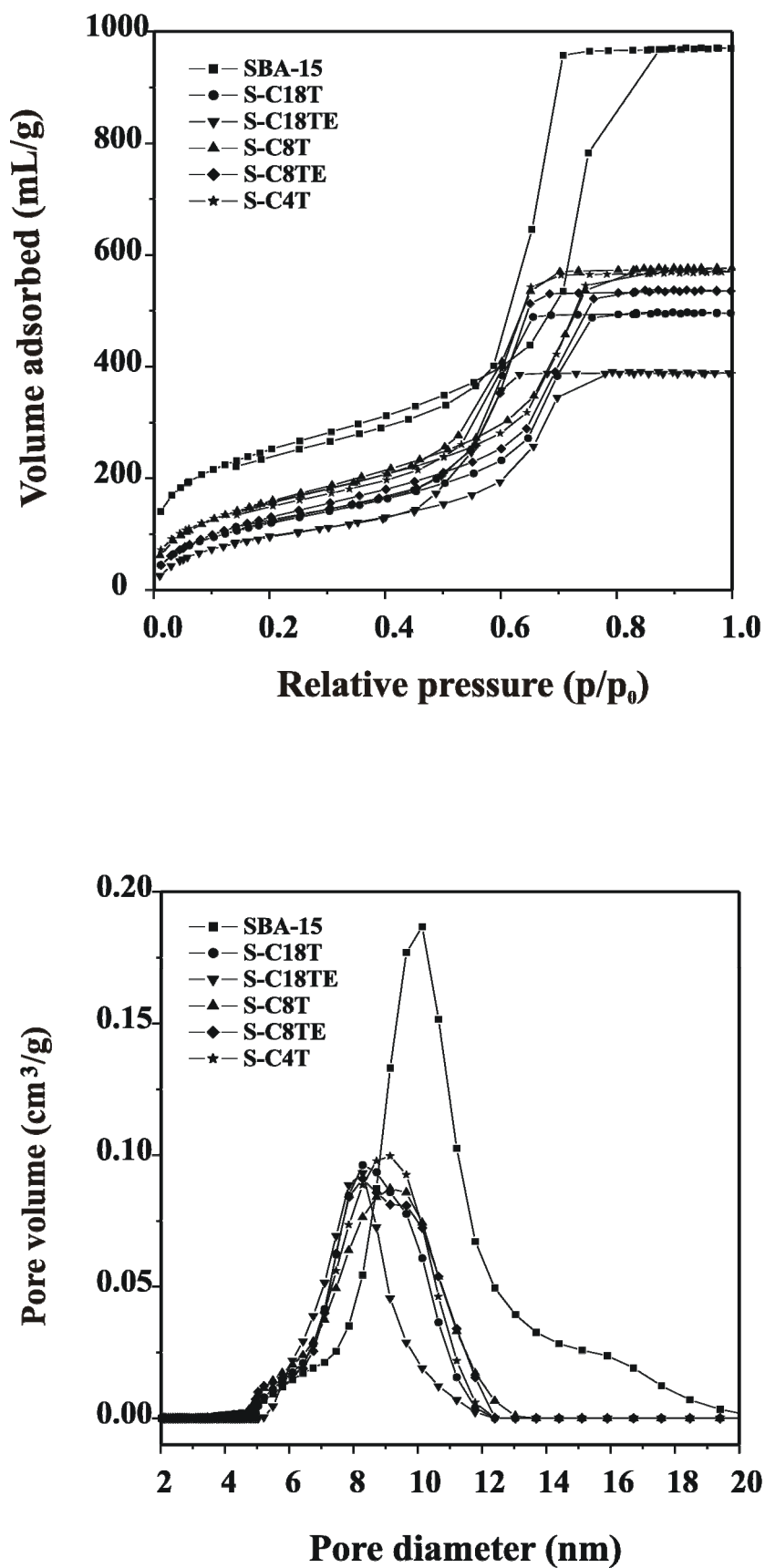


Figure 7.2: Nitrogen sorption isotherms (top) and DFT pore size distribution (bottom) for SBA-15 materials before and after surface modification with trifunctional silanes.

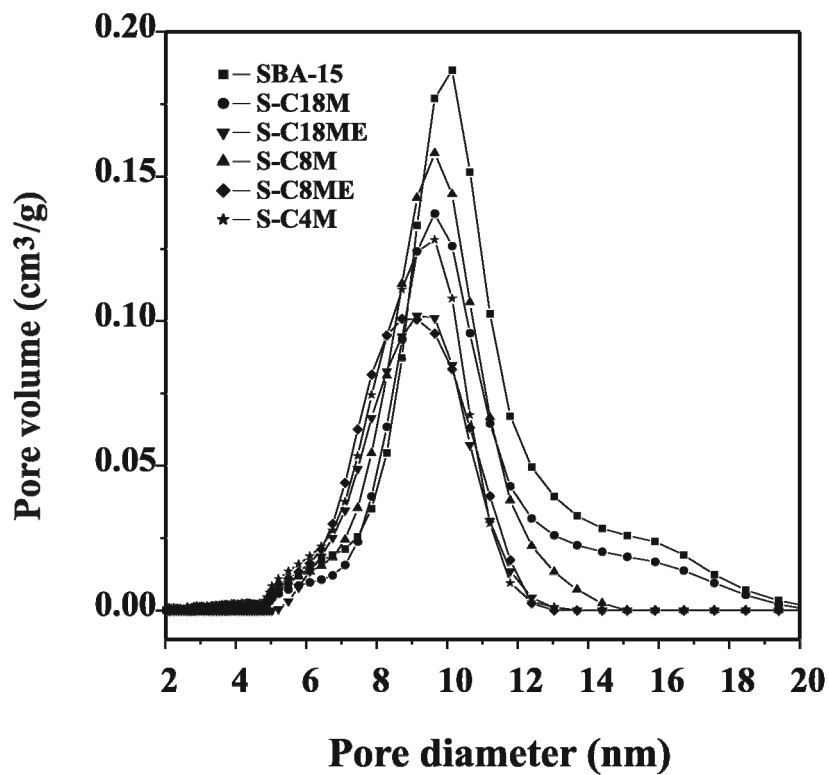
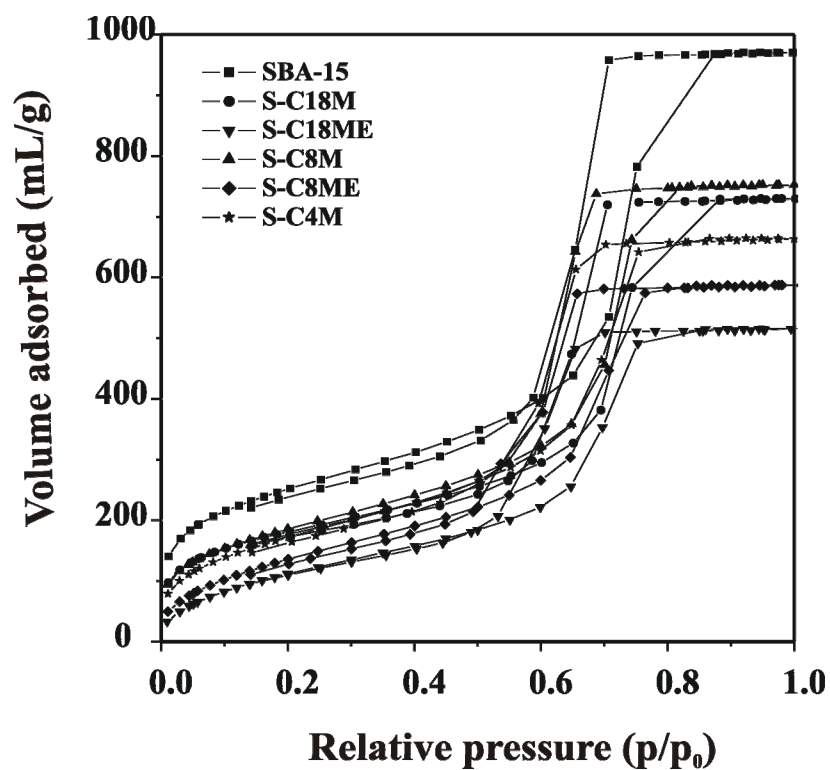


Figure 7.3: Nitrogen sorption isotherms (left) and DFT pore size distribution (right) for SBA-15 materials before and after surface modification with monofunctional silanes.



Table 7.2: Nitrogen sorption parameters for SBA-15 materials before and after surface modification.

Material code	$S_{\text{BET}}$ ( $\text{m}^2/\text{g}$ )	$V_{\text{p}}$ ( $\text{ml}/\text{g}$ )	DFT $D_{\text{pore}}$ ( $\text{nm}$ )	% C	SC ( $\mu\text{mol}/\text{m}^2$ )
SBA-15	735	1.52	10.10	-	-
S-C4T	484	0.88	9.01	6.61	3.75
S-C8T	501	0.89	9.15	9.42	1.73
S-C8TE	428	0.83	8.28	10.60	2.02
S-C18T	380	0.76	8.70	12.92	1.05
S-C18TE	308	0.60	8.28	18.43	1.70
S-C4M	532	1.02	9.35	5.50	2.58
S-C8M	560	1.16	9.64	2.90	0.57
S-C8ME	450	0.91	8.71	8.57	1.48
S-C18M	532	1.13	9.63	1.67	0.11
S-C18ME	378	0.80	9.14	9.40	0.70

### 7.3.4 Small Angle X-ray Diffraction

Figure 7.4 depicts the XRD pattern obtained for the calcined SBA-15 and surface modified SBA-15 materials, which exhibit single diffraction peaks, characteristic of mesoporous materials with a pore structure lacking long-range order. Surface modified materials show the XRD patterns similar to original material which clearly indicate that the hexagonal symmetry and the inorganic wall structure of the SBA-15 material is retained after surface modification.

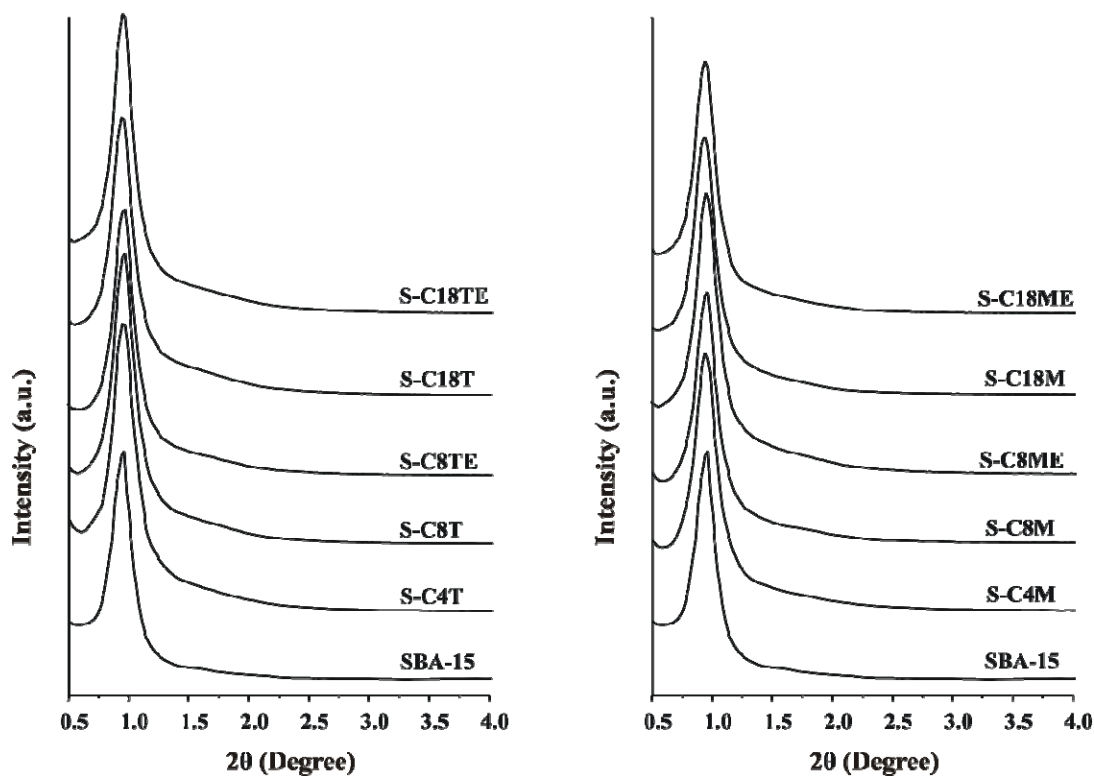


Figure 7.4: XRD patterns for SBA-15 materials before and after surface modification with trifunctional silanes (left) and monofunctional silanes (right).

### 7.3.5 $^{29}\text{Si}$ NMR Spectroscopy

$^{29}\text{Si}$  NMR spectroscopy is employed for the determination of the surface species, amount of alkyl chain attachment and degree of cross linking of the attached alkylsilanes. The  $^{29}\text{Si}$  CP/MAS NMR spectra of the unmodified and surface modified SBA-15 samples are shown in Figure 7.5 and the chemical shifts are reported in Table 7.3. The  $^{29}\text{Si}$  resonances around -92, -102 and -110 ppm originate from the structural units of the SBA-15 support and reflect surface silanol groups,  $\text{Q}^2$ ,  $\text{Q}^3$  and  $\text{Q}^4$  groups, respectively ( $\text{Q}^n$  units =  $\text{Si}(\text{OSi})_n(\text{OH})_{4-n}$ , with  $n = 1$  to 4) [95,97]. After attachment of the butyl, octyl and octadecyl silanes, the intensities of  $\text{Q}^2$  and  $\text{Q}^3$  units, bearing surface hydroxyl groups, are significantly reduced, while the intensity for the  $\text{Q}^4$  units increases. This trend continues for the endcapped samples which exhibit an additional considerable growth for the  $\text{Q}^4$  signal intensity.

The  $\text{Q}^2$  groups are lost in case of materials surface modified with shorter trifunctional chains ( $\text{C}_4$  and  $\text{C}_8$ ) owing to their greater reactivity. The  $\text{Q}^3$  signal intensity for the samples modified with monofunctional alkylsilanes is found to be higher than for those obtained from trifunctional alkylsilanes, which is consistent with the lower surface

coverage. This can be related to the lower reactivity of the former silylation reagent due to the lower probability (only one reactive group available) to react with surface silanols. Further reasons might be the bulky methyl groups of the monofunctional alkylsilane, which provide a steric hindrance for the binding of other alkylsilane chains in close vicinity to a surface-bound alkylsilane, and the lack of cross-linking reactions due to the presence of a single reactive group.

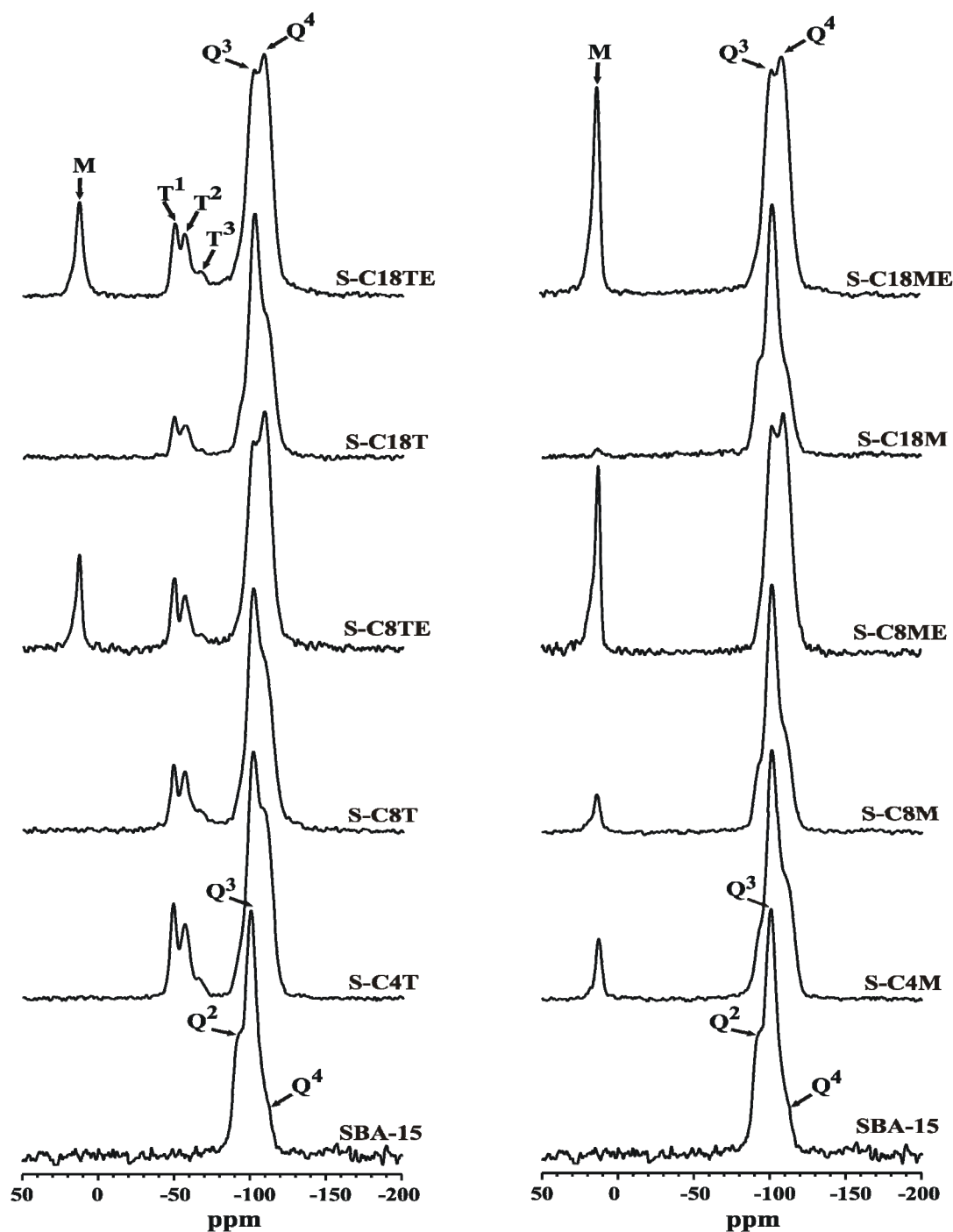


Figure 7.5:  $^{29}\text{Si}$  CP/MAS NMR spectra of SBA-15 materials before and after surface modification with trifunctional silanes (left) and monofunctional silanes (right).

For the endcapped materials, an additional peak at about 13 ppm [ $M = R_3Si(OSi-)$ ] is found arising from the trimethylsilyl groups of the endcapping reagent. For sample, S-C8ME and S-C18ME samples, this peak also contains a small signal component from the attached monofunctional alkylsilane chains of the first surface modification step. This peak has very low intensity in the case of material modified with  $C_{18}$  monofunctional chain (S-C18M) because only a small amount of  $C_{18}$  monofunctional chains are bound to the SBA-15 surface, as indicated by the very low surface coverage.

In the case of materials modified with trifunctional chains, the presence of  $T^1$ ,  $T^2$  and  $T^3$  peaks (at about -49 ppm, -56 ppm and -65 ppm) prove the attachment and cross-linking of the chains on the SBA-15 silica surface ( $T^n = RSi(OSi)_n(OH)_{3-n}$ , with  $n=1, 2, 3$ ) [54].  $T^1$  species are referred to trifunctional groups without cross-linking,  $T^2$  species in these samples indicate partial cross-linking and  $T^3$  is referred to complete cross-linking.

Table 7.3:  $^{29}Si$  CP/MAS chemical shift values for SBA-15 materials before and after surface modification.

Material code	$^{29}Si$ Chemical Shift (ppm)						
	Q <sup>2</sup>	Q <sup>3</sup>	Q <sup>4</sup>	T <sup>1</sup>	T <sup>2</sup>	T <sup>3</sup>	M
SBA-15	-92.3	-101.1	-111.0	-	-	-	-
S-C4T	-	-101.5	-109.7	-48.8	-56.3	-64.8	-
S-C8T	-	-101.6	-109.9	-48.7	-56.2	-65.7	-
S-C8TE	-	-101.1	-109.0	-49.8	-56.0	-65.5	13.3
S-C18T	-92.4	-101.8	-110.3	-48.7	-56.2	-	-
S-C18TE	-	-102.0	-109.2	-49.9	-56.1	-65.3	13.2
S-C4M	-92.4	-101.8	-110.7	-	-	-	13.7
S-C8M	-92.2	-101.6	-110.7	-	-	-	12.9
S-C8ME	-	-101.7	-109.3	-	-	-	12.8
S-C18M	-92.7	-101.7	-111.3	-	-	-	13.2
S-C18ME	-	-102.3	-109.6	-	-	-	12.6

### 7.3.6 $^{13}C$ NMR Spectroscopy

$^{13}C$  NMR spectroscopy is used to study the organic components after attaching alkylsilanes to the SBA-15 silica surface. Figure 7.6 depicts experimental  $^{13}C$  CP/MAS NMR spectra for the surface modified SBA-15 silica materials which show typical signals

from aliphatic carbons [165]. The  $^{13}\text{C}$  chemical shifts of the various species are reported in Table 7.4.

Table 7.4:  $^{13}\text{C}$  chemical shifts and assignment of surface modified SBA-15 materials.

Sample	Carbon position	$^{13}\text{C}$ shift (ppm)	Sample	Carbon position	$^{13}\text{C}$ shift (ppm)
S-C4T	OCH <sub>3</sub>	49.6	S-C4M	Si(CH <sub>3</sub> ) <sub>2</sub> R	-2.2
	C-4	10.2		C-4	12.9
	C-1	12.1		C-1	17.7
	C-2, C-3	25.9		C-2, C-3	26.4
S-C8T	OCH <sub>3</sub>	50.3	S-C8M	Si(CH <sub>3</sub> ) <sub>2</sub> R	-2.0
	C-8	10.7		C-8	12.7
	C-1	12.8		C-1	18.0
	C-2, C-7	23.3		C-2, C-7	23.2
	C-4, C-5	30.2		C-4, C-5	30.1
	C-3, C-6	32.9		C-3, C-6	32.7
S-C8TE	OCH <sub>3</sub>	49.9	S-C8ME	Si(CH <sub>3</sub> ) <sub>2</sub> R, Si(CH <sub>3</sub> ) <sub>3</sub>	0.2
	Si(CH <sub>3</sub> ) <sub>3</sub>	0.1		C-8	13.5
	C-8	13.2		C-1	18.6
	C-1	17.4		C-2, C-7	23.4
	C-2, C-7	23.3		C-4, C-5	30.5
	C-4, C-5	30.2		C-3, C-6	33.5
	C-3, C-6	32.9			
S-C18T	OCH <sub>3</sub>	50.1	S-C18M	Si(CH <sub>3</sub> ) <sub>2</sub> R	-1.8
	C-1, C-18	12.6		C-1, C-18	16.8
	C-2, C-17	22.8		C-2, C-17	23.6
	C-3 – C-16	30.4		C-3 – C-16	30.2
S-C18TE	OCH <sub>3</sub>	50.7	S-C18ME	Si(CH <sub>3</sub> ) <sub>2</sub> R, Si(CH <sub>3</sub> ) <sub>3</sub>	0.5
	Si(CH <sub>3</sub> ) <sub>3</sub>	0.4		C-1, C-18	16.9
	C-1, C-18	13.1		C-2, C-17	23.3
	C-2, C-17	23.5		C-3 – C-16	30.4
	C-3 – C-16	31.3			

In the materials surface modified with octadecyl (C<sub>18</sub>) trifunctional silanes, the C-1 and C-18 resonate at about 13 ppm, while for monofunctional samples they occur at about 17 ppm. The low field shifts of the former signals for the SBA-15 samples surface modified with the monofunctional silanes are attributed to the electronic effects from the methyl groups bound to the silicon atom. The C-2 and C-17 resonate at about 23 ppm and on the other hand, a strong peak from the internal carbons (C3-C16) of octadecyl chains appears at about 30 ppm. It is well known that  $^{13}\text{C}$  chemical shifts of the methylene carbons located in the inner part of alkyl chain are very sensitive to the conformational

states [166-168]. The methylene carbons in all trans conformation have a chemical shift between 34.2 and 32.8 ppm according to their molecular packing and motional state while the chemical shift of those in a mixed trans-gauche conformation is upfield shifted [166,168-169]. The maximum shift of methylene carbons due to conformation difference was reported as ~5 ppm [170]. Hence, the chemical shift of the C3-C16 peak, at 30 ppm, for octadecyl chains on the SBA-15 surface indicates that the carbons are in a mixed trans-gauche conformation. There is an additional peak around 50 ppm in case of materials surface modified with trifunctional silanes which can be assigned to methoxy groups bound to silicon. This signal could be explained by non-reacted methoxy groups of the alkylsilanes. Another more likely explanation is the presence of methoxy groups which were released during the hydrolysis of the trifunctional silanes and which are subsequently bound to the surface silanol groups [146]. In case of the monofunctional material (S-C18M), the additional methyl groups bound to the silicon atom of the alkylsilane resonate at about -1.8 ppm.

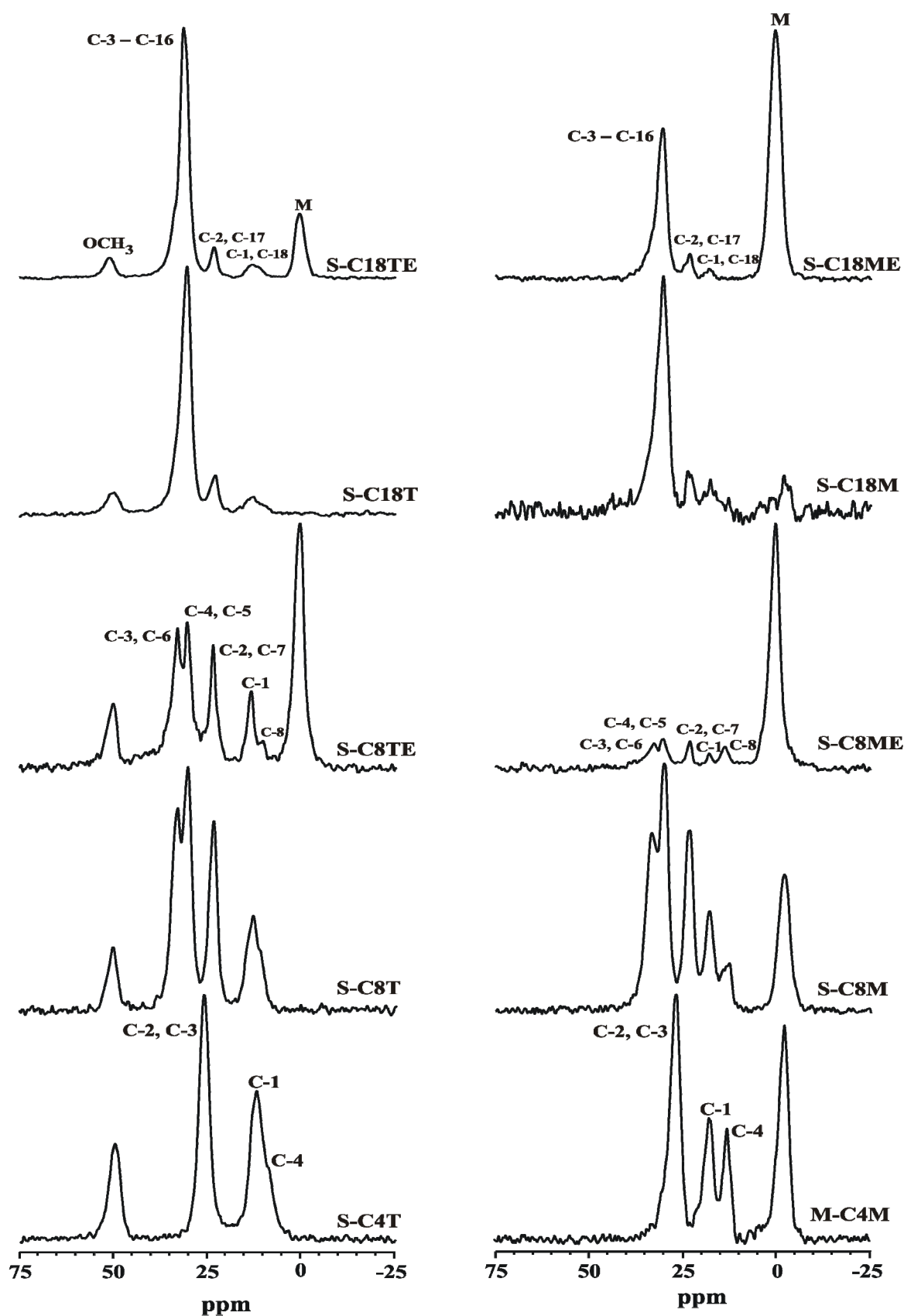


Figure 7.6:  $^{13}\text{C}$  CP/MAS NMR spectra of SBA-15 materials before and after surface modification with trifunctional silanes (left) and monofunctional silanes (right).

In the samples surface modified with octyl silanes, carbons C-1 and C-8 resonate at 13 ppm and 11 ppm for trifunctional sample (S-C8T), while for monofunctional sample they occur at about 18 ppm and 13 ppm, respectively. The low field shift of this resonance can be attributed to the electronic effects from the methyl groups bound to the silicon atom as shown in case of ocadecyl chains. The signal at around 23 ppm points to carbons C-2 and C-7, carbons C-4 and C-5 are visible by a resonance around 30 ppm while the signal at about 33 ppm arises from carbons C-3 and C-6. The additional methyl groups bound to the silicon atom of the monofunctional octylsilane appear at about -2.0 ppm. In the samples surface modified with butyl silanes, carbons C-4 and C-1 resonate at 12 and 10 ppm for trifunctional sample while they are shifted to 17 and 13 ppm for monofunctional sample. The signal for carbons C-2 and C-3 appears at about 26 ppm. For the trifunctional samples, the additional  $^{13}\text{C}$  resonance at around 50 ppm stems from the nonreacted methoxy groups and the methylene groups attached to silicon atom appear at about -2.0 ppm in monofunctional samples.

The trimethylsilyl groups after endcapping with HMDS resonate at about 0.1 ppm and 0.4 ppm for samples S-C8TE and S-C18TE, respectively. In samples S-C8ME and S-C18ME, this signal appears at 0.2 ppm and 0.5 ppm, respectively. In the latter case, the signal also contains a spectral component from the methyl groups of the attached dimethylalkyl silane.

### 7.3.7 FTIR Measurements

FTIR spectroscopy can be used to probe the structural features of the attached alkyl chains. In general, the conformational properties of attached alkyl chains can be studied by several conformation-sensitive vibrational bands [110-111]. Among these, the symmetric and antisymmetric  $\text{CH}_2$  stretching bands ( $2800\text{-}3000\text{ cm}^{-1}$ ) are the most intense signals, and in the majority of cases are easily accessible. Their positions as a function of external parameters, like temperature, pressure or sample constitution, can be used for a qualitative discussion of the conformational order in the aliphatic chains. Hence, changes in the positions of these bands are directly related to the alteration of the *trans/gauche* ratios. A band shift towards lower wavenumbers reflects an increase in conformational order (i.e., higher amount of *trans* conformers and reduced mobility), while a shift towards higher wavenumbers points to an increasing conformational disorder with a higher amount of *gauche* conformers and thus enhanced chain flexibility.



Similar information can in principle be derived from the bandwidths, although the respective alterations are typically less pronounced [105].

Variable temperature FTIR studies were performed for the present surface modified SBA-15 materials in a temperature range between 193 K and 353 K. Representative FTIR spectra, covering the region of the CH<sub>2</sub> and CH<sub>3</sub> stretching bands, are shown in Figure 7.7 and 7.8. The analysis of these conformational orders in a temperature range from 193 K to 353 K is important because temperature is important during chromatographic separations and shape selectivity can be affected by column temperature, especially for certain classes of solutes with rigid and well-defined molecular shapes.

The bands are assigned according to previously reported literature [108,150-153,155]. The CH<sub>3</sub> groups exhibit antisymmetric (CH<sub>3</sub>-a) and symmetric (CH<sub>3</sub>-s) stretching modes near 2962 cm<sup>-1</sup> and 2872 cm<sup>-1</sup> while for the CH<sub>2</sub> groups these modes occur near 2927 cm<sup>-1</sup> (CH<sub>2</sub>-a) and 2857 cm<sup>-1</sup> (CH<sub>2</sub>-s), respectively. For the sample S-C4T (see Figure 7.7) the symmetric CH<sub>2</sub> band is split into two bands at 2866 cm<sup>-1</sup> and 2852 cm<sup>-1</sup> at 193 K. According to Fox and Martin [154-155], this split can arise from coupling between the two methylenes. A similar split-up of this IR band has also been reported earlier for similar systems [99,156-157]. At higher temperatures, the splitting of bands becomes successively smaller showing an increasing conformational disorder with increasing temperature.

For the sample S-C8T, at 193 K the antisymmetric and symmetric CH<sub>2</sub> stretching bands are visible at 2929 cm<sup>-1</sup> and 2857 cm<sup>-1</sup>, respectively. Upon temperature increase, these bands are slightly shifted towards higher wavenumbers to reach values of 2930 cm<sup>-1</sup> and 2858 cm<sup>-1</sup>, respectively, at 353 K. For the sample S-C8TE, the antisymmetric and symmetric CH<sub>2</sub> stretching bands appear at 2929 cm<sup>-1</sup> and 2856 cm<sup>-1</sup> and are showing a wavenumber shift of 2 cm<sup>-1</sup> towards higher values at higher temperatures. Such shifts for the CH<sub>2</sub> stretching bands are well documented for many materials [97,100,105].

In the case of S-C18T sample, at 193 K two bands appear at 2925 cm<sup>-1</sup> for antisymmetric CH<sub>2</sub> stretching band and 2854 cm<sup>-1</sup> for symmetric CH<sub>2</sub> stretching band. These bands are found to shift towards higher wavenumbers with increasing sample temperature and are shifted to 2927 cm<sup>-1</sup> and 2856 cm<sup>-1</sup>, respectively at 353 K. For the sample S-C18TE, these bands are shifted from 2924 cm<sup>-1</sup> and 2854 cm<sup>-1</sup> to 2927 cm<sup>-1</sup> and 2857 cm<sup>-1</sup>. Here we observe a higher frequency shift of almost 3 cm<sup>-1</sup> pointing to an increasing conformational disorder with a higher amount of the gauche conformers and thus higher alkyl chain mobility [158].

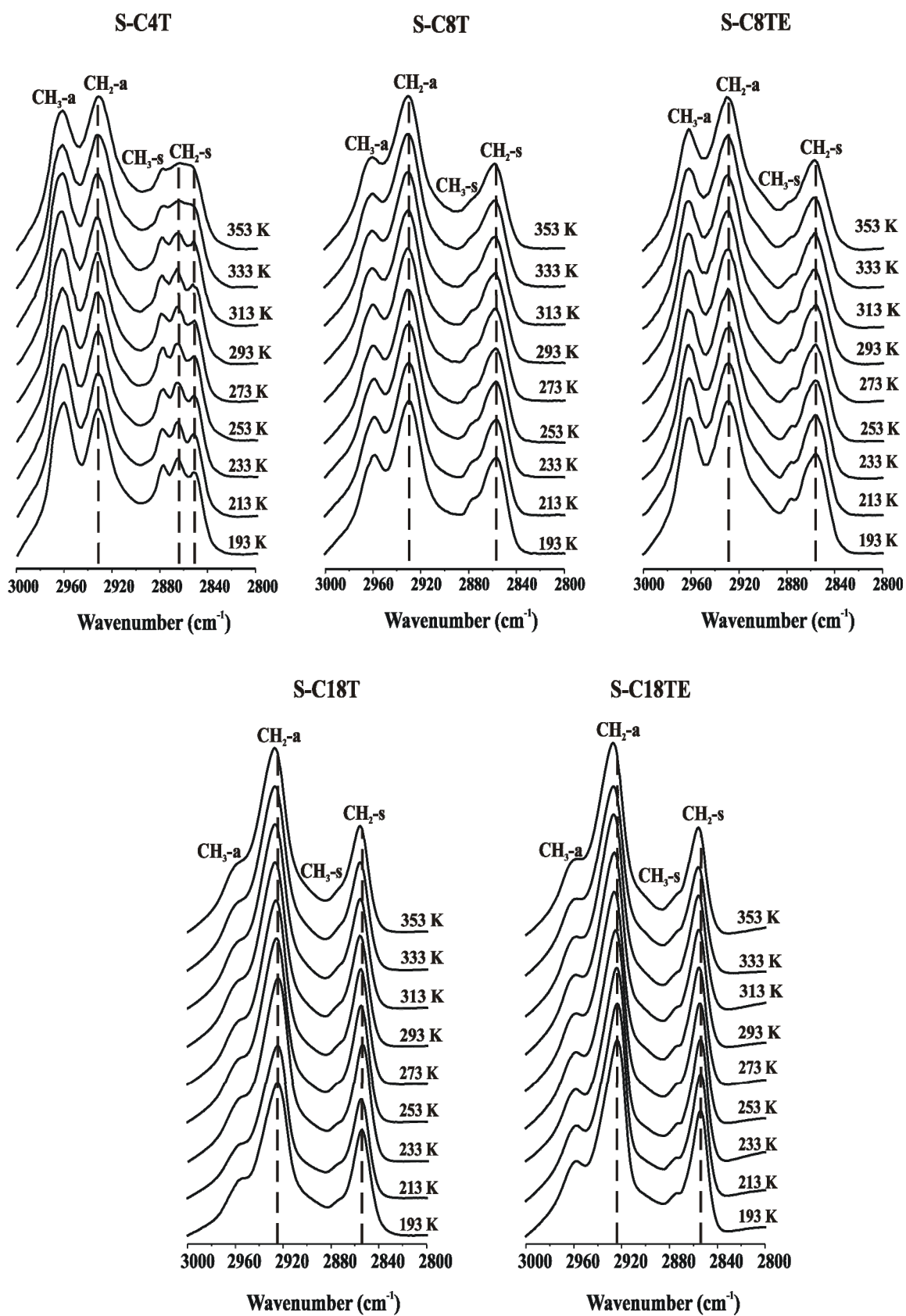


Figure 7.7: Variable temperature FTIR spectra of SBA-15 materials surface modified with trifunctional alkylsilanes.

Figure 7.8 shows the FTIR spectra of SBA-15 materials surface modified with monofunctional chains. Here, two methyl groups are bound to the silicon atom in the alkyl chains which explains the higher relative intensity of the antisymmetric  $\text{CH}_3$  stretching bands. For the sample S-C4M, there is no split-up of the symmetric  $\text{CH}_2$  band, as observed for sample S-C4T. In the sample S-C8M, the antisymmetric  $\text{CH}_2$  stretching band appears at  $2926\text{ cm}^{-1}$  and shifting to  $2928\text{ cm}^{-1}$ . While the symmetric  $\text{CH}_2$  stretching band appears at  $2857\text{ cm}^{-1}$  and shifting to  $2858\text{ cm}^{-1}$ . In the sample S-C8ME, the antisymmetric and symmetric  $\text{CH}_2$  stretching bands are showing an increase of  $2\text{ cm}^{-1}$  upon temperature increase. For samples surface modified with the monofunctional octyl chains, the  $\text{CH}_2$  stretching bands appear at lower wavenumbers owing to the lower conformational order of the monofunctional octyl chains as compared to the trifunctional ones.

In the sample S-C18M, the antisymmetric and symmetric  $\text{CH}_2$  stretching bands appear at  $2927\text{ cm}^{-1}$  and  $2855\text{ cm}^{-1}$  and are shifting to  $2928\text{ cm}^{-1}$  and  $2856\text{ cm}^{-1}$ , respectively. For the sample S-C18ME, there is a shift of  $2\text{ cm}^{-1}$  in wavenumber as the temperature is increasing. The  $\text{CH}_2$  stretching bands appear at higher wavenumbers in materials surface modified with the monofunctional octadecyl chains as compared to corresponding trifunctional materials. This implies that the conformational order in the samples surface modified with monofunctional octadecyl chains is higher than in the trifunctional materials despite the higher carbon content (and thus higher surface coverage) of the latter SBA-15 materials. A possible explanation might be given by the stronger intermolecular interactions of the methyl groups bound to the silicon atom for the monofunctional samples, comprising chain–chain as well as chain–silica surface interactions, and which imposes a higher chain order than for the trifunctional samples.

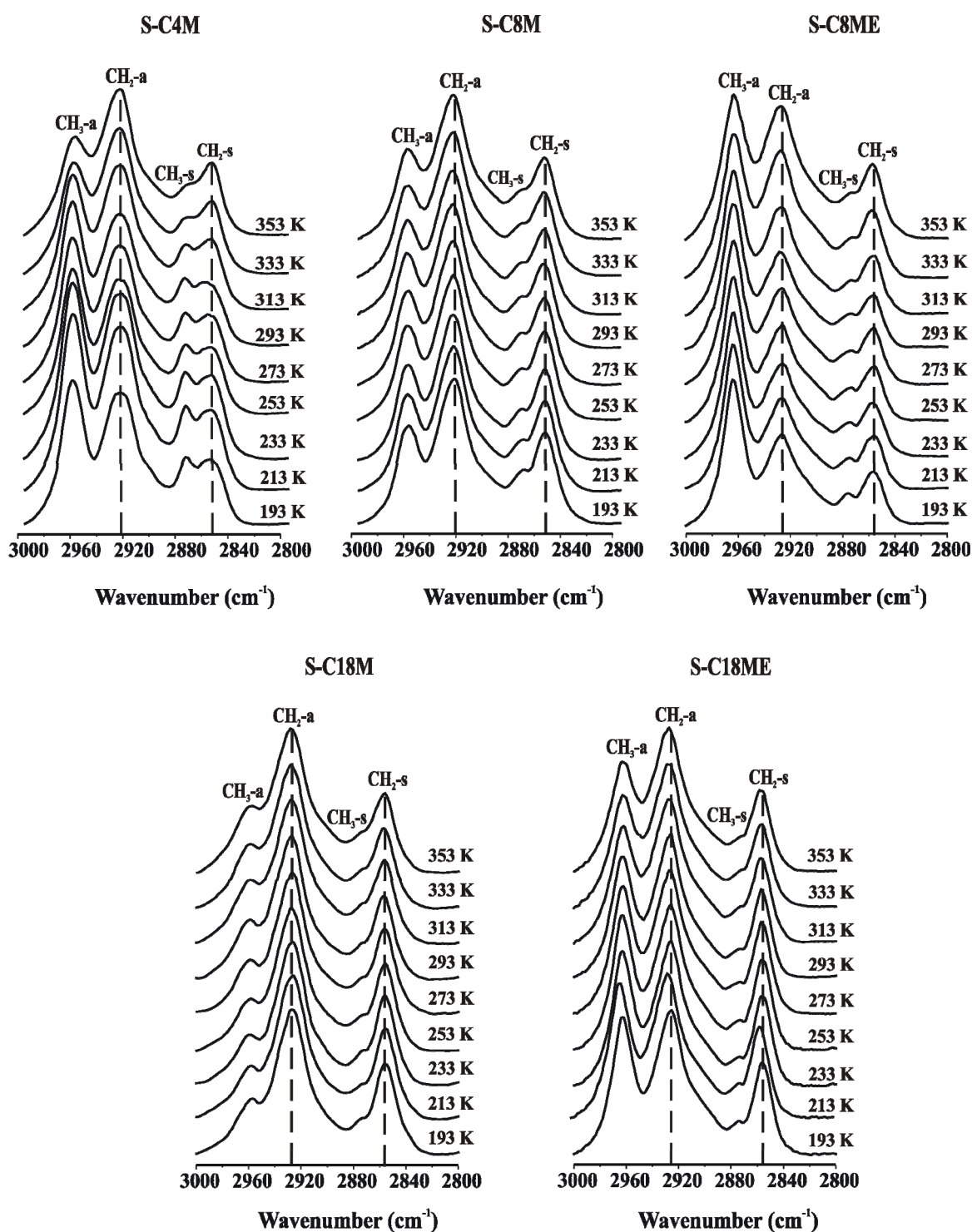


Figure 7.8: Variable temperature FTIR spectra of SBA-15 materials surface modified with monofunctional alkylsilanes.

### 7.3.8 HPLC Measurements

The chromatographic performance of surface modified SBA-15 silica spheres was tested using a test mixture, NIST SRM 870, which consists of five organic components (uracil,

toluene, ethylbenzene, quinizarin and amitriptyline) under controlled conditions, i.e., mobile phase, flow, and temperature.

Figure 7.9 shows the separation chromatograms of the aforementioned test mixture by using the surface modified SBA-15 silica columns with a mobile phase of acetonitrile/water- 50/50 (v/v) at a flow rate of 1.0 ml min<sup>-1</sup>. The eluent time of organic components under these separation conditions follows the order: uracil<toluene<ethylbenzene<quinizarin<amitriptyline. As expected, for reversed-phase chromatography, the more polar compounds elute faster than the less polar molecules [19].

In the majority of the cases, well-separated peaks for uracil, toluene, ethylbenzene, quinizarin, and amitriptyline can be observed. Surface coverage and alkyl chain lengths are the main factors which affect the chromatographic performance of the stationary phases. Hence, the test mixture is well separated with good peak shapes for the stationary phases with higher surface coverage for the alkylsilanes. Endcapping also improves the peak shapes and the chromatographic performance. However, like the trend for longer alkylsilane chains, the increasing hydrophobicity of the surface, in general, also increases the elution time. Materials with low surface coverages often yield tailing peaks for basic analytes because of their interaction with residual silanols. At higher surface coverage, only a small number of silanols remains, and symmetric peak shapes are observed [164].

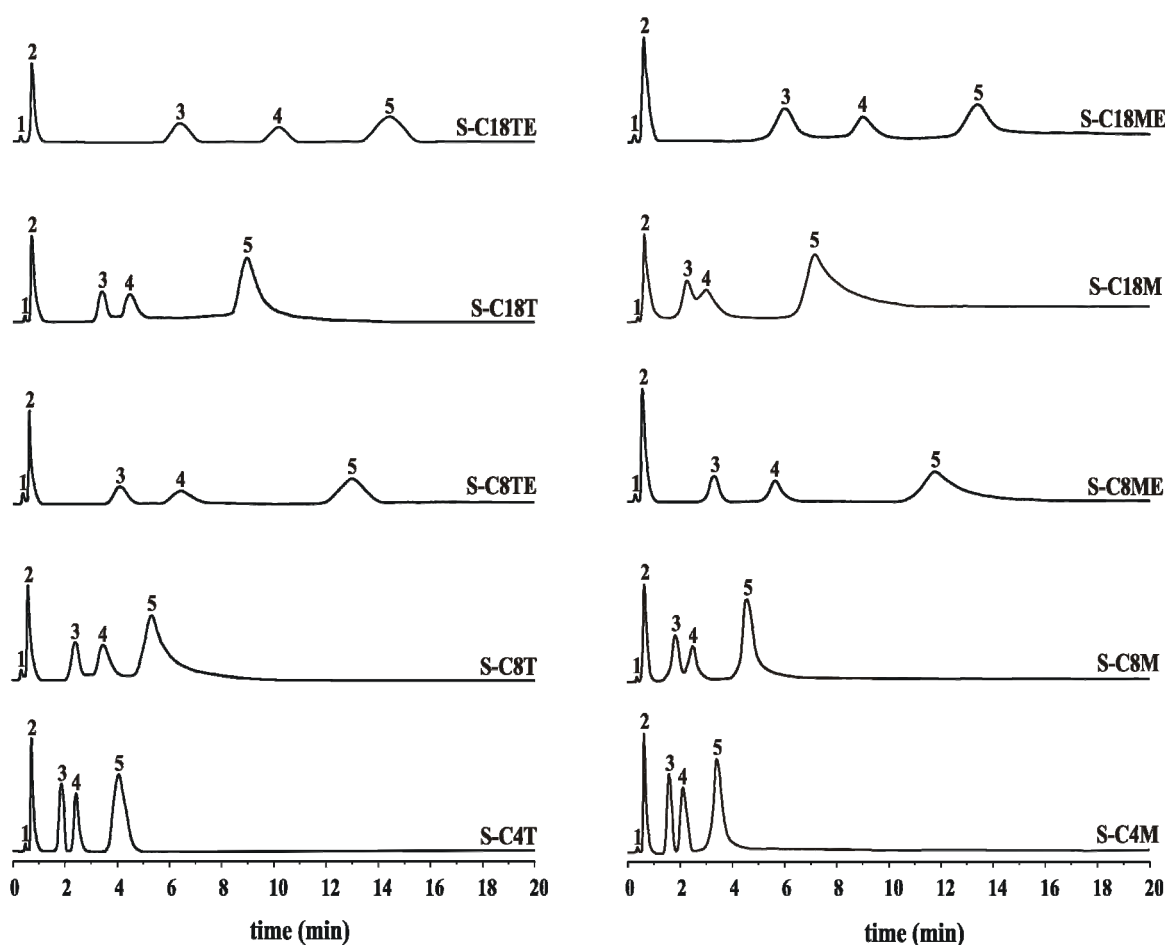


Figure 7.9: HPLC diagrams for test mixture SRM 870 mixture: uracil (1), toluene (2), ethylbenzene (3), quinizarin (4) and amitriptyline (5) using a acetonitrile/water mixture (50/50, v/v) as the mobile phase at flow rate of 1.0 ml/min at 254 nm for SBA-15 materials before and after surface modification.

## 7.4 Concluding Remarks

Mesoporous SBA-15 silica spheres were prepared using triblock copolymer and their spherical morphology was confirmed by SEM analysis. SBA-15 materials with desired surface properties were prepared by surface modification using mono- and trifunctional alkyl chains with different lengths. The mesoporosity and hexagonal pore symmetry of the material is retained after surface modification and this was confirmed by nitrogen sorption and XRD studies. Alkyl chain attachment and chain cross-linking were studied by  $^{29}\text{Si}$  and  $^{13}\text{C}$  NMR spectroscopies. FTIR and  $^{13}\text{C}$  NMR measurements revealed a low conformational order of the alkyl chains in case of monofunctional materials as compared to trifunctional materials, owing to different intermolecular interactions for both types of

alkyl chains, resulting in lower surface coverage for monofunctional materials. For the alkylsilanes with shorter chain lengths higher surface coverages were found, as they can also bind to the interior of the mesopores. The chromatographic performance of all samples was tested. A better separation performance was found for the SBA-15 silica materials with higher surface coverage. A further improvement of the chromatographic separation performance of materials surface modified with longer alkyl chains could be achieved by subsequent endcapping with HMDS. Here, the increased hydrophobicity also yielded longer elution times. In summary, these studies have demonstrated that such mesoporous SBA-15 silica materials are promising candidates for chromatographic applications.





# Chapter 8

## Summary

Silica gels have been the most widely used stationary phase as they are very stable at high pressure, and they yield reproducible separation efficiencies. However, the chromatographic silicas which are commercially available are amorphous, and have low surface area and broad pore size distribution. They also have certain limitations, such as adsorptivity towards basic analytes due to interactions with the silanol groups as well as lack of pH stability. The improvement of the starting silica materials with controllable particle and pore sizes has considerably improved their performance in chromatographic applications. In this dissertation, ordered mesoporous MCM-41 silica spheres and mesoporous spheres of the SBA-15 type were synthesized and their spherical morphology was confirmed by SEM analysis. The unique properties of these silica materials are their high surface areas, the narrow pore size distribution and the adjustable pore size, which put the basis for new chromatographic applications.

The development of organic-inorganic hybrid stationary phases is one of the most important advances in the field of chromatography that make reversed-phase high-performance liquid chromatography as a widely used separation technique. In this dissertation, ordered MCM-41 and SBA-15 silica materials were surface modified with alkyl chains of different lengths, octadecyl ( $C_{18}$ ), octyl ( $C_8$ ), and butyl ( $C_4$ ) chains, using mono and trifunctional silylating agents and employing different preparation methods. In case of materials surface modified with  $C_8$  and  $C_{18}$  alkyl chains, subsequent endcapping of remaining silanols was carried out using HMDS. All the materials were characterized before and after surface modification using various characterization techniques. The elemental composition was determined by elemental analysis, and the morphology of the materials was studied by SEM analysis. The information about mesoporosity, pore size, pore volume, surface area and pore symmetry of the materials was obtained by nitrogen sorption and XRD studies.  $^{29}\text{Si}$  NMR spectroscopy was employed for the determination of the surface species, amount of alkyl chain attachment and degree of cross linking of the

attached alkylsilanes.  $^{13}\text{C}$  NMR spectroscopy was used to study the organic components after attaching alkylsilanes to the MCM-41 and SBA-15 silica surfaces. Recent studies have shown that the conformational order, chain dynamics, and their concomitant effects on retention and selectivity (i.e., separation performance), depend on various factors, such as alkyl chain lengths, chain packing, chain surface coverage, supporting material, temperature and pressure. Therefore, Fourier transform infrared spectroscopy – through analysis of the symmetric and antisymmetric  $\text{CH}_2$  stretching bands – was used to get information about the conformational order of the alkyl chains. The materials surface modified with monofunctional chains exhibited a low conformational order of the alkyl chains as compared to trifunctional materials, and this is attributed to the lower surface coverage for monofunctional materials.

In the first part, MCM-41 spheres with trimodal pore size distribution have been prepared via the pseudomorphic route, using commercial Prontosil silica spheres. These MCM-41 silica spheres were surface modified with octadecyl ( $\text{C}_{18}$ ) alkyl chains using a trifunctional silylating agent (*n*-octadecyltrimethoxysilane). Surface modification of MCM-41 silica was carried out by using direct grafting and surface polymerization methods in order to vary the degree of surface hydrophobicity. The materials prepared using surface polymerization method showed higher surface coverages as compared to the materials prepared by direct grafting method. The chromatographic performances of these  $\text{C}_{18}$  alkyl modified MCM-41 stationary phases were tested with a mixture of alkyl benzenes, and were also compared with the data for commercial Prontosil. The better properties of the present systems can be attributed to their high surface area, well-defined pore size and uniform particle size.

In the next part, after optimization of the reaction conditions, highly ordered MCM-41 silica spheres with uniform mesopores were prepared by the pseudomorphic transformation route using Kromasil silica. The surface modification was carried out using the surface polymerization method. The effect of alkyl chain length and functionality of the alkyl ligands during surface modification was probed by using alkylsilanes of two different alkyl chain lengths and functionalities, octyl ( $\text{C}_8$ ) and butylsilanes ( $\text{C}_4$ ). The shorter chains are able to bind to the interior mesopore walls while on the other hand, because of steric hindrance, longer chains primarily bind to the outer surface and only few chains are attached within the mesopores, leaving a large fraction of non-reacted surface silanol groups which are considered to lead to surface hydrophilicity. The residual silanol groups are weakly acidic, and cause peak tailing for basic solutes

which reduces the resolution and column efficiency in chromatographic applications. Endcapping of these silanols, for instance, by hexamethyldisilazane (HMDS) overcomes this problem and provides a better performance during chromatographic separation. Nitrogen sorption studies revealed that the MCM-41 samples which were surface modified with the trifunctional alkylsilanes exhibited a stronger reduction in surface area, pore size and total pore volume than those from surface modification with monofunctional silanes. In general, the pore size distribution is broadened after surface modification which reflects a non-uniformity of the surface modified MCM-41 channels. The strongest reduction in surface area and pore volume was observed for the two samples which were endcapped with HMDS. From the substantial reduction of these surface quantities, it is clear that smaller trimethylsilyl groups can deeply penetrate into channels resulting in a better surface coverage with enhanced surface hydrophobicity.  $^{29}\text{Si}$  NMR spectroscopy showed that the  $\text{Q}^3$  signal intensity for the samples modified with monofunctional alkylsilanes is higher than for those obtained from trifunctional alkylsilanes, which is consistent with the lower surface coverage. This can be related to the lower reactivity of the former silylation reagent due to the lower probability (only one reactive group available) to react with surface silanols. Further reasons might be the bulky methyl groups of the monofunctional alkylsilane, which provide a steric hindrance for the binding of other alkylsilane chains in close vicinity to a surface-bound alkylsilane, and the lack of cross-linking reactions due to the presence of a single reactive group. Variable temperature FTIR studies were performed for the present surface modified MCM-41 materials. Upon temperature increase, the  $\text{CH}_2$  stretching bands were shifting towards higher wavenumbers, which points to an increase in conformational disorder and enhanced chain mobility with increasing temperature. For MCM-41 samples surface modified with the monofunctional alkylsilanes, the  $\text{CH}_2$  stretching bands appear at slightly lower wavenumbers as compared to the trifunctional materials which is due to the lower conformational order of the monofunctional chains.

The chromatographic performance of all samples was tested using a test mixture, NIST SRM 870. A better separation performance was found for the MCM-41 samples with higher surface coverage. For the materials modified with shorter alkylsilanes sharper peaks of better symmetry were observed. Endcapping was found to improve the peak shapes. However, the increased hydrophobicity yielded longer elution times.

A comprehensive study was also conducted on alkyl bonded mesoporous MCM-41 silica materials prepared using supercritical carbon dioxide ( $\text{sc-CO}_2$ ) as reaction medium.

The surface coverages of the resulting materials are found to be higher than the organic solvent based materials which were prepared by the surface polymerization method, which is explained by the greater accessibility of silanols in *sc*-CO<sub>2</sub>. The resulting materials were characterized using nitrogen sorption analysis, XRD, <sup>29</sup>Si and <sup>13</sup>C NMR spectroscopy. A qualitative study of the conformational order was made by the analysis of the symmetric and antisymmetric CH<sub>2</sub> stretching bands of the IR spectra.

In the final part, mesoporous SBA-15 silica spheres were obtained using the triblock copolymer in acidic media. SBA-15 materials have a hexagonal pore structure like MCM-41. However, they have larger pore diameters which are almost double as compared to MCM-41 materials. The specific surface areas and specific pore volumes are somewhat smaller than that of MCM-41 materials, but pore walls are thicker as compared to MCM-41 materials. Therefore, also the thermal and hydrothermal stability of these materials are better. By surface modification with organic groups, the mesoporous SBA-15 silica spheres can be used as a stationary phase in HPLC to separate both small aromatic molecules as well as biomolecules, such as proteins. Here, a systematic study of C<sub>4</sub>, C<sub>8</sub> and C<sub>18</sub> alkyl modified SBA-15 materials is reported which were prepared by surface polymerization using tri- and monofunctional silanes. For the materials surface modified with C<sub>8</sub> and C<sub>18</sub> alkyl chains, the remaining silanol groups were endcapped by hexamethyldisilazane (HMDS). Nitrogen sorption isotherms of SBA-15 materials have been used to obtain information about the mesoporosity. A typical irreversible IV type isotherm with a H1 hysteresis loop was observed, and the plateau value was lowered for all the samples with increase in surface coverage. This indicates that the attached alkyl chains are located inside the mesoporous channels, and hence reduce the pore dimension of the parent SBA-15 silica material. The degree of organization was investigated by XRD which shows that SBA-15 materials have a pore structure lacking long-range order. Surface modified SBA-15 materials showed XRD patterns similar to the original material which clearly indicate that the hexagonal symmetry and the inorganic wall structure of the SBA-15 material is retained after surface modification. <sup>29</sup>Si NMR measurements revealed that after attachment of the butyl, octyl and octadecyl silanes, the intensities of Q<sup>2</sup> and Q<sup>3</sup> units, bearing surface hydroxyl groups, were significantly reduced, while the intensity for the Q<sup>4</sup> units was found to increase. This trend continued for the endcapped samples which exhibited an additional considerable growth for the Q<sup>4</sup> signal intensity. From <sup>13</sup>C NMR and FTIR measurements, information about the conformation and mobility of the attached alkyl chains was obtained.

The application of surface modified SBA-15 silica materials as a stationary phase was tested by separating a mixture of organic molecules using the test mixture. Surface coverage and alkyl chain lengths were found to be the main factors which affect the chromatographic performance of these stationary phases. Hence, the test mixture was well separated with good peak shapes for the stationary phases with higher surface coverage for the alkylsilanes. It has been shown that generally the alkylsilanes with shorter chains give better peaks, and endcapping was found to improve the peak shapes and the chromatographic performance of the materials modified with longer alkyl chains. However, the increasing hydrophobicity of the surface, in general, also increases the elution time.

In summary, it was demonstrated that ordered mesoporous MCM-41 and SBA-15 silica materials can be used as stationary phases in chromatography after surface modification with alkylsilanes. On the basis of the present investigations it can be stated that surface properties of the MCM-41 and SBA-15 silica supports, type of silylating agent, and surface modification scheme play important roles for determining the surface attachment, conformational order and mobility of the alkyl chains of these stationary phase materials, which in turn determine their chromatographic performances.



# Chapter 9

## Zusammenfassung

Silikagele haben sich als stationäre Trägerphasen in der Adsorptionschromatographie weitgehend durchgesetzt. Sie weisen in der Regel, auch unter erhöhtem Druck, eine sehr gute Stabilität auf und zeichnen sich durch eine gute Reproduzierbarkeit der erzielten Trennwirkung aus. Allerdings sind kommerziell erhältliche Silikagele in der Regel amorph. Sie besitzen eine geringe Oberfläche und weisen eine breite Verteilung der Partikeldurchmesser auf. Desweiteren sind bei der Anwendung dieser Materialien verschiedene Einschränkungen bekannt, wie beispielsweise das Adsorptionsvermögen bei basischen Analyten, bedingt durch Wechselwirkungen mit den Hydroxylgruppen an der Oberfläche, oder die geringe pH-Stabilität. Die Verbesserung der Ausgangs-Silikagele durch Verwendung von Materialien mit gut regulierbarer Teilchen- und Porengröße hat die Einsatzmöglichkeiten dieser Systeme in der Chromatographie erheblich verbessert.

Im Rahmen dieser Dissertation wurden zwei geordnete mesoporöse Silikagele, MCM-41 und SBA-15, hergestellt und deren kugelförmige Gestalt durch SEM-Messungen bestätigt. Zu den besonderen Eigenschaften dieser Silikagele zählen deren große Oberfläche, eine enge Porengrößenverteilung und eine anpassbare Porengröße, die Grundvoraussetzungen für neue chromatographische Anwendungen sind.

Die Entwicklung von neuen Stationärphasen auf der Basis organisch-anorganisch Hybridsysteme ist einer der wichtigsten Fortschritte auf dem Gebiet der Chromatographie, was letztlich die Umkehrphasen-HPLC zu einer der vorherrschenden Trennmethode gemacht hat. In dieser Arbeit wurden geordnete MCM-41- und SBA-15-Silika-Materialien durch Alkylketten unterschiedlicher Länge, Octadecyl ( $C_{18}$ ), Octyl ( $C_8$ ) und Butyl ( $C_4$ ), oberflächenmodifiziert, wobei mono- und trifunktionale Silylierungsreagenzien eingesetzt und verschiedene Präparationstechniken angewendet wurden. Im Falle der Oberflächenmodifizierung mit  $C_8$ - und  $C_{18}$ -Alkylketten wurden die verbliebenen Silanolgruppen anschließend durch Reaktion mit HMDS

(Hexamethyldisilazan) alkyliert. Alle Materialien wurden vor und nach der Oberflächenmodifizierung mit Hilfe verschiedener Messmethoden charakterisiert. Die Probenzusammensetzung wurde über die chemische Elementaranalyse ermittelt. Rasterelektronenmikroskopische Messungen lieferten Aussagen über die Oberflächenstruktur. Informationen über den mesoporösen Charakter (Porengröße, Porenvolumen, Teilchenoberfläche) und zur Poren-Symmetrie wurden aus Stickstoffsorptions- und Röntgenbeugungsmessungen erhalten.

$^{29}\text{Si}$  NMR-Messungen dienten der Bestimmung der Strukturkomponenten an der Silika-Oberfläche, der Anzahl der gebundenen Alkylketten sowie des Vernetzungsgrads der angehenden Alkylsilane.  $^{13}\text{C}$  NMR-Messungen wurden zur Charakterisierung der organischen Komponenten nach Anbindung der Alkylsilane an die MCM-41- und SBA-15-Oberflächen eingesetzt. Aus früheren Untersuchungen war bekannt, dass die Alkylkettenkonformation und -dynamik, und die damit verbundenen Einflüsse auf Retention und Selektivität (d.h. Trennwirkung), von verschiedenen molekularen Parametern, wie Alkylkettenlänge, Kettenpackung, Oberflächenbeladung, Art des verwendeten anorganischen Trägers, Temperatur und Druck, abhängen. Deshalb wurden IR-spektroskopische Messungen (Analyse von  $\text{CH}_2$ -Streckschwingungen) zur Bestimmung der Konformationsordnung durchgeführt. Die durch monofunktionale Ketten modifizierte Materialoberfläche wies, verglichen mit der durch trifunktionale Ketten modifizierten Oberfläche, eine geringere Konformationsordnung der Alkylketten auf. Dieser Effekt wird der niedrigeren Oberflächenbeladung der monofunktionalen Materialien zugeschrieben.

Im ersten Abschnitt der Arbeit wurden über das sog. pseudomorphe Herstellungsverfahren, unter Verwendung von kommerziellem Silikagel mit definierter Kugelform (Prontosil), sphärische MCM-41-Silikapartikel mit trimodaler Porengrößenverteilung hergestellt. Die so erhaltenen MCM-41-Materialien wurden mittels Octadecylketten ( $\text{C}_{18}$ ), durch Einsatz eines trifunktionalen Silylierungsreagenz (n-Octadecyltrimethoxysilan), oberflächenmodifiziert. Die Anbindung erfolgt entweder direkt oder über Oberflächenpolymerisation, was eine Variation des hydrophoben Charakters der Oberfläche ermöglichte. Die durch Oberflächenpolymerisation hergestellten Materialien weisen generell eine höhere Oberflächenbeladung auf als die Materialien, die durch das direkte Anbindungsverfahren hergestellt wurden. Das chromatographische Verhalten dieser alkylierten, stationären MCM-41-Phasen wurde mittels eines Gemisches aus Alkylbenzolen getestet, und die Ergebnisse wurden



mit den Resultaten für kommerzielle Prontosil-Säulen verglichen. Die beobachteten verbesserten Trenneigenschaften der hier hergestellten Stationärphasen werden der größeren Oberfläche, der definierten Porengröße und der einheitlichen Partikelgröße zugeschrieben.

Im nächsten Abschnitt der Arbeit wurden, ausgehend von Kromasil-Silikagel und nach Optimierung der Reaktionsbedingungen, ebenfalls über die pseudomorphe Syntheseroute hoch geordnete MCM-41-Silika-Kugeln mit einheitlicher Porengröße hergestellt. Die Oberflächenmodifikation wurde über das Oberflächenpolymerisations-Verfahren durchgeführt. Die Auswirkungen der Alkylkettenlänge und der Funktionalität der verwendeten Alkyliganden wurde mittels zweier unterschiedlicher Alkylkettenlängen, Octyl- ( $C_8$ ) und Butylsilane ( $C_4$ ), und funktioneller Gruppen ausgetestet. Die kürzeren Ketten konnten auch an die inneren Porenwände angebunden werden. Aus sterischen Gründen wurden die längeren Ketten vorwiegend an den äußeren Oberflächen angebunden, während in diesem Fall nur wenige Ketten die inneren Poren erreichen. Hieraus ergab sich eine große Anzahl verbliebender Oberflächen-Silanolgruppen, was wiederum zu einem verstärkten hydrophilen Oberflächencharakter dieser Systeme führt. Diese Silanolgruppen sind schwach sauer und bewirken bei basischen Lösungen ein sog. „Peak tailing“, welches die Auflösung und die Effizienz der Säulen bei der chromatographischen Trennung verringert. Das Abschirmen dieser Silanol-Gruppen, vorzugsweise durch Alkylierung mittels HMDS, führte deshalb zu deutlich verbesserten Trenneigenschaften. Stickstoffsorptionsmessungen ergaben, dass die MCM-41-Proben, die mit trifunktionalen Alkylsilanen modifiziert wurden, eine stärkere Verringerung der Oberfläche, der Porengröße und des Gesamtvolumens aufweisen als die mit monofunktionalen Silanen modifizierten Proben. In der Regel verbreiterten sich die Porengrößenverteilung nach der Oberflächenmodifizierung, was die Unregelmäßigkeit bei der oberflächenmodifizierten MCM-41-Kanäle widerspiegelt. Die stärkste Abnahme der Oberfläche und des Porenvolumens wurde bei den beiden mittels HMDS behandelten Proben beobachtet. Die deutliche Verringerung dieser Oberflächenparameter zeigte, dass die kleineren Trimethylsilyl-Gruppen weiter in die Kanäle vordringen können und durch die bessere Beladung der hydrophobe Charakter der MCM-41-Oberfläche zunimmt.

$^{29}\text{Si}$ -NMR-Messungen zeigten, dass die  $Q^3$ -Signalintensität für die mit monofunktionalen Alkylsilanen modifizierten Proben, im Vergleich zu den mit trifunktionalen Alkylsilanen modifizierten Proben, größer ist. Die daraus resultierende

niedrigere Oberflächenbeladung konnte auf die geringere Reaktivität des erstgenannten Silylierungsmittels, das nur über eine reaktive Gruppe verfügte, zurückgeführt werden. Weitere Gründe sind die sperrigen Methylgruppen des monofunktionalen Alkylsilans, die nach Anbindung für weitere Alkylsilan-Ketten ein sterisches Hindernis darstellen. Ebenfalls ist keine Quervernetzung möglich, da hier nur eine funktionelle Gruppe vorhanden ist. An den oberflächenmodifizierten MCM-41-Materialien wurden temperaturabhängige FTIR-Messungen durchgeführt. Mit ansteigender Temperatur verschoben sich die CH<sub>2</sub>-Streckschwingungsbanden zu höheren Wellenzahlen, was eine Abnahme der Konformationsordnung und Erhöhung der Alkylketten-Beweglichkeit anzeigte. Die CH<sub>2</sub>-Streckschwingungsbanden der mit monofunktionalen Alkylsilanen modifizierten MCM-41 Proben lagen bei etwas niedrigeren Wellenzahlen als die der mit trifunktionalen Alkylsilanen behandelten Materialien, was wiederum eine geringere Konformationsordnung der monofunktionalen Ketten anzeigte.

Das chromatographische Verhalten aller Proben wurde mit der Testmischung „NIST SRM 870“ überprüft. Ein besseres Trennverhalten erzielte man für die MCM-41-Proben mit höherer Oberflächenbeladung. Bei den mit kürzeren Alkylsilanen modifizierten Materialien wurden schärfere Peaks mit besserer Symmetrie beobachtet. Die Alkylierung mit HDMS ergab eine verbesserte Peakform. Jedoch hatte der daraus resultierende stärkere hydrophobe Charakter der Silika-Oberfläche längere Eluationszeiten zur Folge.

Eine umfangreiche Studie wurde ebenfalls an mesoporösen MCM-41 Materialien durchgeführt, bei denen die Alkylketten über superkritisches Kohlenstoffdioxid (sc-CO<sub>2</sub>) als Reaktionsmedium angebunden wurden. Die Oberflächenbeladung der resultierenden Materialien war größer als die in Gegenwart organischer Lösungsmittel durch Oberflächenpolymerisation dargestellten Materialien, was auf die bessere Zugänglichkeit der Silanolgruppen in superkritischem Kohlenstoffdioxid zurückgeführt wurde. Diese Materialien wurden mit Hilfe von Stickstoffsorptions-, Röntgen- sowie <sup>29</sup>Si und <sup>13</sup>C NMR-Messungen charakterisiert. Zur Bestimmung der Konformationsordnung der gebundenen Alkylketten wurden wiederum IR-spektroskopische Verfahren eingesetzt.

Im abschließenden Abschnitt wurden mesoporöse SBA-15 Silikakugeln mit Hilfe von geeigneten Triblock-Copolymeren in sauren Medien hergestellt. SBA-15-Materialien besitzen ebenfalls eine hexagonale Porenstruktur wie MCM-41, allerdings mit einem beinahe doppelt so großen Porendurchmesser. Die spezifische Oberfläche und das Porenvolumen sind etwas kleiner als bei den MCM-41-Systemen. Die Porenwände sind

dagegen dicker, was sowohl die thermische als auch die hydrothermische Beständigkeit verbessert. Die durch organische Gruppen modifizierten mesoporösen SBA-15-Kugeln können ebenfalls als stationäre Phase in der HPLC verwendet werden. Sie trennen sowohl Aromaten als auch Biomoleküle, wie beispielsweise Proteine.

Es wurden systematische Studien an C<sub>4</sub>-, C<sub>8</sub>- und C<sub>18</sub>-modifizierten SBA-15-Materialien vorgenommen, die über Oberflächenpolymerisation mit mono- und trifunktionalen Silylierungsmitteln dargestellt wurden. Bei den mit C<sub>8</sub>- und C<sub>18</sub>-Alkylketten modifizierten SBA-15-Materialien wurden die verbleibenden Silanolgruppen durch HMDS alkyliert. Stickstoffsorptionsmessungen wurden durchgeführt, um Informationen über den mesoporösen Charakter der Proben zu erhalten. In diesem Zusammenhang wurde eine typische Typ IV-Isotherme mit einer H1-Hysterese-Schleife beobachtet, und der Plateauwert nahm mit steigender Oberflächenbeladung der Proben ab. Dies zeigte, dass die Alkylketten in den mesoporösen Kanälen gebunden sind und daher die Porendimensionen der SBA-15-Materialien entsprechend abnehmen. Röntgenuntersuchungen zeigten, dass die SBA-15-Materialien eine Porenstruktur mit geringerer Langreichweite besitzen. Die oberflächenmodifizierte SBA-15-Materialien wiesen die gleiche Röntgenmuster auf wie das Ausgangsmaterial, d.h. die hexagonale Symmetrie und die Struktur der anorganischen Wände des SBA-15 Materials blieben auch nach der Oberflächenmodifizierung erhalten. <sup>29</sup>Si NMR-Messungen ergaben, dass sich nach dem Anbinden der Butyl-, Octyl- und Octadecylsilanen die Intensität der Q<sup>2</sup>- und Q<sup>3</sup>-Signale, die für die Zahl der Hydroxylgruppen an der Oberfläche stehen, deutlich abnehmen, während die Intensität des Q<sup>4</sup>-Signals ansteigt. Für die zusätzlich mit HMDS behandelten Proben ergibt sich ebenfalls ein beträchtlicher Intensitätsanstieg der Q<sup>4</sup>-Signale. Aus den <sup>13</sup>C NMR- und IR-Messungen wurden Informationen über Konformation und Beweglichkeit der angehängten Alkylketten erhalten.

Der Einsatz von oberflächenmodifizierten SBA-15-Materialien als stationäre Phase wurde durch mittels Auftrennung einer Testmischung aus verschiedenen organischen Molekülen überprüft. Dabei erwiesen sich die Oberflächenbeladung und die Alkylkettenlänge als die entscheidenden Faktoren, welche für das Chromatographieverhalten dieser stationären Phasen wesentlich sind. Demzufolge wurde die Testmischung mit Hilfe der stationären Phasen sauber getrennt, die eine höhere Oberflächenbeladung an Alkylsilanen aufwiesen. In der Regel ergaben die Stationärphasen, die mit kürzerkettigen Alkylsilanen modifiziert wurden, schärfere HPLC-Peaks und die zusätzliche Alkylierung mit HMDS hatte eine Verbesserung der

Peakform und des Chromatographieverhaltens zur Folge. Jedoch führte die damit verbundene Hydrophobizität der Oberfläche auch bei diesen SBA-15-Materialien zu längeren Eluationszeiten.

Zusammenfassend lässt sich feststellen, dass geordnete mesoporöse MCM-41- and SBA-15-Silikagele nach Oberflächenmodifizierung mit Alkylsilanen grundsätzlich als Stationärphasen in der Chromatographie verwendet werden können. Die im Rahmen dieser Arbeit durchgeführten Untersuchungen haben gezeigt, dass die Oberflächeneigenschaften der MCM-41- and SBA-15-Silikagele, das verwendete Silylierungsmittel und das Verfahren zur Oberflächenmodifizierung einen entscheidenden Einfluss auf die Oberflächenanbindung, die Konformationsordnung und Mobilität der Alkylketten haben, was sich wiederum auf das Verhalten dieser Stationärphasen während des chromatographischen Trennprozesses auswirkt.

## References

- [1] L.R. Snyder, J.J. Kirkland, Introduction to modern liquid chromatography, Wiley, New York ; Chichester, 1979.
- [2] Y.V. Kazakevich, R. LoBrutto, HPLC for Pharmaceutical Scientists, Wiley Interscience, 2007.
- [3] J. Kirkland, *Chromatographia* 8 (1975) 661.
- [4] K.S.W. Sing, D.H. Everett, R.A.W. Haul, L. Moscou, R.A. Pierotti, J. Rouquerol, T. Siemieniewska, *Pure and Applied Chemistry* 57 (1985) 603.
- [5] J.Y. Ying, C.P. Mehnert, M.S. Wong, *Angewandte Chemie-International Edition* 38 (1999) 56.
- [6] K.W. Gallis, J.T. Araujo, K.J. Duff, J.G. Moore, C.C. Landry, *Advanced Materials* 11 (1999) 1452.
- [7] A.L. Doadrio, E.M.B. Sousa, J.C. Doadrio, J.P. Pariente, I. Izquierdo-Barba, M. Vallet-Regi, *Journal of Controlled Release* 97 (2004) 125.
- [8] C.T. Kresge, M.E. Leonowicz, W.J. Roth, J.C. Vartuli, J.S. Beck, *Nature* 359 (1992) 710.
- [9] J.S. Beck, J.C. Vartuli, W.J. Roth, M.E. Leonowicz, C.T. Kresge, K.D. Schmitt, C.T.W. Chu, D.H. Olson, E.W. Sheppard, S.B. Mccullen, J.B. Higgins, J.L. Schlenker, *Journal of the American Chemical Society* 114 (1992) 10834.
- [10] Q.S. Huo, D.I. Margolese, U. Ciesla, D.G. Demuth, P.Y. Feng, T.E. Gier, P. Sieger, A. Firouzi, B.F. Chmelka, F. Schuth, G.D. Stucky, *Chemistry of Materials* 6 (1994) 1176.
- [11] Q.S. Huo, D.I. Margolese, G.D. Stucky, *Chemistry of Materials* 8 (1996) 1147.
- [12] A. Sayari, *Recent Advances and New Horizons in Zeolite Science and Technology* 102 (1996) 1.
- [13] C.G. Wu, T. Bein, *Science* 266 (1994) 1013.
- [14] C.G. Wu, T. Bein, *Science* 264 (1994) 1757.
- [15] C.G. Wu, T. Bein, *Chemistry of Materials* 6 (1994) 1109.
- [16] C. Huber, K. Moller, T. Bein, *Journal of the Chemical Society-Chemical Communications* (1994) 2619.
- [17] P.T. Tanev, M. Chibwe, T.J. Pinnavaia, *Nature* 368 (1994) 321.
- [18] J. Rathousky, A. Zukal, O. Franke, G. Schulzekloff, *Journal of the Chemical Society-Faraday Transactions* 90 (1994) 2821.
- [19] A.V. Neimark, P.I. Ravikovitch, M. Grun, F. Schuth, K.K. Unger, *Journal of Colloid and Interface Science* 207 (1998) 159.
- [20] N.K. Raman, M.T. Anderson, C.J. Brinker, *Chemistry of Materials* 8 (1996) 1682.
- [21] A. Sayari, P. Liu, *Microporous Materials* 12 (1997) 149.
- [22] A. Galarneau, J. Iapichella, K. Bonhomme, F. Di Renzo, P. Kooyman, O. Terasaki, F. Fajula, *Advanced Functional Materials* 16 (2006) 1657.
- [23] T. Martin, A. Galarneau, F. Di Renzo, D. Brunel, F. Fajula, S. Heinisch, G. Cretier, J.L. Rocca, *Chemistry of Materials* 16 (2004) 1725.
- [24] C. Boissiere, M. Kummel, M. Persin, A. Larbot, E. Prouzet, *Advanced Functional Materials* 11 (2001) 129.
- [25] M. Grun, A.A. Kurganov, S. Schacht, F. Schuth, K.K. Unger, *Journal of Chromatography A* 740 (1996) 1.
- [26] M. Grun, I. Lauer, K.K. Unger, *Advanced Materials* 9 (1997) 254.

- [27] A. Galarneau, J. Lapichella, D. Brunel, F. Fajula, Z. Bayram-Hahn, K. Unger, G. Puy, C. Demesmay, J.L. Rocca, *Journal of Separation Science* 29 (2006) 844.
- [28] A. Kurganov, K. Unger, T. Issaeva, *Journal of Chromatography A* 753 (1996) 177.
- [29] M. Raimondo, G. Perez, N. Sinibaldi, A. DeStefanis, A.A.G. Tomlinson, *Chemical Communications* (1997) 1343.
- [30] C. Thoelen, K. Van de Walle, I.F.J. Vankelecom, P.A. Jacobs, *Chemical Communications* (1999) 1841.
- [31] C. Boissiere, A. van der Lee, A. El Mansouri, A. Larbot, E. Prouzet, *Chemical Communications* (1999) 2047.
- [32] Y.F. Lu, H.Y. Fan, A. Stump, T.L. Ward, T. Rieker, C.J. Brinker, *Nature* 398 (1999) 223.
- [33] T. Martin, A. Galarneau, F. Di Renzo, F. Fajula, D. Plee, *Angewandte Chemie-International Edition* 41 (2002) 2590.
- [34] D.Y. Zhao, Q.S. Huo, J.L. Feng, B.F. Chmelka, G.D. Stucky, *Journal of the American Chemical Society* 120 (1998) 6024.
- [35] D.Y. Zhao, J.L. Feng, Q.S. Huo, N. Melosh, G.H. Fredrickson, B.F. Chmelka, G.D. Stucky, *Science* 279 (1998) 548.
- [36] A. Vinu, M. Hartmann, *Chemistry Letters* 33 (2004) 588.
- [37] D.Y. Zhao, J.Y. Sun, Q.Z. Li, G.D. Stucky, *Chemistry of Materials* 12 (2000) 275.
- [38] A. Galarneau, D. Desplandier-Giscard, F. Di Renzo, F. Fajula, *Catalysis Today* 68 (2001) 191.
- [39] A.M. Liu, K. Hidajat, S. Kawi, D.Y. Zhao, *Chemical Communications* (2000) 1145.
- [40] M. Mesa, L. Sierra, B. Lopez, A. Ramirez, J.L. Guth, *Solid State Sciences* 5 (2003) 1303.
- [41] K. Kosuge, P.S. Singh, *Chemistry of Materials* 13 (2001) 2476.
- [42] Y.R. Ma, L.M. Qi, J.M. Ma, Y.Q. Wu, O. Liu, H.M. Cheng, *Colloids and Surfaces a-Physicochemical and Engineering Aspects* 229 (2003) 1.
- [43] A. Stein, B.J. Melde, R.C. Schroden, *Advanced Materials* 12 (2000) 1403.
- [44] A.P. Wight, M.E. Davis, *Chemical Reviews* 102 (2002) 3589.
- [45] J.W. Wiench, Y.S. Avadhut, N. Maity, S. Bhaduri, G.K. Lahiri, M. Pruski, S. Ganapathy, *Journal of Physical Chemistry B* 111 (2007) 3877.
- [46] U. Schubert, *New Journal of Chemistry* 18 (1994) 1049.
- [47] R. Maoz, J. Sagiv, *Journal of Colloid and Interface Science* 100 (1984) 465.
- [48] S.R. Wasserman, G.M. Whitesides, I.M. Tidswell, B.M. Ocko, P.S. Pershan, J.D. Axe, *Journal of the American Chemical Society* 111 (1989) 5852.
- [49] U. Trudinger, G. Müller, K.K. Unger, *Journal of Chromatography* 535 (1990) 111.
- [50] C.P. Tripp, M.L. Hair, *Langmuir* 11 (1995) 1215.
- [51] L.C. Sander, K.A. Lippa, S.A. Wise, *Analytical and Bioanalytical Chemistry* 382 (2005) 646.
- [52] L.C. Sander, S.A. Wise, *Analytical Chemistry* 67 (1995) 3284.
- [53] M.J. Wirth, H.O. Fatunmbi, *Analytical Chemistry* 65 (1993) 822.
- [54] M. Pursch, L.C. Sander, K. Albert, *Analytical Chemistry* 68 (1996) 4107.
- [55] L.C. Sander, S.A. Wise, *Analytical Chemistry* 56 (1984) 504.
- [56] J.J. Kirkland, M.A. Vanstraten, H.A. Claessens, *Journal of Chromatography A* 691 (1995) 3.
- [57] K. Kailasam, A. Fels, K. Müller, *Microporous and Mesoporous Materials* 117 (2009) 136.

- [58] K. Kailasam, S. Mascotto, S. Gross, C. Maccato, K. Müller, *Journal of Materials Chemistry* 20 (2010) 2345.
- [59] L.O. Healy, V.P. Owens, T. O'Mahony, S. Srijaranai, J.D. Holmes, J.D. Glennon, G. Fischer, K. Albert, *Analytical Chemistry* 75 (2003) 5860.
- [60] B. McCool, C.P. Tripp, *Journal of Physical Chemistry B* 109 (2005) 8914.
- [61] J.R. Combes, L.D. White, C.P. Tripp, *Langmuir* 15 (1999) 7870.
- [62] Y. Shin, T.S. Zemanian, G.E. Fryxell, L.Q. Wang, J. Liu, *Microporous and Mesoporous Materials* 37 (2000) 49.
- [63] T. Welsch, H. Frank, G. Vigh, *Journal of Chromatography* 506 (1990) 97.
- [64] G.B. Cox, *Journal of Chromatography A* 656 (1993) 353.
- [65] N.H.C. Cooke, K. Olsen, *Journal of Chromatographic Science* 18 (1980) 512.
- [66] A. Pryde, *Journal of Chromatographic Science* 12 (1974) 486.
- [67] M. Kruk, M. Jaroniec, *Chemistry of Materials* 13 (2001) 3169.
- [68] F.o. Rouquerol, J. Rouquerol, K.S.W. Sing, *Adsorption by powders & porous solids : principles, methodology and applications*, Academic Press, San Diego, Calif., 1999.
- [69] P.I. Ravikovitch, S.C. O'Donnell, A.V. Neimark, F. Schuth, K.K. Unger, *Langmuir* 11 (1995) 4765.
- [70] S.J. Gregg, K.S.W. Sing, *Adsorption, surface area, and porosity*, Academic Press, London ; New York, 1982.
- [71] C. Sangwichien, G.L. Aranovich, M.D. Donohue, *Colloids and Surfaces A: Physicochemical and Engineering Aspects* 206 (2002) 313.
- [72] S. Brunauer, P.H. Emmett, E. Teller, *Journal of the American Chemical Society* 60 (1938) 309.
- [73] C.P. Jaroniec, M. Kruk, M. Jaroniec, A. Sayari, *Journal of Physical Chemistry B* 102 (1998) 5503.
- [74] A.S.M. Chong, X.S. Zhao, *Journal of Physical Chemistry B* 107 (2003) 12650.
- [75] L. Jelinek, E.S. Kovats, *Langmuir* 10 (1994) 4225.
- [76] L. Gurvitsch, *J. Phys. Chem. Soc. Russ.* 47 (1915) 805.
- [77] E.P. Barrett, L.G. Joyner, P.P. Halenda, *Journal of the American Chemical Society* 73 (1951) 373.
- [78] M. Kruk, M. Jaroniec, A. Sayari, *Langmuir* 13 (1997) 6267.
- [79] Y. Zhang, F.L.Y. Lam, Z.F. Yan, X.J. Hu, *Chinese Journal of Chemical Physics* 19 (2006) 102.
- [80] L.A. Solovyov, S.D. Kirik, A.N. Shmakov, V.N. Romannikov, *Microporous and Mesoporous Materials* 44 (2001) 17.
- [81] L.A. Solovyov, A.M. Astachov, M.S. Molokeyev, A.D. Vasiliev, *Acta Crystallographica Section B-Structural Science* 61 (2005) 435.
- [82] M. Imperor-Clerc, P. Davidson, A. Davidson, *Journal of the American Chemical Society* 122 (2000) 11925.
- [83] G.A. Zickler, S. Jahnert, W. Wagermaier, S.S. Funari, G.H. Findenegg, O. Paris, *Physical Review B* 73 (2006).
- [84] M. Mehring, *Principles of high-resolution NMR in solids*, Springer-Verlag, Berlin ; New York, 1983.
- [85] A. Abragam, *The Principles of Nuclear Magnetism*. [With plates.], Clarendon Press, Oxford, 1961.
- [86] R.R. Ernst, G. Bodenhausen, A. Wokaun, *Principles of nuclear magnetic resonance in one and two dimensions*, Clarendon Press, Oxford, 1987.
- [87] K. Schmidt-Rohr, H.W. Spiess, *Multidimensional solid-state NMR and polymers*, Academic Press, London, 1994.

- [88] J.M. Thomas, J. Klinowski, *Adv. Catal.* 33 (1985) 199.
- [89] J.F. Haw, T. Xu, *Adv. Catal.* 42 (1998) 115.
- [90] E.R. Andrew, *Proc. Nucl. Magn. Reson. Spectrosc.* 8 (1971) 1.
- [91] E.R. Andrew, W.S. Hinshaw, *Physics Letters A* 43 (1973) 113.
- [92] A. Pines, M.G. Gibby, J.S. Waugh, *Journal of Chemical Physics* 59 (1973) 569.
- [93] S.R. Hartmann, E.L. Hahn, *Physical Review* 128 (1962) 2042.
- [94] G.E. Maciel, D.W. Sindorf, *Journal of the American Chemical Society* 102 (1980) 7606.
- [95] D.W. Sindorf, G.E. Maciel, *Journal of the American Chemical Society* 103 (1981) 4263.
- [96] R. Mendelsohn, M.A. Davies, J.W. Brauner, H.F. Schuster, R.A. Dluhy, *Biochemistry* 28 (1989) 8934.
- [97] S. Singh, J. Wegmann, K. Albert, K. Müller, *Journal of Physical Chemistry B* 106 (2002) 878.
- [98] K.M. Merz, B.t. Roux, *Biological membranes : a molecular perspective from computation and experiment*, Birkhauser Boston, Boston, 1996.
- [99] L.C. Sander, J.B. Callis, L.R. Field, *Analytical Chemistry* 55 (1983) 1068.
- [100] G. Srinivasan, L.C. Sander, K. Müller, *Analytical and Bioanalytical Chemistry* 384 (2006) 514.
- [101] G. Srinivasan, C. Meyer, N. Welsch, K. Albert, K. Müller, *Journal of Chromatography A* 1113 (2006) 45.
- [102] K. Kailasam, G. Srinivasan, K. Müller, *Journal of Chromatography A* 1134 (2006) 81.
- [103] K. Kailasam, M.M. Natile, A. Glisenti, K. Müller, *Journal of Chromatography A* 1216 (2009) 2345.
- [104] G. Srinivasan, K. Müller, *Journal of Chromatography A* 1110 (2006) 102.
- [105] G. Srinivasan, M. Pursch, L.C. Sander, K. Müller, *Langmuir* 20 (2004) 1746.
- [106] G. Srinivasan, A. Kyrilidis, C. McNeff, K. Müller, *Journal of Chromatography A* 1081 (2005) 132.
- [107] J.G. Dorsey, W.T. Cooper, J.F. Wheeler, H.G. Barth, J.P. Foley, *Analytical Chemistry* 66 (1994) R500.
- [108] R.G. Snyder, *Journal of Chemical Physics* 47 (1967) 1316.
- [109] H. Farida, B.C. James, *J. Am. Chem. Soc.* 93 (1989) 2053.
- [110] R.G. Snyder, M.W. Poore, *Macromolecules* 6 (1973) 708.
- [111] A. Badia, L. Cuccia, L. Demers, F. Morin, R.B. Lennox, *Journal of the American Chemical Society* 119 (1997) 2682.
- [112] Y. Xiang, Y. Liu, M.L. Lee, *Journal of Chromatography A* 1104 (2006) 198.
- [113] C.G. Horvath, B.A. Preiss, S.R. Lipsky, *Analytical Chemistry* 39 (1967) 1422.
- [114] L.C. Sander, S.A. Wise, *Advances in Chromatography* 25 (1986) 139.
- [115] N. Tanaka, Y. Tokuda, K. Iwaguchi, M. Araki, *Journal of Chromatography* 239 (1982) 761.
- [116] K.B. Sentell, A.N. Henderson, *Analytica Chimica Acta* 246 (1991) 139.
- [117] M. Pursch, D.L. Vanderhart, L.C. Sander, X.H. Gu, T. Nguyen, S.A. Wise, D.A. Gajewski, *Journal of the American Chemical Society* 122 (2000) 6997.
- [118] C.A. Doyle, T.J. Vickers, C.K. Mann, J.G. Dorsey, *Journal of Chromatography A* 877 (2000) 25.
- [119] J.E. Pemberton, M.K. Ho, C.J. Orendorff, M.W. Ducey, *Journal of Chromatography A* 913 (2001) 243.
- [120] C.A. Doyle, T.J. Vickers, C.K. Mann, J.G. Dorsey, *Journal of Chromatography A* 877 (2000) 41.



- [121] K.B. Sentell, *Journal of Chromatography A* 656 (1993) 231.
- [122] S. Neumann-Singh, J. Villanueva-Garibay, K. Müller, *Journal of Physical Chemistry B* 108 (2004) 1906.
- [123] M. Pursch, L.C. Sander, H.J. Egelhaaf, M. Raitza, S.A. Wise, D. Oelkrug, K. Albert, *Journal of the American Chemical Society* 121 (1999) 3201.
- [124] M.W. Ducey, C.J. Orendorff, J.E. Pemberton, L.C. Sander, *Analytical Chemistry* 74 (2002) 5576.
- [125] S.J. Klatte, T.L. Beck, *Journal of Physical Chemistry* 97 (1993) 5727.
- [126] I. Yarovsky, M.I. Aguilar, M.T.W. Hearn, *Journal of Chromatography A* 660 (1994) 75.
- [127] S.J. Klatte, T.L. Beck, *Journal of Physical Chemistry* 99 (1995) 16024.
- [128] I. Yarovsky, M.L. Aguilar, M.T.W. Hearn, *Analytical Chemistry* 67 (1995) 2145.
- [129] K.B. Sentell, J.G. Dorsey, *Journal of Chromatography* 461 (1989) 193.
- [130] R.C. Zeigler, G.E. Maciel, *Journal of the American Chemical Society* 113 (1991) 6349.
- [131] M. Pursch, S. Strohschein, H. Handel, K. Albert, *Analytical Chemistry* 68 (1996) 386.
- [132] G. Srinivasan, S. Neumann-Singh, K. Müller, *Journal of Chromatography A* 1074 (2005) 31.
- [133] B. Liu, W.C. Wang, X.R. Zhang, *Physical Chemistry Chemical Physics* 6 (2004) 3985.
- [134] P. Schuster, G. Zundel, C. Sandorfy, *The hydrogen bond : recent developments in theory and experiments. Vol.3*, North-Holland Publishing Co., Amsterdam ; Oxford, 1976.
- [135] K. Kailasam, K. Müller, *Journal of Chromatography A* 1191 (2008) 125.
- [136] J. Iapichella, J.M. Meneses, I. Beurroies, R. Denoyel, Z. Bayram-Hahn, K. Unger, A. Galarneau, *Microporous and Mesoporous Materials* 102 (2007) 111.
- [137] H. Engelhardt, P. Orth, *J. of Liq. Chromatogr.* 10 (1987) 1999.
- [138] Y.V.S. Rao, D.E. De Vos, P.A. Jacobs, *Angewandte Chemie-International Edition* 36 (1997) 2661.
- [139] A. Galarneau, D. Desplantier, R. Dutartre, F. Di Renzo, *Microporous and Mesoporous Materials* 27 (1999) 297.
- [140] T.J. Barton, L.M. Bull, W.G. Klemperer, D.A. Loy, B. McEnaney, M. Misono, P.A. Monson, G. Pez, G.W. Scherer, J.C. Vartuli, O.M. Yaghi, *Chemistry of Materials* 11 (1999) 2633.
- [141] B.A. Grimes, S. Lüdtkke, K.K. Unger, A.I. Liapis, *Journal of Chromatography A* 979 (2002) 447.
- [142] K.T. Moller, C.D. Starr, S.A. Johnson, *A parent's guide to cleft lip and palate*, University of Minnesota Press, Minneapolis, 1990.
- [143] J. Tudor, D. OHare, *Chemical Communications* (1997) 603.
- [144] S. Zheng, L. Gao, J.K. Guo, *Materials Chemistry and Physics* 71 (2001) 174.
- [145] M. Pursch, R. Brindle, A. Ellwanger, L.C. Sander, C.M. Bell, H. Haendel, K. Albert, *Solid State Nucl. Magn. Res.* 9 ( 1997) 191.
- [146] C.R. Kessel, S. Granick, *Langmuir* 7 (1991) 532.
- [147] G.S. Caravajal, D.E. Leyden, G.R. Quinting, G.E. Maciel, *Analytical Chemistry* 60 (1988) 1776.
- [148] R. Anwander, I. Nagl, M. Widenmeyer, G. Engelhardt, O. Groeger, C. Palm, T. Roser, *Journal of Physical Chemistry B* 104 (2000) 3532.
- [149] P.A. Bianconi, F.C. Schilling, T.W. Weidman, *Macromolecules* 22 (1989) 1697.
- [150] N. Sheppard, *Journal of Chemical Physics* 17 (1949) 74.

- [151] G.J. Szasz, N. Sheppard, D.H. Rank, *Journal of Chemical Physics* 16 (1948) 704.
- [152] M. Maroncelli, S.P. Qi, H.L. Strauss, R.G. Snyder, *Journal of the American Chemical Society* 104 (1982) 6237.
- [153] R.G. Snyder, M. Maroncelli, S.P. Qi, H.L. Strauss, *Science* 214 (1981) 188.
- [154] J.J. Fox, A.E. Martin, *Proceedings of the Royal Society of London Series a-Mathematical and Physical Sciences* 167 (1938) 0257.
- [155] J.J. Fox, A.E. Martin, *Proceedings of the Royal Society of London Series a-Mathematical and Physical Sciences* 175 (1940) 0208.
- [156] J.M. Chalmers, P.R. Griffiths, *Handbook of vibrational spectroscopy*, Wiley, Chichester, 2002.
- [157] S. Morita, Y. Ozaki, I. Noda, *Applied Spectroscopy* 55 (2001) 1622.
- [158] H.L. Casal, H.H. Mantsch, *Biochimica Et Biophysica Acta* 779 (1984) 381.
- [159] L.R. Snyder, J.J. Kirkland, J.L. Glajch, *Practical HPLC method development*, Wiley, New York ; Chichester, 1997.
- [160] C.C. Landry, A.G. Eklund, S.T. Jull, K.W. Gallis, *Abstracts of Papers of the American Chemical Society* 219 (2000) U113.
- [161] R.P.W. Scott, P. Kucera, *Journal of Chromatographic Science* 13 (1975) 337.
- [162] L.C. Sander, S.A. Wise, *Journal of Separation Science* 26 (2003) 283.
- [163] D.A. Barrett, V.A. Brown, P.N. Shaw, M.C. Davies, H. Ritchie, P. Ross, *Journal of Chromatographic Science* 34 (1996) 146.
- [164] Y.F. Cheng, T.H. Walter, Z.L. Lu, P. Iraneta, B.A. Alden, C. Gendreau, U.D. Neue, J.M. Grassi, J.L. Carmody, J.E. O'Gara, R.P. Fisk, *Lc Gc North America* 18 (2000) 1162.
- [165] O.H. Han, Y.K. Bae, S.Y. Jeong, *Bulletin of the Korean Chemical Society* 29 (2008) 405.
- [166] W. Gao, L. Reven, *Langmuir* 11 (1995) 1860.
- [167] L.Q. Wang, J. Liu, G.J. Exarhos, K.Y. Flanigan, R. Bordia, *Journal of Physical Chemistry B* 104 (2000) 2810.
- [168] O.H. Han, Y. Paik, Y.S. Moon, S.K. Lee, T.Y. Kim, Y.H. Lee, W.I. Lee, *Chemistry of Materials* 19 (2007) 3615.
- [169] J. Liu, Y. Shin, Z.M. Nie, J.H. Chang, L.Q. Wang, G.E. Fryxell, W.D. Samuels, G.J. Exarhos, *Journal of Physical Chemistry A* 104 (2000) 8328.
- [170] A.E. Tonelli, F.C. Schilling, *Accounts of Chemical Research* 14 (1981) 233.



# Tahira Yasmin

Nationality: Pakistani

Date of birth: 07 November 1978

Place of birth: Chakwal, Pakistan

---

## Education

- Sep. 2002–Feb. 2005 Quaid-i-Azam University, Islamabad, Pakistan  
**M.Phil** in Physical Chemistry
- Sep. 2000–June 2002 Quaid-i-Azam University, Islamabad, Pakistan  
**M.Sc.** in Chemistry
- Mar. 1996–Oct. 1998 Punjab University, Lahore, Pakistan  
**B.Sc.** in Chemistry and Biology

---

## Publications

Yasmin T. and Müller K., (2010). Synthesis and surface modification of mesoporous MCM-41 silica materials, *Journal of Chromatography A*, 1217, 3362–3374.

Yasmin T. and Müller K., (2010). Synthesis and Characterization of Surface Modified SBA-15 Silica materials and their Application in Chromatography, Manuscript to be submitted.

Yasmin T. and Müller K., (2010). Structural Characterization of Alkyl Bonded MCM-41 Silica Materials Prepared by Supercritical Fluid Approach, Manuscript to be submitted

Kailasam K., Yasmin T. and Müller K., (2010). Evaluation of alkyl grafted MCM-41 silica spheres by HPLC and various physico-chemical techniques, Manuscript to be submitted